Naturally Inspired Multi-layer Composite Films on Planar and Modulated Surfaces

A Thesis Submitted to the University of London for the Degree of Doctor of Philosophy

By

Iffat Fatima Patel

Supervisor: Professor Gleb B. Sukhorukov

Dr Himadri Gupta

School of Engineering and Materials Science

Queen Mary University of London

April 2015

Declaration

I certify that the present work is prepared solely by me during the course of my studies at Queen Mary University of London. It has not been submitted for a degree at this or any other university. Any words and/or figures from the work of other people are fully acknowledged according to standard referencing.

This thesis fully complies with the regulations set by the University of London and the Queen Mary University of London.

Iffat F. Patel

March 2015

Abstract

Biomimetics is a field of engineering which aims to mimic what has been present in nature. High ceramic-content biomineralized structures like abalone nacre and antler bone have a layered-architecture at the nano- and microscale, consisting of a majority phase of elastic reinforcement platelets or fibrils embedded in a minority viscoelastic phase of proteins and polysaccharides. The synthesis of such systems artificially has attracted widespread interest, with a goal to designing tough composites with adaptable mechanical properties

The results of synthesis pathways towards fabricating such materials are reported herein, including a chemical infiltration route, where growth occurs inside precursor organic multilayers. The structural and mechanical similarities with natural biomineralized systems will also be explored. TGA was used to calculate the rate of mineralization within multilayer films, micromechanical-testing techniques were implemented to compare synthetic composite's mechanical performance with natural biomineralized tissues like nacre. Finally, the mineralization process in three-dimensional multi-layer assembly is discussed using nano-patterning techniques.

To gain a better reading on the presented work and contents discussed, an introduction followed up by comprehensive literature review over polymer assemblies and composite natural and man-made film are presented. Following this, the experimental section containing materials, methods and instruments are described in Chapter 4. In Chapter 5, infiltration process in layer-by-layer films on planar films producing flat substrates is reported. Chapter 6 describes peculiarities of multilayer films made of biopolymers and the chemical infiltration process in such structures, while Chapters 7 and 8 present the research data and analysis of multilayer films with chemical infiltration made modulated nano-imprinted surfaces using both synthetic and biological polymers assessing the bio-mimicking mineralisation in these systems. Finally, Chapters 9 and 10 present conclusions and future outlook.

Table of contents

Acknowledgements

I would like to express my special appreciation and thanks to my PhD supervisor Professor Gleb Sukhorukov, who has been a tremendous mentor and positive influence, who always provided his constant encouragement and guidance over time. I would also like to thank Dr Himadri Gupta for his expertise, help and concern all the while.

It was a great honour for me to work with our collaborators at A Star Institute of Materials and Engineering, I am grateful to Dr Maxim Kiryukhin for his advice and support whilst conducting research in Singapore.

I am especially thankful to all my colleagues and friends, Dr Zofia Luklinska for her expert opinion on imaging techniques; Dr Andy Bushby and Mr. Jonathon Hills for all the guidance they provided throughout my PhD studies. A warm thanks goes out to all the members of our research group, for a lovely working atmosphere and positive exchange of skills and research ideas.

This thesis is dedicated entirely to my beloved parents and my two sisters, Elaynah and Nusrat, words cannot express how grateful I am for their ongoing support, my mum who was a constant pillar of enlightenment throughout. Your prayer for me was what sustained me thus far.

Finally, I would also like to thank my partner, Karl, for his patience who had faith in me during the writing period, and encouraged me to strive towards reaching the finishing line.

List of figures

List of tables

Nomenclature

AFM	Atomic force microscopy
Alg	Sodium alginate
BSA	Bovine serum albumin
Coll	Collagen
E	Young's Modulus
G	Grams
GPa	Gigapascal
HA	Hyaluronic acid
kPa	Kilopascal
LBL	Layer-by-layer
Mw	Molecular weight
NP	Nanoparticle
PAH	Poly (allyl amine hydrochloride) (70 kDa)
PDADMAC	Poly (diallyldimethylammonium chloride) (100-200 kDa)
PEM	Poly electrolyte multilayers
PEI	Polyethyleneimine
pK_a	Acid dissociation constant
PLL	Poly (L-lysine)
PLL Alg	Poly (L-lysine)-alginate
PMMA	Poly(methylmethacrylate), (100 kDa)
PSS	Poly (4-sodium styrene sulfonate) (70 kDa)
SANS	Small angle neutron scattering
SEM	Scanning electron microscopy

SFA	Surface force apparatus
TEM	Transmission electron microscopy
TGA	Thermogravimetric Analysis
TOF SIMS	Time of flight, secondary ion mass spectroscopy
XRD	X-ray diffraction

1. Introduction

Over the past decade research in the field of nanotechnology and nanocomposites has experienced a significant explosion. Nanostructured composite materials give way to an encouraging new generation of ultrasensitive sensors, optoelectronic devices with added performance features. In turn, rigid biological systems are increasingly becoming a source of inspiration for the fabrication of next generation, advanced, functional materials. With the recent developments in nanotechnology, the research of biomaterials and bio-inspired materials has expanded to the micro- and nano- scale, which has promoted a breakthrough in the design of advanced functional materials. Undergoing evolution for millions of years, many biological tissues and materials have realized a unification of their structure and mechanical properties. They are made of inorganic and organic constituents, arranged in complicated multiscale structures, which possess a unique combination of light weight, high strength and toughness, which is difficult to be achieved by artificial metallic, ceramic, polymeric composites.

More recently, inspired by structural models and the outstanding mechanical properties of rigid biological materials, innovative, novel artificial and hierarchal structural materials; including nacre-like materials have been fabricated artificially. As an alternative and feasible approach for the fabrication of bio-inspired rigid structural material, the hierarchal assembly of micro- and nano-building blocks into bulk materials is an attractive feature (1,2) The excellent integrated mechanical properties with hierarchical structure have inspired chemists and materials scientists to develop biomimetic strategies for artificial nacre materials (3)

The goal of this study is the development of biomimetic materials based on a naturally occurring material found in nature- as the armour system of seashells, exhibiting remarkable engineering properties. Nacre-inspired artificial materials are highly desired and will provide a good perspective for next-generation, bio-inspired materials. It is a hard and elastic composite material made up of biopolymers as elastic and inorganic particles acting as a reinforcement mechanism (4). To unravel the scientific principles buried in nacre, the single-crystal growth of calcium carbonate and the hierarchical structure of nacre have been comprehensively studied, indicating that nature has adopted an elaborate strategy to create nacre. An exceptional hierarchal arrangement of the organic and inorganic components conveys extraordinary mechanical properties.

Discussion is focused on the effect of the layered structure, interface, and component loading on strength and toughness of nacre-mimic layered nanocomposites. In this investigation, the focus relies on construing a layer-by-layer assembly arrangement of the structure and reinforcement with an organic phase. This is further investigated on three-dimensional modulated surfaces created through Nano-patterning techniques.

Much progress has been made in exploring multiscale and hierarchical structures, investigating the remarkable mechanical properties of nacre, and understanding of the relationship between them. It is possible to specifically tailor the modulation of these nanocomposites and this still remains an ongoing challenge with the aim of achieving control on the nanometre scale within the field of nanoscience and nanotechnology.

2. Literature review

This literature review focuses on the preparation and application of layer-by-layer assembly with polyelectrolytes, the development of composites, both synthetic and biological in addition to the growth of calcium carbonate within natural and synthetic materials. The different strategies, previously applied will be highlighted and the potential application of this technology explored.

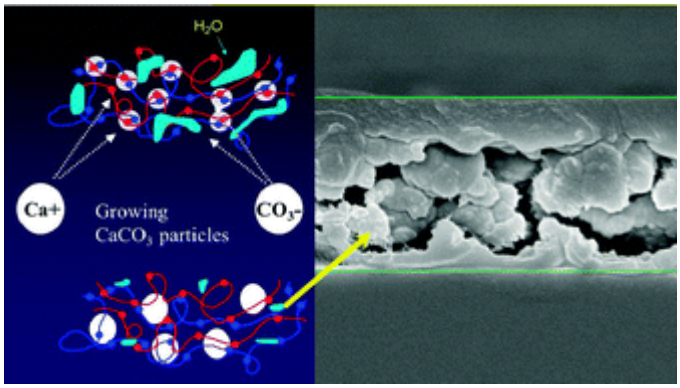

Figure 2.1. Cross section of polyelectrolyte multilayer, infiltrated with calcium and carbonate ions to mimic structures present in naturally occurring materials, a result of this research.

2.1. Polyelectrolytes

2.1. Biomimetics and layer-by-layer synthesis

Investigations have been ever increasing in the development of complex shapes and smart materials. Natural materials are a classic example of the morphological diversity and versatility (figure 2.2) and there has been an ever-increasing passion for humans to mimic and copy nature's ideologies (5).

Figure 2.2. Natural shells made of nacre which are being pursued for their amazing hierarchal organisation and strength (6)

In line with this the layer-by-layer technique has continuously evolved and the production of biomimetic materials and layer-by-layer deposition is an exciting area of research.

When considering the synthesis of materials it is crucial to think about the hierarchal organization, complex shapes and control of the size, shape and polymorph under ambient conditions in aqueous environments (7) the role of the organic matrix has attracted a lot of interest and the mineralization process has been carefully analysed by various research groups which shall be discussed further.

The interface structure of biological composites ultimately determines the load that they can bear. The width, stiffness and content of reinforcing material directs the dynamic stresses which are present in the material (8-9). Biological systems which have a greater width can easily adapt to the relatively high dynamic stresses.

Triple helix collagen molecules have a diameter of approximately 1.5 nm and length of 300 nm (10). Collagen is present in natural organisms in the form of an insoluble

network of fibrous bundles helping tissue to maintain mechanical properties which include elasticity, compression, shape and strength. It is feasible for mineralized invertebrae tissue which result in mechanical support and strain storage energy in bone. The mechanical properties and anisotropy of collagen fibres are known to be regulated by the orientation and composition of fibres. Research found the Young's modulus of single collagen Type I fibrils were in the range of 5 GPa. For this reason collagen is seen as a potentially versatile material which can be incorporated within PEM films in order to give structural characteristics and provide organisation at a molecular level (11-13).

2.2. Nature and nacre

Some of the most architecturally desirable systems are present in nature (14) Structures are adaptable to their function; biological composites have complex and intelligent structural organisations that comprise of both organic, mineral components- resulting in ductile and brittle behaviour. These components are designed at the nanoscale throughout the system. The layered arrangement within these naturally occurring composites contribute significantly to their advanced mechanical properties. In relation to Biomimetics, scientists (15-19) aim to continuously challenge themselves by attempting to manufacture synthetic materials which exhibit similar structures and superior mechanical properties leading to advanced and multifunctional composites.

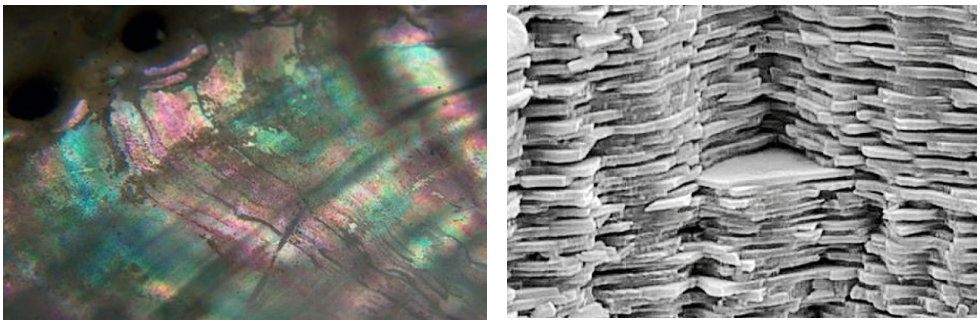

Figure 2.3. Displaying the surface of albone nacre shell (20) and a micrograph of the cross section of nacre (21), displaying the layered structure which results in the high mechanical integrity the material displays.

Biological examples include tendons, connective tissue, deer antlers- used as high impact defensive weapons, and nacre- found in shell, used for protection, nacre gains its known reference 'Mother of Pearl' from its shimmering effect whilst lining the inside of the mollusc shell (figure 2.3) (22-23).

Naturally occurring materials have many attributes (24) that are reflected in the day to day function of organisms.Tendon is a soft connective tissue, the structural units are based on collagen fibres which can be up to 300 microns in diameter, in addition to this there is a complex network consisting of fibroblasts (up to 86% wt.) and water (55%-wet wt.) (25). The network is connected in a complex interwoven manner whereby muscular tension is transmitted for equal force distribution- particularly in areas of movement- the joints (26). The bundles of collagen make up the collective fibril bundles, which are aligned parallel to the long axis of the tendon (27). The structural organization within tendons adapt it to withstanding specific loading conditions in that it is susceptible to cyclic loading, whilst experiencing shear and compressive stresses in addition to tension throughout a lifetime (28,29).

Nacre is an exceptional hybrid material with its structure and related mechanical properties and taken here as model to mimic the construction of new material (30). Nacre is an organic component produced by bivalves, gastropods and cephalopods structured to serve its purpose by protecting the soft muscle secreted by molluscs. Modulus, bending strength and fracture toughness of nacre are compared with a synthetic alumina ceramic material. (31-33).

It is therefore desirable to attain the characteristics of nacre and synthesis a material which can perform the same way. Many investigations have been conducted in order to attempt this. Nacre shell is an attractive target for such a process with its inner nacreous layer composed of aragonite platelets and proteins. In order to develop new methods for new generation materials a biomimetic approach is followed which investigates biological structures and establishes a relationship between structure and properties (34-35).

This edible muscle if often targeted by marine predators; however the presence of nacre's hard shell-like material covers the muscle as well as withstanding the crushing impact of enemy teeth, thus reducing the likely hood of being consumed. The shimmering colour of the nacre shell is attributed to its layered hexagonal aragonite (crystallised calcium carbonate) platelets with a thickness of around 0.5 μm (similar to the wavelength of light) causing interference in the different wavelengths of visible light, giving it a beautiful iridescent appearance (36). A fully developed albone shell can be up to 150-200 mm in diameter and primarily composed of two main layers with different phases. A brittle layer which lies on the outer side, being composed of larger sized crystals of calcite and an inner layer which comparatively is made up of 95% volume of aragonite and 5% volume of proteins and polysaccharides. The aragonite platelets

combined with water present at the interface and addition of elastic proteins (chitin and lustrins) fform an organic matrix of layered sheets 10-50 nm wide (37). This is where the composite framework is effective and strength and the toughness of a naturally existing material is displayed. It is this structure that is appealing to science (38-40). The mechanical capabilities of nacre offers a balance in strength and elasticity (41-42), enabling it to build resistance against high impact loads and provide its viscoelastic properties (figure 2.4). Studies have demonstrated that nacre not only displayed advanced structural properties when analysed under the Dark field TEM (demonstrating its ability to respond as a single crystal, instead of its actual sub-divided highly crystalline matrix), but possessed high biocompatibility (43-44).

This demonstrates the use of combined materials in tissue engineering, thus combining superior properties for advances in technology. Another study compared naturally occurring nacre and artificially prepared nacre using polyelectrolyte multilayers and found ultimate tensile strength (UTS) of natural nacre to be 130 MPa and young's modulus of 64 GPa (36), whilst the artificial nacre possessed values for UTS of (100±10) MPa and Young's modulus of (11±2) GPa. The difference in Young's modulus was explained through the clay platelet constituents, where bulkier blocks of $CaCO_3$ were used to prepare the artificial nacre, causing additional friction when one $CaCO_3$ slides against another.

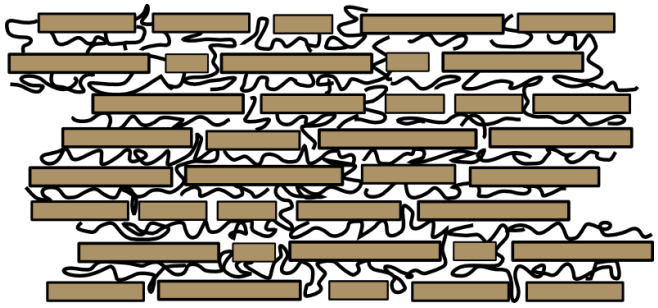

Figure 2.4. Schematic displaying the brick-and mortar structure which provides reinforcement to the structure at a micro level, each platelet has a relative thickness of 5 microns (21).

The scientific studies indicate how closely controlled fabrication and observation at the nanoscale can produce composites with impressive mechanical properties, yet none that exceed that of naturally occurring materials. Despite the relatively weak components that make up nacre, collectively the constituents make up a material with outstanding mechanical integrity when the material is designed and controlled at such a level it can lead to an increased level of control. When synthesizing a material with bespoke requirements it is necessary to maintain a high level of control at the Nano, micro level design.

2.1.1. Collagen- A naturally occurring polymer

The most abundant protein present in the body is collagen, it constitutes approximately 25% of protein mass. More than twenty known different types of collagen are present in the human body (45). A general definition that can be given to collagen is as a protein which contains one domain where three polypeptide chains associate to form a triple helix and the sequence of such domains comprise if repeating triplets of amino acids (46).

Among them Type I collagen is the most common forms of collagen, primarily found in the extracellular matrix of skin, tendon and bones to provide shape and strength

(47). Resistance to macroscopic extension of tissue- like tendon is provided by the arrangement of large axially, densely packed collagen type I collagen fibrils.

Type II, VI, IX and XI are present in different proportion, different cross linking to provide to provide a dense matrix of stress bearing fibrils and resistance to compression. For this reason, collagen classification based on the primary structure is carried out by measuring the length of the triple helical domain. Type I collagen is used in this study.

Physical properties and chemical composition of Collagen

The triple helix collagen molecules have a diameter of approximately 1.5 nm and length of 300 nm. Collagen is not found in the human body in the liquid state like blood or plasma, it is in the form of an insoluble network of fibrous bundles helping tissues to maintain properties like elasticity, compression, shape and strength (48). It is capable of being mineralized in vertebrae tissues offering mechanical support and strain storage energy in bone (49). Collagen molecules are naturally found in the body and have inherent properties including biocompatibility, low toxicity, biodegradability and less prone to immunological reactions. The mechanical properties and anisotropy of collagen fibres is known to be regulated by the orientation and composition of fibres. The Young's modulus of single collagen Type I fibrils were (5±3) GPa (50). Type I collagen is the most common protein in connective tissues; it's made of a repetitive amino acid sequence (51).

The structure includes; two α1 and one α2 chains form three peptide subunits which can fold into unique triple helical structure with three domains: NH_2 terminated helical, triple helical, and –COOH terminated helical domain NH group of one glycyl sequence forms hydrogen bond with CO group of adjacent chain and another one with

hydroxyl group of 4-hydroxyproline in third position of triplet. Hence it's also known as telopeptide collagen or tropocollagen.

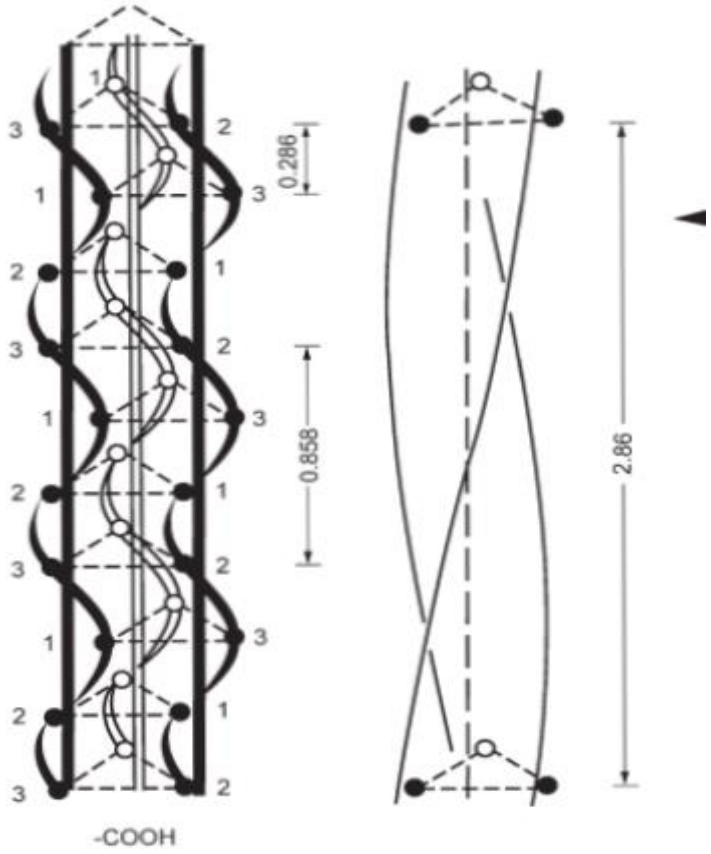

Figure 2.5. The figure above displays a schematic of the triple helix typically found in the helical structure of collagen with a carboxylic acid and amine functional group at either end. The structure shows (Gly-Pro-Pro) in glycine is designated by 1, proline in x position by 2, proline in y position by 3. (7, 16)

Morphology of collagen molecules changes drastically on conversion of collagen type I monomers into collagen fibrils (figure 2.5). Typical collagen fibrils are undetermined in length and diameter are in a broad range (10-500 nm) depending on age of collagen and tissue type (52).

It has been observed that collagen fibrils of 100 μm have three domains (52) clearly visible: a finely pointed (alpha), central region of uniform diameter (shaft), coarser tip (beta). Lateral aggregation of fibrils varied in 100-140 nm diameter with cylindrical and twisted conformations (53). From this it can be ascertained that

collagen is a versatile component and can take many shapes and configurations. This makes the challenge greater in synthesizing architectural designs with collagen.

2.2. Mechanosensing, actuation and controlling dynamic loading behaviour

All living organisms use composite materials; the composites aid in providing protection, motility and signal sensing as well as mechanical strength and support. Nature's models are now being used as the carbon prototype to drive research in the direction of mechanosensors and actuators. Of course it is vital that the structure-function relationship of these living organisms can be transferred in to a range of structural solutions through research and development.

When engineering a material a 'top down' approach is usually taken whereby a material is selected to fabricate a component with an established goal and design plan in mind; this is the common engineering phenomena. In contrast, nature works with a 'bottom-up' approach and the material and structure are grown according to their levels of hierarchy implementing self-assembly in a biological environment (54). Having said this, the environment that natural organisms and structures develop in also fulfil many criteria including steady temperatures, pressure and pH conditions which are desirable for proliferation for the existence of life (55-56).

Biomimetic materials science requires the study of pre-existing materials which represent solutions of multifaceted problems, thus making it more challenging to apply the principles of engineering directly to biological systems.

Many investigations have focused on the quasi-static loading events of composite materials in both nature and synthetic applications. There is an issue with recreating the service life loading conditions in these composite materials. High impact loading, dynamic loading and fatigue assessments include a few as all of these loading conditions rely on time dependence and mechanics of the localised structure. Nature

has demonstrated the high impact loading conditions of natural materials including bone, deer antlers and the common nacre sea shells (57-58). All share the same design at the nanoscale whereby a stiff reinforcement scaffold of high volume fractions is surrounded by an amorphous interfacial region, the changes taking place in the amorphous morphology result in dynamic mechanical responses thus allowing the analysis of mechanical properties.

Fratzl and Barth, (59) presented the mechanosensory systems of spiders and actuation systems in plants which demonstrates the combination of engineering models and classical biology. According to Fratzl and Barth, the process of mechanical sensing is described as the reverse of those by with actuators generate mechanical forces. Refined data processing is required for the interpretation of mechanical signals such as tactile input and generation of complex movement signals. When considering a biological species like the Cupiennius salei; the spider demonstrates sophisticated sensory filtering which biologically takes place outside of the central nervous system (60). A slit-system embedded on the exoskeleton of the spider allows it to detect advanced level vibrations which are used in courtship for prospective mates.

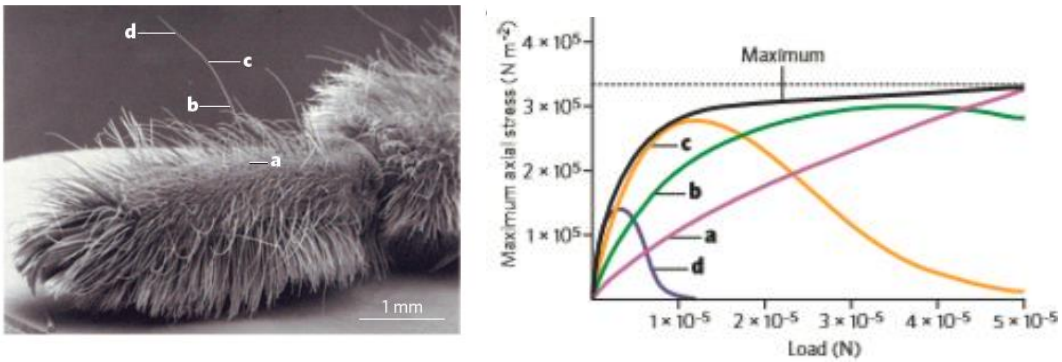

Figure 2.6. The image on the left indicates the various positions the measurements were made (a,b,c and d). The dependence on increasing the stimulus or force on these receptors is indicated in the graph on the right, as a measure of maximum axial stress at each point (59).

The system locally enhances the mechanical compliance of the exoskeleton resulting in a deformation of the slit by micro-forces; this amazing structure-function relation can be demonstrated in nature as the exoskeleton has a stiffness which equates to that close to bone (figure 2.6). In turn the mechanosensitive sensilla can protrude from the surface and deflect by direct flow or the frictional forces of airflow.

Fratzl and Barth identified that the cuticular modulus was of 15 MPa at low frequencies. As the frequency of vibration increased to 112 Hz the modulus also increased up to 70 MPa. This is clearly demonstrated in the curve whereby the dependence on increasing the stimulus or force on different positions of the receptors is indicated. Ultimately the mechanical adaptability of the cuticle is a result of the degree of crosslinking of the matrix and is enhanced by the modification of various structural properties including the proportion of fibres within matrix, water content and also the orientation of the fibres. Materials like chitin and cellulose found in these structures are versatile. The receptor hairs are therefore well designed and demonstrate a classic example in nature with a light-weight, high strength characteristic which is adaptable according to the force of the stimuli (59).

2.2.1. The History behind layer-by-layer synthesis

The layer-by-layer technique involves controlling both the vertical and lateral distribution of layers, a three-dimensional material can be synthesised with control over the shape, dimensions and composition over various length scales.

The binding of monolayers using cationic and anionic colloidal nanoparticles was first discovered the early 20th century (61). Immersion in suspensions of opposite charge lead to the production of multilayer films one layer at a time (61). Tracing back to the seminal work of Langmuir and Blodgett (62), research evolved from the two

dimensional assembly of architectural films produced in liquid, air and solid interfaces. The Langmuir film was developed through satisfying the unsaturated surface valence forces, The LB multilayer films as they soon came to be known as were producing film architectures with structure and composition designed for a specific function. An amphiphilic surfactant bearing two chemically distinctive termini branches controlled the orientation of the substrate, the exposed end then adhered to the counterpart. The control of chemical species in this way was pivotal to the understanding the synthesis and dimensional assemblies of the individual components.

By 1991 Decher (63-64) continued this concept through the growth of soluble organic polyelectrolytes resulting in the formation of controlled architecture-multilayer polymer films based on the propagation of the layer-by-layer assembly of charged polyelectrolytes to create an electrostatically bound super lattice structure. Essentially, alternating the charge of a polyelectrolyte solution each time resulted in monolayers of oppositely charged ions being attracted to one another. As this process is repeated, a multilayer is formed and this effectively can be manipulated to ascertain desired characteristics of a material (63-64).

2.3. Polyelectrolytes

Polymers are highly superior in that they display qualities that can be easily manipulated to best suit the desired application. Polyelectrolytes are made from polymers, which are many repeating monomers units joined together through a polymerisation reaction, these groups are prone to dissociate in aqueous solutions and result in the generation of free ions which in turn produces a solution which is electrically conductive (65-66).

A correlation can be found between the number of repeating monomer units and the molecular weight of the polymer, and it is this idea that governs several physical properties of polymer materials, including glass transition temperature, T_g (the transition from an amorphous polymer displaying a rubber like behaviour to behaviour of a brittle glassy material), melting points, stiffness, viscoelastic properties and toughness.

If the solution is positively charged it is a polycation, conversely, if it is negatively charged it is a polyanion. The dissociation behaviour of a polyelectrolyte determines the degree in which it dissociates in water. A strong polyelectrolyte will completely dissociate in water, comparable to a weaker polyelectrolyte which undergoes partial dissociation only- the pH of a weak polyelectrolyte effectively.

The conformation of the polymers strongly determine their mechanical properties, thus influencing mechanical properties of the overall composite performance. The Lennard-Jones theory illustrates that as the distance between atoms decreases the force and changes from attraction to repulsion, hence the closer together the negative groups on the polymer chain the stronger the repulsive forces between the atoms (67-68).

2.3.1. Surface energy of solutions

Depending on the characteristics of a surface, liquid can display various behaviour, on a smooth surface this behaviour is characterised by the surface free energy and strength of the force between the surface and liquid.

Materials including PMMA and biopolymers make suitable materials for the layer-by-layer process. Biopolymers are ideal because they contain a low number of

electronegative atoms within the polymer chain, since polar groups increase surface energies. This will allow sufficient level of polyelectrolyte adsorption through its increased wettability. Complete wetting means that the droplet would have a low contact angle and cover more of the surface (69) Pre-treatment of a substrate, primarily dipping PMMA substrate into PEI solution, is effective in enhancing adhesion between polyelectrolyte layers. Similarly, pre-treatment of a surface using piranha solution (3:1 sulphuric acid to hydrogen peroxide) also contributes to high adhesion by sterilising and removing any impurities on the surface that may prevent contact between the polyelectrolyte and the substrate surface.

2.4. Polyelectrolyte multilayer

Electrostatic interactions are responsible for the attraction between charged polyelectrolyte multilayers. It was Decher, who was first to develop polyelectrolyte multilayers, the process involved formation of a multilayer on a charged substrate material (70-71). Hybrid materials include two moieties, organic and inorganic, combined at a molecular level, material classification depends on the type of interaction which bonds the inorganic and organic species. When creating an inorganic composite, two moieties, organic and inorganic are combined at a molecular scale. These material components can either have weak van der Waals, hydrogen bonding or weak electrostatic interactions. This arises when a dipole is initiated momentarily from the constant movement of electrons.

Van der Waals forces consist of interactions between atoms with a permanent dipole induced by electronegativity or temporary dipoles. Other common forces include covalent and ionic bonding (figure 2.7 overleaf). The strength of interaction between polymer chains increases with increased polymer chain length. A longer chain will

allow more points of contact for bonding interaction. This is likely to occur across the whole length of the chain, thus more energy would be required to overcome the bonding (72). If the polymer has a high Mw then longer chains are going to be present. It can be deduced that the longer chains will have a higher degree of entanglement. These entanglements are the key success behind strong plastics and polymer composites (73).

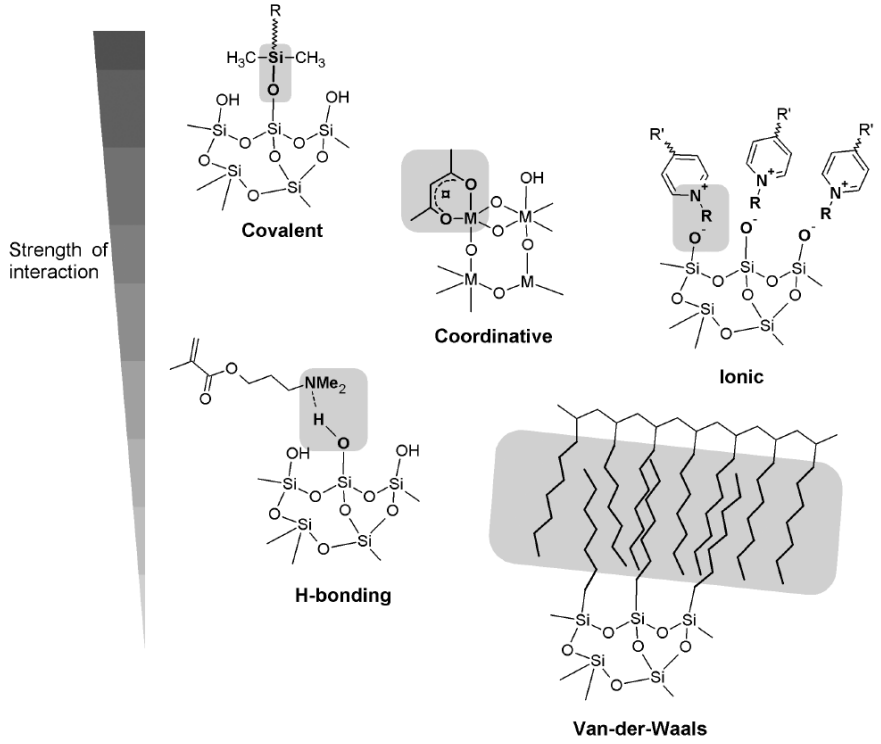

Figure 2.7. Displaying the bonding forces present in composite materials (74).

2.4.1. Physicochemical aspects of layer-by-layer assembly

The primary layer of deposition serves to charge the surface, this primer can consist of aminoalkylchloro- or alkoxysilane groups which anchor to the hydroxyl groups on a silicon surface (75-76). It was established that at neutral pH the exposed amine functionality is protonated thus exposing a positively charged surface. The multiple electrostatic reactions can bind this surface with a water soluble anionic

polyelectrolyte. The polyelectrolyte monolayer overcompensates for the positive charge of the primer and this results in a negatively charged surface (77-78).

This gives the opportunity to enable sequential deposition of cationic and anionic polyelectrolytes (figure 2.8). The resultant multilayer demonstrates a high level of regularity and the individual polymer layers can have insulating, magnetic or semiconducting features depending on the addition of active components (79-80).

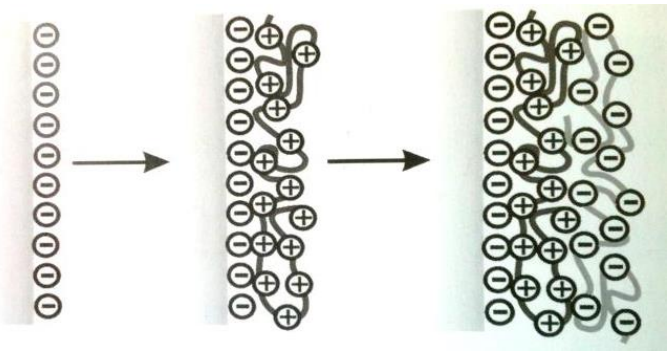

Figure 2.8. Iterative formation of layer-by-layer electrostatic multilayers by alternately dipping in solutions of polyanions and polycations (76).

The use of redox active organic polyelectrolyte multilayers using a solution phase self-assembly technique was implemented in various pieces of work (81-82). Cationic polyviologens with anionic sulfonated polyelectrolytes resulted in the production of multilayer films which actively controlled thickness. Amongst the other functionalities and interactions that can be used to build up layer-by-layer films are: hydrogen bonding, stero-complexation of stereoregular polymers, charge-transfer interactions and specific bio-recognition events.

The layer-by-layer deposition can be modified by controlling the relevant parameters including; pH, salt concentration, and polyelectrolyte charge density. The electrostatically driven layer-by-layer process has the advantage of producing films with desired thickness. Polymers, proteins, viruses, colloids and dyes are a few of the

species which can be used for the formation of these films with Nano-scale precision (83-84).

It is a well-known fact that the solution ionic strength and the charge density of a polymer will influence the degree of polymerisation and plays a major part in the film deposition process. Manipulating the pH of the polyelectrolyte solution can also give a way to control the charge density of the polyelectrolyte chains (84). For (PSS/PAH) systems the pH becomes a crucial factor when it is too close or higher than the pK_a of PAH as the maximum thickness of the films is reached when the polyelectrolytes are weakly charged (85). The average pK_a of the acid-base moieties can also be shifted depending on the environment. For instance the pH is significantly lowered within a multilayer film than in the solution directly. An exciting concept of the layer-by-layer process is the ability to merge different functionalities into one unique system. The versatile nature of the process can reveal engineering designs of increasing scientific and technological interest (85).

2.4.2. Nucleation and bio-mineralization

The process of biomineralization involves the production of a new crystalline phase. Nucleation therefore plays a crucial role in the primary building blocks of bio mineralisation in a complex structure (86). The classical theory of nucleation takes into account the spontaneous formation of spherical molecular clusters with size dependent free energies that continue to grow when the value is greater than the size of the critical radius.

$$G = \frac{4\pi}{3} r^3 G_v + 4\,\pi r^2 \gamma \qquad (1)$$

where G_v is the Gibbs volume energy and γ is the interfacial energy. The critical radius r_c is found by setting the derivative of G equal to zero

$$\frac{dG}{dr} = 4\,\pi r_c^2 G_v + 8\,\pi r_c \gamma = 0 \qquad (2)$$

Yielding:

$$r_c = -\frac{2\gamma}{G_{v_1}} \qquad (3)$$

Where γ the surface energy, and *Gv* is is Gibbs energy per volume (87-88).

Taking all these factors into consideration, the formation of biomimetic structures using controlled layer-by-layer assembly is ideal (87-88). Not only can the thickness of the multicomponent film can be controlled, the composition and function can also be monitored. The charge self-regulation can control the deposition along each step of the process, which is elementary in the layer-by-layer process.

The combination of bio macromolecules such as proteins and polysaccharides play a determining role in the morphological control in the formation of bio minerals (89). A number of in-vitro studies for the nucleation and growth of bio minerals demonstrated that their morphologies are influenced by the extracted organic components. Studies in this region focused primarily on the development of the inorganic components of naturally occurring materials like bone, nacre and mollusc shell (90-91). Newly developed inorganic/organic composites displayed a change in morphological properties of the material itself. In these investigations, thin film calcium-carbonate crystals were grown via a combination of polymer thin film and simpler acidic polymers like poly-acrylic acid and (PAA) and poly-glutamic acid (PGA) (92-93).

Much research has been conducted on strengthening mechanisms through the process of biomineralization (94) as an attempt to optimize designs for novel materials. The superior mechanical performance of naturally occurring materials like nacre were

originally attributed to its unique microstructure. Over the past decade, research on the mechanical behaviour and modelling of nacre has deduced that the microstructural arrangement has a high degree of influence on the performance and strength of this materials as described in the parameters below (95).

i. A staggered arrangement of nacre platelets which present a brick and mortar model to describe the behaviour of nacre platelets.
ii. Nano-asperities on platelets were detected through the Finite-Element Analysis model based on friction mechanisms (95).
iii. The mineral bridges, which connect the protein layer between adjacent mineral platelets increase the toughening mechanism which in turn results an increase of strength.

Investigations of limnetic nacre resulted in a higher degree of mineralization with a thicker nacre layer, ultimately occupying 80 % of the total thickness of the shell. The mechanical performance is also limited according to the water content of the shell, as the water content is increased the Young's modulus and ultimately the strength decreases significantly. This has an impact on the material ductility and hardness of the shell itself (95).

2.4.3. Artificial thin films and layer-by-layer assembly

It was during the 1970's that Lowenstam proposed his theory of organic matrix mediated mineralisation. The majority of bio-minerals are composed of calcium carbonate, phosphate, oxalates and silica or iron oxides (96).

Figure 2.9. Artificial layering of shell structure. Demonstrating the complexity of the structure which arises in the high performance of natural materials (97).

The nucleation kinetics play an important role in the development of these structures and this shall be explored further (98-99). The primary concept that organics can control the nucleation, growth and form of inorganic materials; this is the process which generates the hierarchal composite structures (100) with unique physical and chemical properties (figure 2.9). Through careful preparation and control of parameters it is possible to exploit the principles of biomineralization to prepare novel materials as seen in the classical nacre model (101).

2.3. Mechanical properties of poly electrolyte multilayer

The interface of composite materials can determine the mechanical response of a material; Figure 2.10 shows an SEM image of a PEM multilayer film (36), a proven method of duplicating natural materials through spontaneous organisation took place. The composites are favourable and the arrangement is displayed in the following illustration.

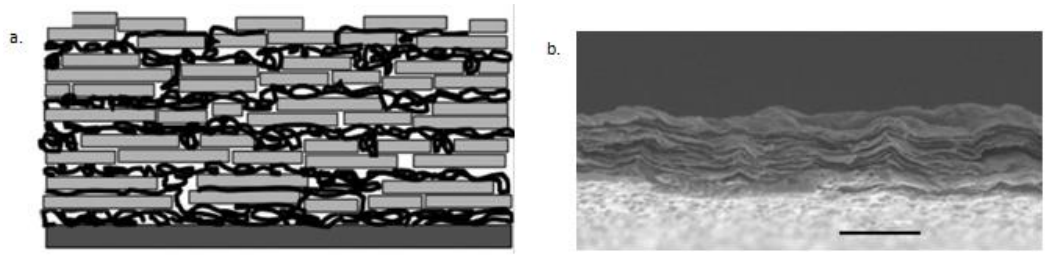

Figure 2.10. Schematic of the polyelectrolyte and clay platelet structure b. SEM of such a film, scale bar: 2 (36)

Table 1 displays the increase in mechanical properties including the Young's modulus as the number of deposition cycles is increased and the SEM image identifies the formation of individual layers in the composite. This coincides with the schematic of the brick and mortar arrangement which is present in natural materials, it is the filler material which gives rise to the increase in mechanical properties and this can be manipulated.

Table 1. Displays the relationships between the strength of PEM films in relation to the deposition cycle (36).

Deposition Cycles	Ultimate Stress (MPa)	Ultimate Strain	Young's Modulus (GPa)
50	95	0.07	9
100	106	0.08	10
200	109	0.10	13

Euler's model of critical stress demonstrates the collapse of elastic shells to estimate the Young's modulus of a PEM film. If the film reaches a critical thickness it can withstand template dissolution, resulting in free-standing structures. This is desirable when considering applications like release-on-demand of cargo from the individual chambers through laser radiation it is critical to maintain the strength of the structure. The theory of elasticity predicts the existence of critical stress above which the elastic shell can buckle. Nano-indentation tests (149) demonstrated a Young's modulus of

(4±1) GPa for PEM shells. The mechanical stability of the PEM chambers was high and therefore proves to have robust characteristics for application in solid-state delivery systems.

The overall performance of natural materials is determined by the microstructure and hierarchal organisation of the individual components and these are strongly influenced by interactions, barrier properties and basic biomimetic concepts (102). Wood for example has strength with is comparable to the strongest steels and antlers, shell and bone have a toughness which is an order of magnitude greater that engineering ceramics due to their resistance to fracture which is measured by the toughness (J_c-fracture energy per unit area) (103-104). Natural materials are made from a small number of polymeric and ceramic building blocks whereby nature fabricates a remarkable range of structured composites. Hydroxyapatite or aragonite platelets are dispersed in a helical matrix of collagen (105), so it can be demonstrated that it is not so much the individual building blocks but their arrangement within natural composites which result in extraordinary properties (106-107).

Further to this, the calcium carbonate crystallization from a supersaturated solution of calcium carbonate was conducted on a chitin substrate, the chitin matrix for the crystallization was prepared by spin coating the solution onto glass substrates and then analysed through SEM. The investigation successfully prepared uni-axially orientated calcium carbonate thin film crystals on chitin matrices by using natural peptides. The peptide ensured a consistent arrangement of the acidic groups by specific interaction with the chitin and stabilization of amorphous calcium carbonate, these factors ultimately led to the formation of uniaxial orientated calcium carbonate films. The design of the organic matrices are therefore crucial when considering the growth of

the calcium carbonate, especially within inorganic/organic hybrid materials which in turn exhibit a level or morphological control (108-110)

2.3.1. Freestanding layer-by-layer thin films

Monolayers of nanoparticles on oppositely charged layers of polyelectrolyte thin films are typically assembled on glass or silicon wafer substrates. The cyclic deposition can result in uniform film deposition through a charge overcompensation phenomena as explained earlier. Research (111-112) carried out in early investigations on preparation of free-standing layer-by-layer thin films thus paving the way for ultrathin membrane synthesis which continues to expand the range of applications the technology can be employed upon (113). When a desired degree of structural sophistication or thickness is achieved, the layer-by-layer assembly is lifted off the substrate. This gives the opportunity to investigate the direct physiochemical properties of the free films.

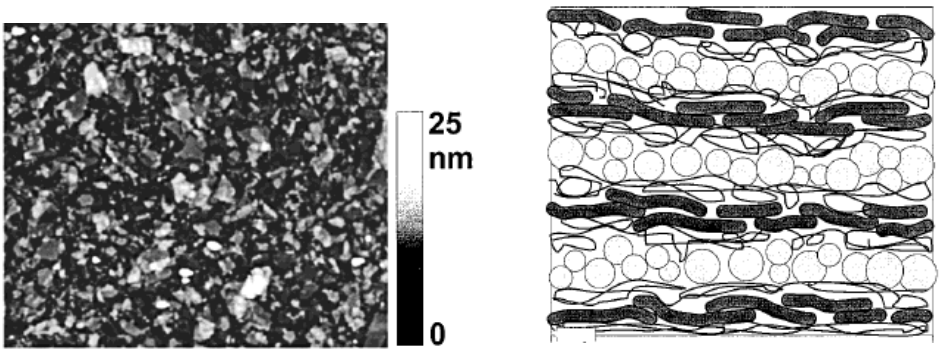

Figure 2.11. a. AFM image of film cast on a silicon substrate with magnatite nanoparticles b. Model structure of magnetic polyelectrolyte clay multilayer, demonstrating different structures (114).

Early experiments made use of organic solvents which were used to 'lift off' the films without damaging the film (figure 2.11) By ensuring that the substrate is hydrophilic

with either a positive or negative charged surface The electrostatic interactions serve as a foundation for the film. A classic example is of cellulose acetate which is insoluble in water but dissolves readily in acetone at room temperature. This research included magnetic nanoparticles (115) resulting in production of a thin film in a range of a few hundred nanometres. Montmorillonite clay platelets were added in order to increase mechanical stability of the films and the schematic can be seen in the figure. The AFM image also characterises the surface topography of the film surface and presents a promising technique which has since been used to produce free standing films, these are films where the substrates has been eliminated.

2.3.2. Deposition methods for casting thin films

When considering the construction of these thin films many methods have been implemented for producing finely controlled thin films. The alternate dipping method has been the oldest implemented and has been used widely (116).

Spin coating has also been used as a successful deposition method and polyelectrolytes are deposited during each cycle. There is a rapid rotation of a spinning disc to which the substrate is attached. Investigations (116) deduced that the surface roughness of the films was independent of the number of deposited pairs on a substrate surface.

Spraying has also been used as a more controlled method of depositing each layer on the substrate surface as demonstrated by researchers (116-117). Small Angle Neutron Scattering, (SANS) data deduced that sprayed (PSS/PAH) polyelectrolyte multilayers are stratified with a substantially decreased level of surface roughness in relation to the same multilayers produced via a dipping process.

On an industrial level the layer-by-layer rolling method allows the implementation of layer-by-layer coating. However, the process is limited because it does not always

yield the same film properties when created on a smaller scale (118). This affirms the importance of the way in which films are deposited on the surface of a substrate.

2.3.3. Layering species

Many polyelectrolytes have been used in the formation of layer-by-layer PEM composites. Those relative to this investigation are discussed further:

PEI is a weak polycation (positively charged) that can be found in its linear state (carrying secondary amine groups) or branched state (carrying both secondary and tertiary amine groups). PEI has the molecular formula (C_2H_5N) n the amine groups carry lone pairs of electrons and, due to their pH dependence, the amine groups are often subjected to protonation. The two hydrogen atoms on the secondary amine group are replaced by two CH_2 groups; whilst three hydrogen's on the tertiary amines are replaced by three CH_2 groups. This leads to the formation of polar bonds due to the electronegativity of nitrogen, thus dipoles are developed increasing its affinity for water and making it readily soluble.

Depending on the strength of the acid, the protonation rate either increases in the presence of low pH values, where the polymer swells, or the rate is slower in higher pH values where polymers are less likely to swell due to their lower charge density (119-120).

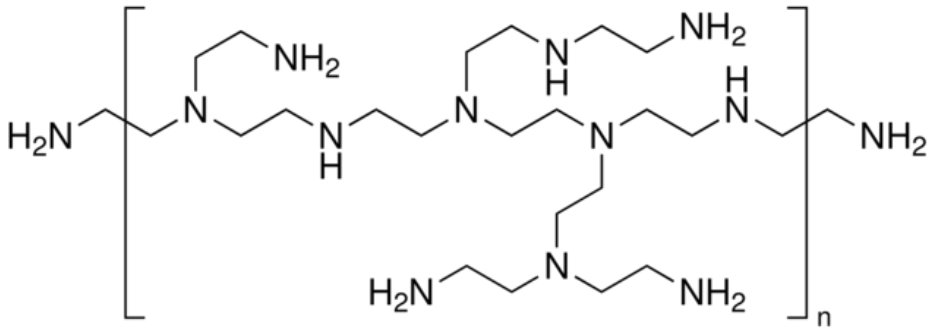

Figure 2.12. Branched PEI used in PEM synthesis (121)

PEI is a synthetic organic molecule and due to this reason it can be used in various applications, the properties it displays, include; the use of its amine groups to bind to a range of transition metal cations (122). Investigations on the toxicity concerns of PEI to several different cell lines (123), PEI has been the main focus in many studies in biomedical and electrical industries, it was used as a primary precursor deposition layer for the fabrication of polyelectrolyte multilayers (125-126)

PSS is a strong polyelectrolyte and carries a negative charge enabling the build-up of layers on positively charged species, through electrostatic interactions between polymeric groups as displayed in figure 2.12-2.16. Its stability over a wide pH range (126). When the charges along weak PE chains are reduced by changing the pH this also reduces the self-repulsion between monomer units (127). This in turn decreases the chain stiffness and increases the surface coverage as it is in a more globular state.

The ionic interactions and van der Waals forces are the foundation of electrostatically bonded PEI and PSS. The large number of opposing charges over compensate each other and lead to the entrapment of polymer coils (128) during the layering process. Varying pH may result in fluctuation of the charge densities leading to changes in the polymer conformations and possibly the affinity for oppositely charged

species and surfaces. Little information has justified whether these conformations between complex molecules are fixed in position or reversible when removed from solutions.

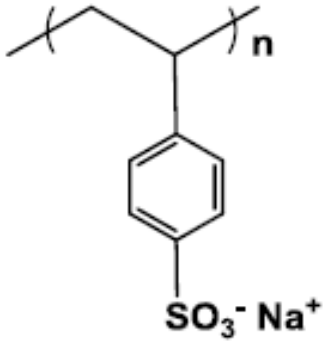

PSS

Figure 2.13. Schematic structure of PSS

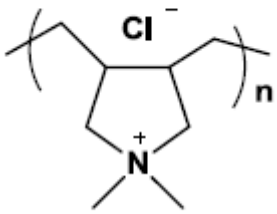

PDADMAC

Figure 2.14. Schematic structure of PDADMAC

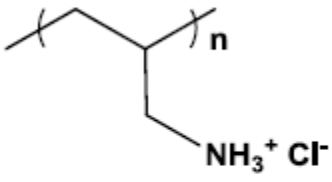

PAH

Figure 2.15. Schematic structure of PAH

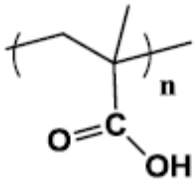

PMA

Figure 2.16. Schematic structure of PMA

2.3.4. Compartmentalised films and three-dimensional structures

In order to increase their generic application research into compartmentalising films for applications like transport, drug delivery and protein storage has been on-going since 1995 (130). The multilayer assembly was designed in order to build up compartments within heterostructures composed of assemblies with a minimum of four interacting species. The pairs of strata would act as blocking layers or barriers towards permeability of macromolecules or ions. The inclusion of nanoparticles within the system would enhance both the property and functions of these films (170).

A purely organic compartmentalised 2-stratum polyelectrolyte film. (PAH/PSS) was deposited directly on to a dense (100nm) exponentially growing poly (glycolic acid) (PGA) films (146). The PSS free chains were able to diffuse through the initial (PGA/PLL) strata thus resulting in an exchange of PGA and PSS chains. As the second layer was deposited the film began to demonstrate barrier properties and this prevented diffusion from taking place. The partial diffusion of the PSS chains resulted in improved mechanical performance of the film and ultimately could be used for embedding active biomolecules within the system. The compartmentalising of these

films is not limited and more complex systems can allow for carefully controlled diffusion between multilayers by incorporating barrier pairs within the system (129).

2.4. Smart and responsive materials

Manipulating the mode and strength of mutually existing interactions can lead to an array of dynamic and responsive coatings. Polymers with inorganic components like carbon nanotubes, inorganic nanoparticles give rise to additional characteristics of the films thus resulting in greater mechanical strength and optical properties as demonstrated in literature (131) during the production of multilayer composites by sequential layering of nanometre scale films.

2.5. Linear and exponential growth of PEM films

Optical methods have been used previously in order to determine the linear increase in film thickness (131,132). Films produced with PSS/PAH showed the characteristic organisation in the direction perpendicular to the substrate with a small interdigitation between the neighbouring polymer layers. In addition to this it was established that the PSS/PAH films behave as glassy materials through characterisation using surface force apparatus (SFA) at ambient temperature (132). Studies went further to propose a theoretical model which demonstrated a linear increase of thickness after the deposition of the first four to five multilayers when deposited on a charged substrate. The model affirms that polyelectrolytes in a solution form complexes with polyelectrolytes of opposite charge on the outer layer of a film. In order to pursue a regular growth of the film with deposition of each layer Shafir and Andelman, (132) describe the significance of reaching strong short range interactions between oppositely charged polymers (133).

The combination of PLL/ sodium alginate (Alg) was found to demonstrate a significant diversion in the growth of layer-by-layer films. The thickness versus the number of layers being positive. The authors concluded that the increment of material deposited at each layer was a consequence of the surface roughness of the previous layer. This was a feasible concept as the surface roughness also provides an increased surface area to which the polyelectrolytes can adsorb onto the surface of the film. PLL/HA and chitosan/ HA have also been described to follow the exponential film growth at pH 4 and 7; the growth can also be manipulated and demonstrates a linear behaviour when PSS is substituted as the polymer (134-135).

The homogeneity of these films was monitored using scanning electron microscopy and atomic force microscopy, which indicated the relevant topography of the film over the surface. The supralinear growth of films was observed post 1999 when PLL-Alg (alginate) lead to the increment of the deposition of each pair of polyelectrolytes increasing and this was due to the surface roughness of the films. The roughness of the film in this system allows space for active sites to be filled for the forthcoming layer deposition.

When considering these biological polymers it was evident that exponential growth behaviour was clearly observed between a pH range of 4 and 7. As the multilayer grows exponentially, the film thickness can dramatically increase to the micrometre range (136). Picart *et al*. 2002 continued their investigation into the PLL-HA multilayer system whereby confocal imaging demonstrated that the PLL not only adsorbs onto the surface of the multilayer but also diffuses throughout the thickness of the whole film. For this reason, the diffusion rate is assumed as constant and it is

also assumed that the uppermost layer will be affected by diffusion thus resulting in a transition between exponential to linear growth in this system.

2.5.1. Growth of the polyelectrolyte multilayer

From previous investigations, it has been established that during the layering process, exponential growth occurs until reaching a critical thickness, before changing to linear growth. Earlier reports have shown that the exponential growth regime has displayed an incremental thickness being significantly larger than that of linear growth (usually hundreds of nanometres versus a few nanometres). Exponential growth is still not entirely understood, though theories have suggested that an increase in surface roughness with each deposited layer may be the cause. Another explanation describing the difference in layers exponentially built up to those linearly built up (137-138) considered the diffusion of polyelectrolytes in and out of the film led to the formation of separate diffusion zones.

The primary zone was found to comprise of the first layering complex only, as it concerned the adhesive properties between the first set of layering species and the substrate surface. The secondary zone was due to the diffusion process occurring following further deposition. This contributed to the exponential growth with increasing number of layers, and although is formed at a secondary stage, it is referred to as the "diffusion zone". The final zone continues to take into consideration the diffusion of polyelectrolytes, whereby layers grow linearly beneath this point. This is due to the concept that further construction of this zone is assumed to inhibit the diffusion process and for this reason the tertiary zone is maintained at a constant thickness (139-141). This adequately outlines the

difference between the growth mechanisms, the schematic (figure 2.17) illustrates this concept further.

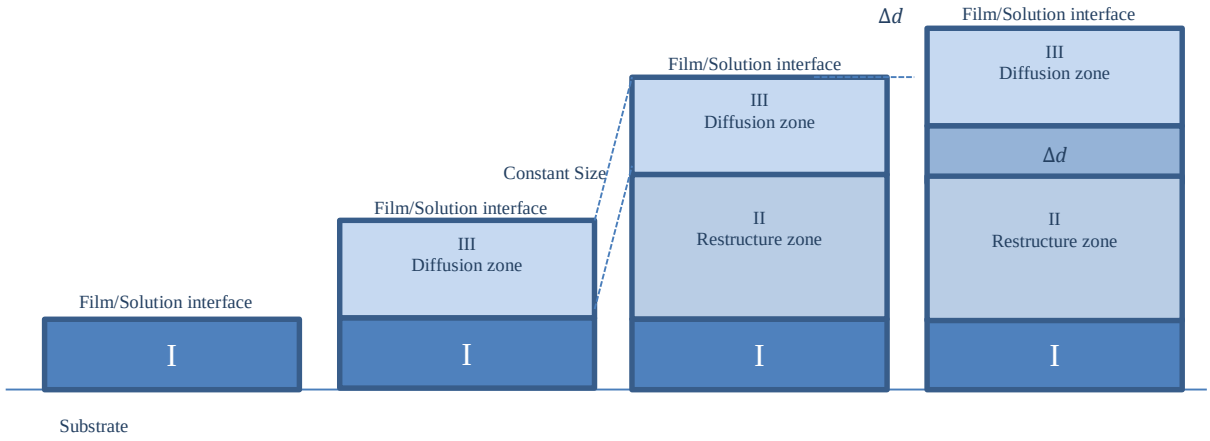

Figure 2.17. Displaying the primary, secondary and tertiary depositions during layer-by-layer assembly as described in previous theories (142).

2.6. Diffusion kinetics

For diffusion to take place, the polymer film needs to be in a state of hydration. Studies concluded that is feasible that there is not always an exact charge compensation between polyanions and polycations (209). The excess of these fixed charges is compensated by the counter ions present in the solution, which results in the Donnan potential. For example, in the (PLL/HA) system, the PLL and HA form complexes on the outer layer of the film, the PLL chains can also diffuse into the multilayer whereby the core of the film remains in thermodynamic equilibrium. The low electrochemical potential of the free PLL chains on the film drive the diffusion process. The emergence of the PLL chains from the solution is also favoured entropically through the diffusion of small cations which are present on the external area of the film resulting in electron-neutrality (143).

The charge overcompensation phenomena is thus introduced and this stimulates an electrostatic barrier. The rinsing step is crucial in these cases because there is a systematic elimination of the free polyelectrolyte chains, whereas the electrostatic barrier will contain the PLL chains within the system. A negative potential well is created upon introduction of the HA solution and once the PLL-HA complexes are formed the electrostatic barrier is also removed. For this reason, the exposure to the solution is also an important controlling parameter as a prolonged time will mean the filling of the negative wells is possible and this phenomena contributes to a structurally organised multilayer (144-145).

Charge distribution within a PEM multilayer is important because it can determine the cohesive properties of the film. The fraction of ionised groups can also be manipulated by tuning the pH of the external solutions. This can result in a change in the Donnan potential of the film, thus influencing the diffusion mechanism and permeation towards electroactive ions (146).

Hoda and Larson (147) explored the diffusion kinetics in relation to PEM film growth and film thickness. The theory concluded that the film thickness of a PEM multilayer is highly dependent on the time taken for both the deposition and rinsing steps. For this reason if the time taken for a polyelectrolyte to diffuse in and out of the whole film is greater than the deposition and rinsing time, the molecules will not have enough time to diffuse through the whole thickness of the film, this is expressed as:

$$Thickness = (Dt)^{1/2} \quad (4)$$

D=diffusion coefficient of the free polyelectrolyte in the film t= deposition (m^2) or rinsing time (s).

Research found (147) that polyanion/polycation pairs which resulted in a strong exothermic reaction resulted in the formation of linearly growing thin films in comparison to the weakly exothermic pairs which demonstrated exponential growth. In order for spontaneous complexations to occur the Gibbs free energy was negative. As a direct effect it seems that throughout these investigations the entropy increase in the system was the driving force for the association of the polyanion/polycation pairs. This was highly associated with the release of water and counter-ions from the polyelectrolyte chains. The counter ion release in polyelectrolytes not only demonstrates the attraction between positive and negative attraction but also demonstrates the importance of electrostatic interactions which allow the deposition of polyelectrolytes for film formation. Ultimately, increasing the entropy in a system is the driving force between the union of polyanions and polycations, the presence and release of water and counter-ions from the polyelectrolyte chains. Thus this process is more of an ion-exchange process rather than just an attraction of oppositely charged species, as a result the related that the film thickness and transition from linear to exponential growth was attributed to the interaction strength of the polyelectrolytes concerned.

2.7. PEM multilayer assembly

In previous investigations (147-149) it has been highly demonstrated that the substrate surface can influence the deposition of the polyelectrolytes on a surface. The interaction of the surface will conduct the initial growth of the PEM film. For this reason pre-treating the substrate with a PEM is common practice (148).

Composite multilayer materials are an active platform for the application of ultrasensitive sensors and optoelectronic devices. The modulation of nanocomposite

functionalities is an element which needs precise control for technical applications. Kiryukhin *et al*, 2011 (149-150) studied the peculiarities of polyelectrolyte multilayer assembly on patterned surfaces. The growth of PEM films on patterned templates with imprinted arrays of micro wells ranging from 2-25 μm and these were extensively studied.

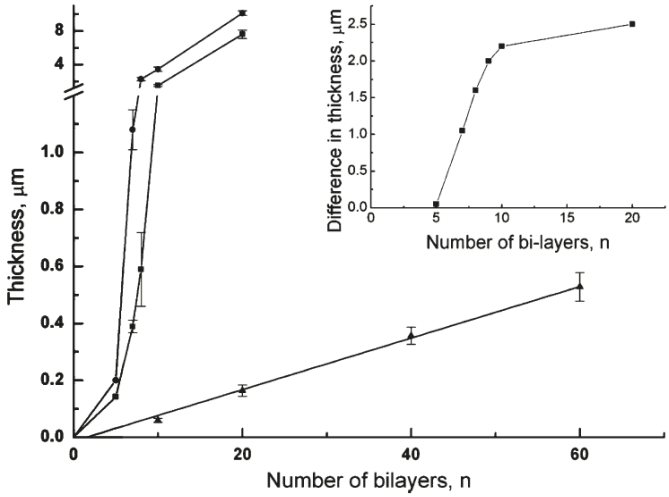

Figure 2.18. Evolution of PEM bilayers constructed at 2 M NaCl (sq) and 0.2 M NaCl (tri) (151)

PSS and PDADMAC were paired together to synthesise PEM thin films. The ionic strength considerably influenced the mechanical strength and structure of the PEM films. Master silicon moulds were essentially utilised in order to fabricate an array of micro wells on PMMA film. The layer-by-layer assembly was then carried out using an automatic dip-coating machine. The surface of the PMMA itself was negatively charged as confirmed by Johnson *et al.* (151), resulting in a uniform distribution of carboxylate groups on the surface. The sacrificial PMMA layer was used in order to fabricate a patterned layer-by-layer film; PMMA acted as a thermal plastic resist and has been used as an established surface patterning technique. This was ideal as in this

investigation the size, shape and arrangement of the micro wells had to be controlled (153-155).

The PMMA displayed an excellent level of pattern conformity with a guaranteed pattern yield. The template was actively dissolved in toluene and the PEM film transferred on a silicon wafer for characterisation. This has been an established method resulting in films of uniform thickness. The critical thickness was determined by the number of bilayers used to construct the film and as the number of bilayers increased the likelihood of three-dimensional microstructures collapsing on dissolution decreased. A greater ionic strength of the solution also resulted in a higher rate of diffusion of macromolecules inside the PEM film reflecting a linear growth regime. Studies concluded that the conformation of polyelectrolytes was influenced strongly by the ionic strength of the solution and the greater number of bilayers was key to achieving three-dimensional, mechanically stable structures which do not collapse (155).

2.8. Application domains of layer-by-layer films

The layer-by-layer technique offers a plethora of opportunities for the process to be implemented in practical applications (156-160). The structure of the material will ultimately define the function of the PEM films. There are five considerable domains in which layer-by-layer is progressively being implemented on a greater scale.

Biomaterial coatings: Protein adsorption has been the main focus of layer-by-layer investigations with the effect of cell behaviour (156). The PEM multilayer was initially

assumed to mimic an extracellular cell matrix thus giving way to favourable conditions for cell adhesion. The PSS-PAH complex also offered a rigid typical coating for endothelialisation. Biodegradable polyelectrolytes were also explored giving the opportunity of drugs or proteins to be delivered with a time-dependent release. Sukhorukov et al. (157) designed hollow target specific-polyelectrolyte capsules for drug delivery (158-160).

Electronic devices and energy conversion: The combination of semi-conductive nanoparticles and conductive polymers has an area for the development of light-emitting diodes with the incorporation of clay nanoparticles. More recently graphene-oxide has been incorporated for as it can enhance properties in electronic conductivity (161).

Biosensors: The stability of PEM multilayers through the hydrogen-bonded network can contribute towards a selective ion separation membrane. Proteins can be successfully embedded within the PEM films to maintain a native secondary structure in combination with thermal stability. In addition to this the incorporation of enzymes like catalase and glucose in enzyme-based diagnostic methods in biosensors are often preferred over others for their improved sensitivity, selectivity and active nature; this is illustrated by the widespread use of enzymes in the selectivity when considering the reactions at the membrane. However, the use of enzymes significantly limits the use of the biosensor, high cost and single use with limited stability are some of the factors. These have been partially overcome by the immobilization of enzymes on an insoluble support. The use of polyvinyl chloride (PVC) in ion-selective electrodes which act as a direct support for enzyme immobilization has milled a way for sensing applications (162-163).

2.9. Assembly of modulated surfaces

Investigations which attempt to mimic nature and the topography and structure of naturally occurring materials often begin on a planar surface. However, naturally occurring materials like bone and nacre do not exist on a naturally occurring modulated surface. When designing these modulated surfaces the long term aim was to begin a series of reactions which would instigate a site-specific release in a controlled manner. This functionality can have a huge impact in drug delivery and micro packaging fields. Polyelectrolytes are used in the formation of these chambers as they provide a versatile material within which the material may be manipulated and grown (164).

A number of methods were implemented in order to fabricate free standing polyelectrolyte films, some of which include direct patterning of pre-fabricated films by solvent-assisted room temperature imprinting, contact printing and lift-off techniques. In addition to this PEMs have been exploited on templates with modulated surface chemistry or topography (165-166). These methodologies often address the formation of two-dimensional structures on flat surfaces only. Fabrication of mechanically-stable patterned films with three-dimensional building blocks is still a challenge.

Nano imprint lithography has been a tried and tested method (167) which results in a high-throughput, low cost method to produce features on a surface at the nanometre level. The imprint process itself can be repeated multiple times when using a durable mould, in addition to this a uniform surface can be created over a large surface area which is highly beneficial during a sample preparation process.

The primary principle of imprint lithography involves two main steps, the first step involves imprinting a material, whereby a mould with nanostructures is applied on a surface in order to duplicate the mould pattern upon application of pressure and heat (above glass transition temperature) at which a thermoplastic becomes a viscous liquid, being able to flow and readily deform in to the shape of the mould in a controlled environment. Imprint lithography is a physical process and has potential to be applied for low-cost mass production of nanostructures in the future. This is a positive step towards the fabrication and implementation of nanostructures in industry and wide-scale applications.

Previous work has also been reported in the fabrication of patterned arrays of PDADMAC-PSS multilayers using a sacrificial PMMA template. PMMA generally displays excellent properties for imprint lithography; it has a small thermal expansion coefficient of ~5 x 10^{-5} per ^{o}C and a small pressure shrinkage coefficient of ~2.6 x 10^{-3} Pa. Similarly the sacrificial template was dissolved via a solvent in order to reveal the polyelectrolyte multi-layered structure. It was necessary to ensure a suitable post-treatment of the polyelectrolyte multilayer was established as the properties of the structure- like stiffness could be affected otherwise and this will be further explored below. Toluene is found to be the most stable solvent in removing the PMMA sacrificial layer in the processing technique (168).

The growth of the multilayer has also been attributed to the size and aspect ratio of the three-dimensional structures which have been imprinted on the templating surface and the conformation of the polyelectrolyte chains in the solutions is thus an influencing parameter on the growth regime of the multilayer.

Imprint technology was used in the design and fabrication on the surface of PMMA films for these multifunctional high performance synthetic micro chambers. PMMA is a typical thermal plastic resist and thermal imprinting on it is an established (169) surface patterning technique as it results in guaranteed pattern fidelity. Research groups have previous reported the formation of PEM films that have been thinner in consistency on the surface of the substrate than in confined geometrics, including those imprinted on polystyrene or pores of polyelectrolyte membranes (170). The thinner membranes were in these cases attributed to the inconsistent and uneven washing steps of the polyelectrolyte during surface treatment and adhesion. It was also established that the water content in the polyelectrolyte multilayer films built from sodium-chloride containing polyelectrolytes solutions were dependent highly on the temperature, humidity and ionic strength of the solution in relation to the number of bilayers (170).

It is essential to take into consideration that polyelectrolytes exist naturally as globular structures in 2 molar ionic strength. An additional parameter for consideration of polyelectrolyte adsorption on oppositely charged surfaces is the size of polymer coils in the solution. This is characterized by the coil end-to-end distance, which has previously been estimated using the scaling theory of flexible polyelectrolytes at high ionic strength, developed by Rubinstein et al. (171). When considering these individual polyelectrolytes, they can pass easily within the three-dimensional structure, reports indicate that the polyelectrolyte can evenly coat the interior of the micro-well, both inside and out. Reports indicated that a film thickness greater that 400 nm was necessary to prevent the collapse of these structures.

2.9.1. Materials Selection

Whether selecting materials on a macro, micro or nano-scale, material selection is very crucial. Researchers make use of various materials engineering charts which display the region in which naturally occurring materials gain a synergy between having a high density and a high Young's modulus (172). This is interesting as it can be compared to synthetic materials, it is visible from these charts (figure 2.19) that naturally occurring materials have a high performance ratio (this being the ratio between the material and dimensional constraints based on the free variable of a specific application e.g. high strength) resulting in desirable properties being selected for various applications.

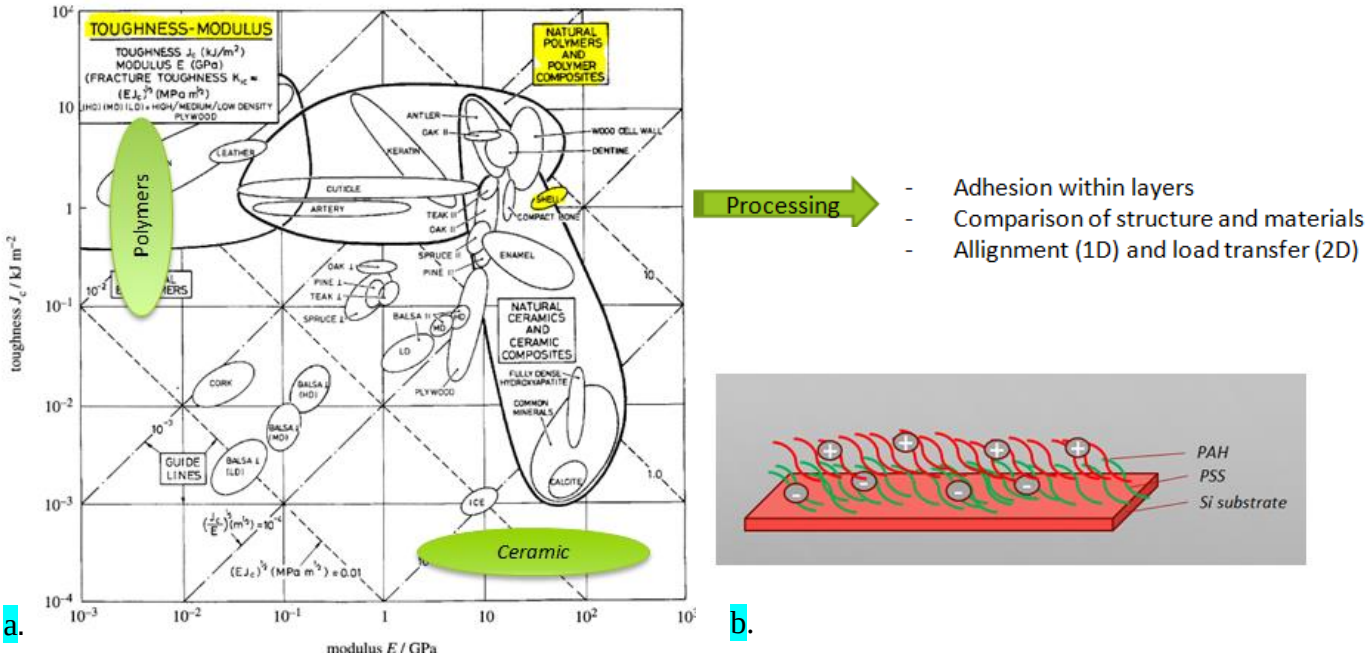

Figure 2.19 a. Modulus vs. Toughness for various groups of materials (172) b. Schematic of layer-by-layer concept and arrangement of polyanions and polycations.

The performance indices give a valid indication of the combinations of material properties which govern performance. From this selection, the most desirable materials can be chosen for specific high performance and high strength applications.

This is necessary at the nano scale and especially within the design of three-dimensional assemblies as the performance of the engineering component is limited by the properties of the material of which it is made and by the organization of the three-dimensional array. Performance indices are primarily governed by design objectives as displayed in figure 2.20, the Young's modulus and density of a material may be classified and when comparing this with figure 2.21 the design can be deduced down to the ideal materials for relative performance indicators via the processing of a mathematical combination of properties.

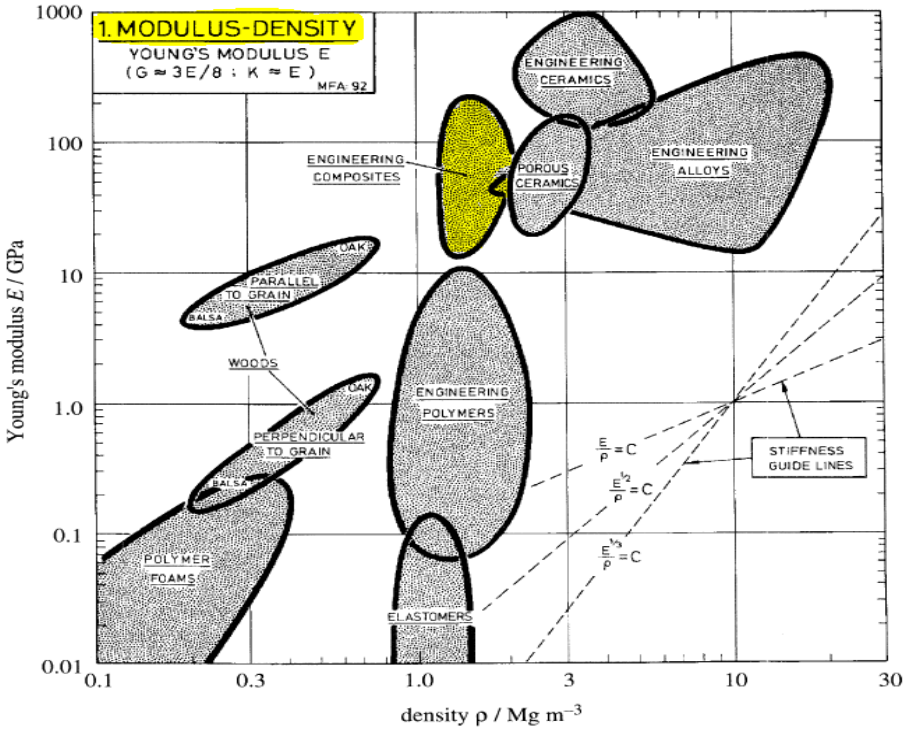

Figure 2.20 An example of a material property chart for engineering materials showing the Young's modulus plotted against density. Guidelines show the slopes of three performance indices (172).

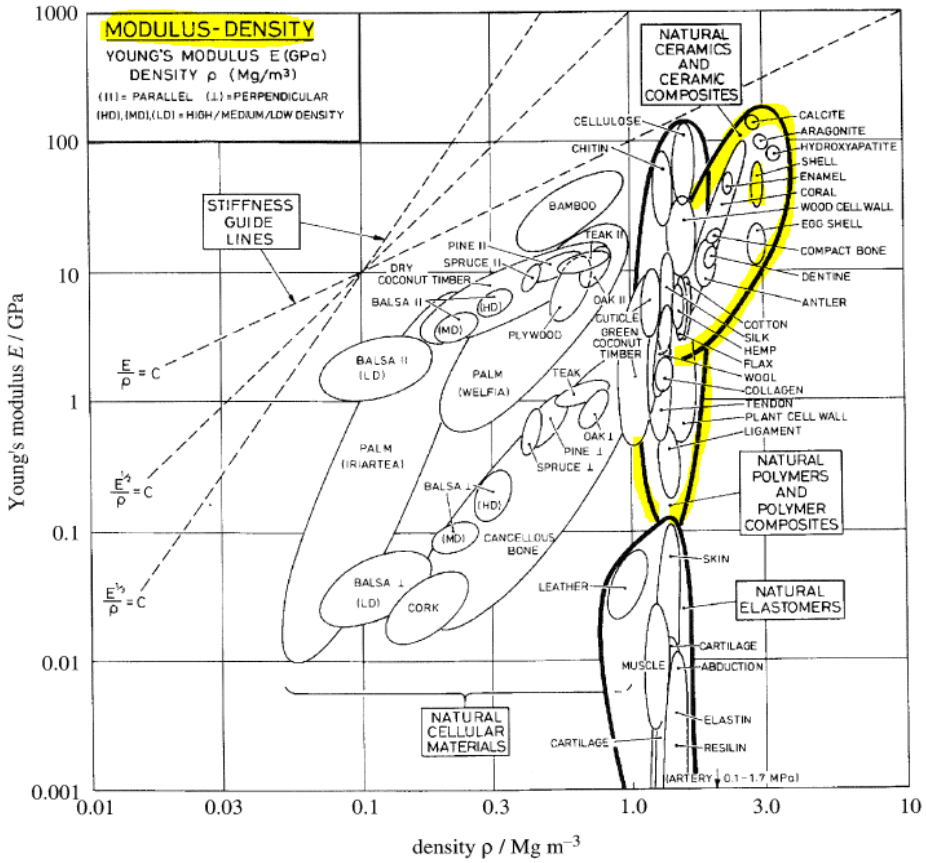

Figure 2.21 Material property chart for natural materials, plotting Young's modulus against density, guidelines identify structurally efficient materials which are light and stiff (172).

It is also necessary to combine the features of a material when devising the manufacturing method and then determining the feasibility of the design on a large scale system. The factors that may influence the development of the material on the large scale have been summarised in figure 2.22, ultimately identifying the importance of the relationship between the orientation of the structure at the nano scale and how this changes when comparing to large scale production.

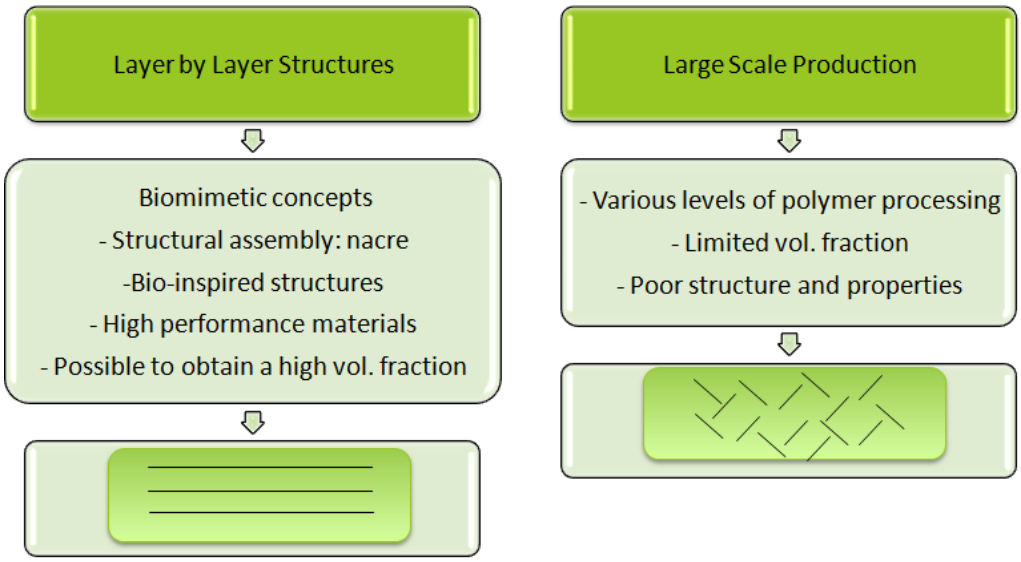

Figure 2.22. Flow chart comparing the differences between large scale production and nano scale.

Improving mechanical function and dynamics as a continuation of current research through incorporation of inorganic fillers within the wells of the three dimensional assemblies as illustrated in figure 2.23. The growth of the inorganic component will be monitored within the walls of the structures.

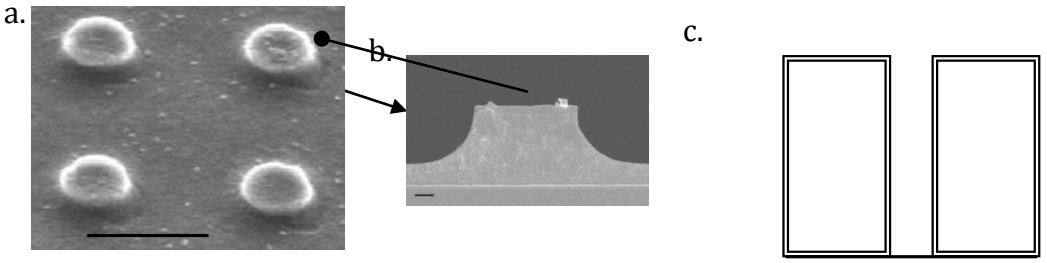

Figure 2.23. (a) And (b) SEM image of $(PDADMAC\text{-}PSS)_n$ films of patterns built at 2M NaCl for 10 bilayers (149) (c) Schematic of structure; displaying the walls where interaction can take place and the layer-by-layer assembly can be manipulated layer-by-layer; incorporate responsiveness and mechanics within the solutions in order to manipulate properties in area of interest.

Previous investigation on these three dimensional assemblies were limited to synthetic materials only. The three dimensional structures may be manipulated in a form to achieve biomimetic structures which are closer to those which occur in naturally occurring materials like nacre, bone and antler. Figure 2.23 illustrates the development

of the three-dimensional structure and gives a positive indication of the growth direction of the structure through layer-by-layer synthesis.

Fabrication and modulation of polyelectrolytes has been further explored on modulated surfaces using polyelectrolyte multilayers. It has been established that a highly ordered array of hollow chambers ranging from 2-25 microns in size (149) were fabricated using a layer-by layer assembly of PAH and PSS polyelectrolytes. The mechanical integrity of these chambers was monitored further to determine the stability conditions which ultimately depend on the chamber geometry. These mechanically stable polyelectrolyte chambers are robust and lead a way for potential alternatives on mechanically robust transport chambers (149). When considering the nanoimprinting process, the process, repeatability and mould durability is of utmost importance. Each time the same mould is used for a sample there is no noticeable change in the PMMA profile or change in the mould itself.

3. Motivation and aims

Decher's concept (174) was further propagated in order to produce ultrathin materials by precise control on the nanometre length scale over the thickness and resulting in thin film production. It still remains a challenge to achieve horizontal multilayer nanocomposites.

As part of synthesising the nanocomposites it is elementary to control the following parameters; the water content (PAH-PSS), multilayer films are built from NaCl containing polyelectrolyte solutions. Controlling the temperature, humidity, and ionic strength of solution, number of bilayers, *n* and the nature of the terminal layer are also a necessity in film formation. Synthesising nanocomposites in order to emulate biological strategies in synthetic materials through layer-by layer processing was the ultimate aim and at the same time trying to attain time-dependent mechanical functionality which is coherent in biological materials.

This investigation will use the layer-by-layer technique in order to synthesise high volume fraction composites which will compose of nanometre thin layers of alternately charged colloidal layers in order to produce an interfacial structure that mimics that displayed in nature. The gap in knowledge will be explored whereby the ability of layer-by-layer multilayers made of prototypical polyelectrolytes (PSS, PAH and PDADMAC) to nucleate and incorporate calcium carbonate, and compare the differences in the inorganic/ organic hybrids formed. In addition to this, biological polymer (HA and collagen) were also nucleated in the same process.

Organic and inorganic compounds can be incorporated within patterned surfaces in order to investigate the mechanics and responsiveness of the nanocomposite. This

investigation further explores this using a dipping-robot which will be utilised in order to fabricate multilayers on the given substrate and ultimately produce free standing structures which can be tested for mechanical performance. Nanoparticles will be used as fillers within the matrix to identify the variation in performance of the PEM multilayers.

Chemical infiltration of the organic layered polyelectrolyte's can be implemented whereby the layered composite can be infiltrated with an inorganic phase as a reinforcement which can potentially lead to static mechanical properties. In the long term it was necessary to think about the impact of research and various levels of polymer processing in order to obtain a uniform, organised structure from natural materials.

The investigation will make use of various analytical techniques; scanning electron microscopy, transmission electron microscopy, thermogravimetric analysis, x-ray diffraction and time-of-flight-secondary ion mass spectroscopy to determine the characteristics and behaviour of the newly synthesized material. In addition to this mechanical performance will be measured using Nano-indentation to determine the Young's modulus and hardness of the relative materials and these will be compared to the materials existing in the natural environment like nacre.

4. Materials, methods and instruments

4.1. Materials List

Below are a list of materials purchased for the synthesis of samples.

- Poly(sodium 4-styrenesulfonate), Mw ~75,000 Sigma Aldrich, UK
- Poly(allylamine hydrochloride), Mw ~58,000 Sigma Aldrich, UK
- Poly(diallyldimethylammonium chloride) wt. % in H_2O. Sigma Aldrich, UK
- Hyaluronic acid sodium salt, Streptococcus equi. Mw ~8,000-15,000, Sigma Aldrich, UK
- Collagen, Type I solution from rat tail, BioReagent, Sigma Aldrich, UK
- Poly(ethyleneimine) solution, Mw ~750,000 Sigma Aldrich, UK
- Calcium chloride, anhydrous Sigma Aldrich, UK
- Sodium carbonate, anhydrous Sigma Aldrich, UK
- Sodium citrate monobasic, anhydrous Sigma Aldrich, UK
- Citric acid, anhydrous Sigma Aldrich, UK
- Trisodium citrate dehydrate, anhydrous Sigma Aldrich, UK
- Glycerol, $\geq$ 99.5 % Sigma Aldrich, UK
- Acetic acid, reagent, $\geq$ 99.7 % Sigma Aldrich, UK
- Hydrochloric acid, concentrate 1 molar. Sigma Aldrich, UK
- Sulphuric acid, 99.99 % Sigma Aldrich, UK
- Hydrogen peroxide solution, 50 wt. % in H_2O Sigma Aldrich, UK
- Toluene, anhydrous, 99.8 % Sigma Aldrich, UK
- Mould- silicon micro well 2µm Kyodo, Japan

4.2. Polymer synthesis

For this investigation three different polyelectrolyte systems were investigated, two are well known synthetic polyelectrolytes and the third are a set of naturally occurring biological polyelectrolytes:

1. (PSS-PAH)
2. (PSS-PDADMAC)- Synthetic polymers
3. (HA-COLLAGEN)- Biopolymers

In addition to this an infiltration solution was also prepared, this consisted of calcium chloride and sodium carbonate. The solutions are prepared freshly on the day of sample synthesis and stored in a cool, dry place. All solutions are dispersed and fully dissolved within their solvent environment for precipitation to occur and for effective synthesis of the composite multilayer.

The polymers were prepared the same way for all sample preparation.

4.3. Biological polymers

4.3.1. *Preparation of the Hyaluronic Acid (HA) solution*

The HA solution was made to a concentration of 1 g/L + 0.15M NaCl by weighing 0.1 g of PSS granules and 0.876 g of NaCl granules. They were both added to a beaker and topped with 100 ml of Milli-Q water. The polymer solutions (figure 4.1) was stirred until the granules of the HA were fully dissolved in the water.

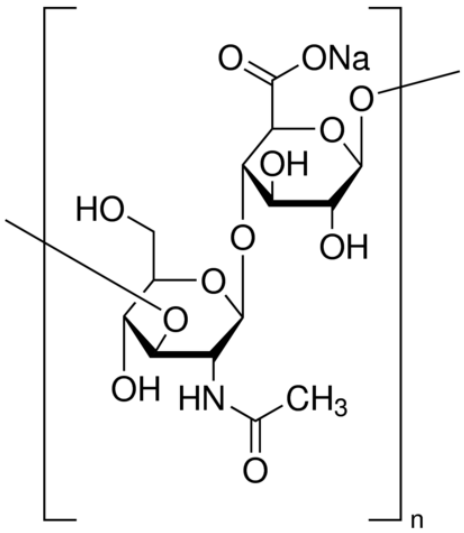

Figure 4.1. Schematic structure of Hyaluronic acid

4.3.2. Preparation of Collagen solution

Preparing the buffer: The sodium citric acid- sodium citrate buffer solution was prepared by adding 11.5 ml of 21.01 g/L of citric acid monohydrate (0.1 M) dissolved in 100 ml Milli Q water. This was then mixed with 88.5 ml of 29.4 g/L of trisodium citrate (0.1 M) which was also dissolved in 100ml Milli Q water. The solutions were stirred together and the pH was recorded at 6. The dialysis membrane was purchased with coated with glycerol for the improvement of its shelf life. This glycerol was washed off the outer surface with Milli Q water for 2-3 minutes. The inside of the membrane with water of the membrane was filled with water and the washing process was repeated for 3 times. The membrane with water was then soaked in water for 10 minutes.

The collagen solution was then prepared by pipetting 15 µm of 5 g/L of the type-I of collagen from rat's tail which holds a concentration of 0.048 g/L in 0.2 M of acetic acid. This acid that comes with the collagen has a pH of 3. The small amount is enough to build layers of collagen fibrils instead of crystals.

The 15 µm was dissolved in 8.6 ml of Milli-Q, stirred and stored in the prepared

dialysis membrane at 40 °C for 3 hours. Once the collagen was removed, water was added to it to increase the pH to pH 5.

Preparation of the natural films based on layer-by-layer deposition of collagen and hyaluronic acid which was carried out using the same method that was mentioned above using the dip coating machine.

4.4. Synthetic Polymers

4.4.1. Preparation of PAH, PSS and PDADMAC

The balance had been calibrated prior to measuring the weight of the sample. The ratio for 400 ml solution of PSS contains 0.8 g of PSS, 400 ml H_20 and 46.8 g NaCl. This give a total of 0.02 g/L and the NaCl is 2 M. The ratio for 400 ml solution PAH contains 0.8 g of PAH, 400 ml H_2O and 46.8 g NaCl. This gives a total of 2 g/L and the NaCl is 2 M. Another polymer to be used in the multilayer formation is PDADMAC. A 250 ml solution prepared in similar fashion using 2.4 ml PDADMAC, 29.5 g NaCl and 250 ml H_2O. This totals to 2 g/L PDADMAC with 2 M NaCl. All solutions were left to stir over night to allow the PAH/PSS to attain a better dispersion in the aqueous solution.

4.4.2. Preparation of PEI

The substrate is then fully dipped PEI to achieve a positive surface. The polymer is extremely viscous and requires extreme care when making the solution. PEI consists of 8 g/L in 100 ml, 400 ml of H_2O to gain 2 g/L. Add 0.43 g PEI with 50 ml H_20. Separately dissolve 0.84 ml HCl in H_2O. The pH is 2-3. 1M NaOH is added to increase the pH to 5. This is stirred simultaneously whilst adding the all the parts of the PEI solution and the pH is adjusted using a pH meter.

4.5. Infiltration solution

Preparation of Sodium- carbonate ($NaC0_3$) and Calcium- chloride ($CaCl_2$)

The solutions are made separately for each. 0.33 M concentration of $NaCO_3$ and $CaCl_2$ where used. The ratio for 250 ml solution of Na_2CO_3 and $CaCl_2$ contained 8.745 g and 9.155 g respectively. Both were left overnight to fully dissolve.

4.6. *Preparing the substrates for film growth*

Thin PMMA sheets and silicon wafer will be used as substrates. Before using the silicon wafer, the substrate is treated with piranha solution (sulphuric acid and hydrogen peroxide) at a ratio of 3:1 (150:50 ml). The silicon wafer should be left in piranha solution for an hour to remove any impurities that would contaminate the layer formation. After this period, the clean surface was then carefully removed using tweezers and rinsed using Milli Q water. Milli Q water was used throughout as opposed to distilled water due to its high purity. The formation of piranha solution is extremely dangerous due to the corrosive chemicals involved and the highly exothermic reaction with temperatures that can reach above 100 ^{o}C so extra care must be taken when handling the chemicals.

4.7. Methods

4.7.1. Casting PMMA substrate

Initial investigations involved synthesizing a PMMA substrate using a spin coating method. This was effective in producing a uniform film upon which the multilayer could then be established. The method below was used in order to do this:

1. Polymethylmethacralate (PMMA) ~ 20% was dissolved in Propylene glycol monomethyl ether acetate (PMA) (2 hours / 90 °C).
2. Substrates were treated with piranha solution (1 hour).
3. PMMA solution was cast on glass slides using a spin coater.
4. Sample was left in oven for 4 hours at 80 °C.
5. Multilayer synthesis was carried out using alternating positive and negative charges through dip coating in solutions.
6. The substrate was dipped into solution and immersed for 15 minutes.
7. The sample was dried for a further 10 minutes and the above repeated.
8. Once the number of bilayers have been established the sacrificial layer can be removed from the glass substrate by immersing slide in water for 24 hours and letting the film come up to the surface of the solution.
9. Films were then prepared for various characterization procedures.

The multilayer was built using a manual dipping process as illustrated in the schematic below.

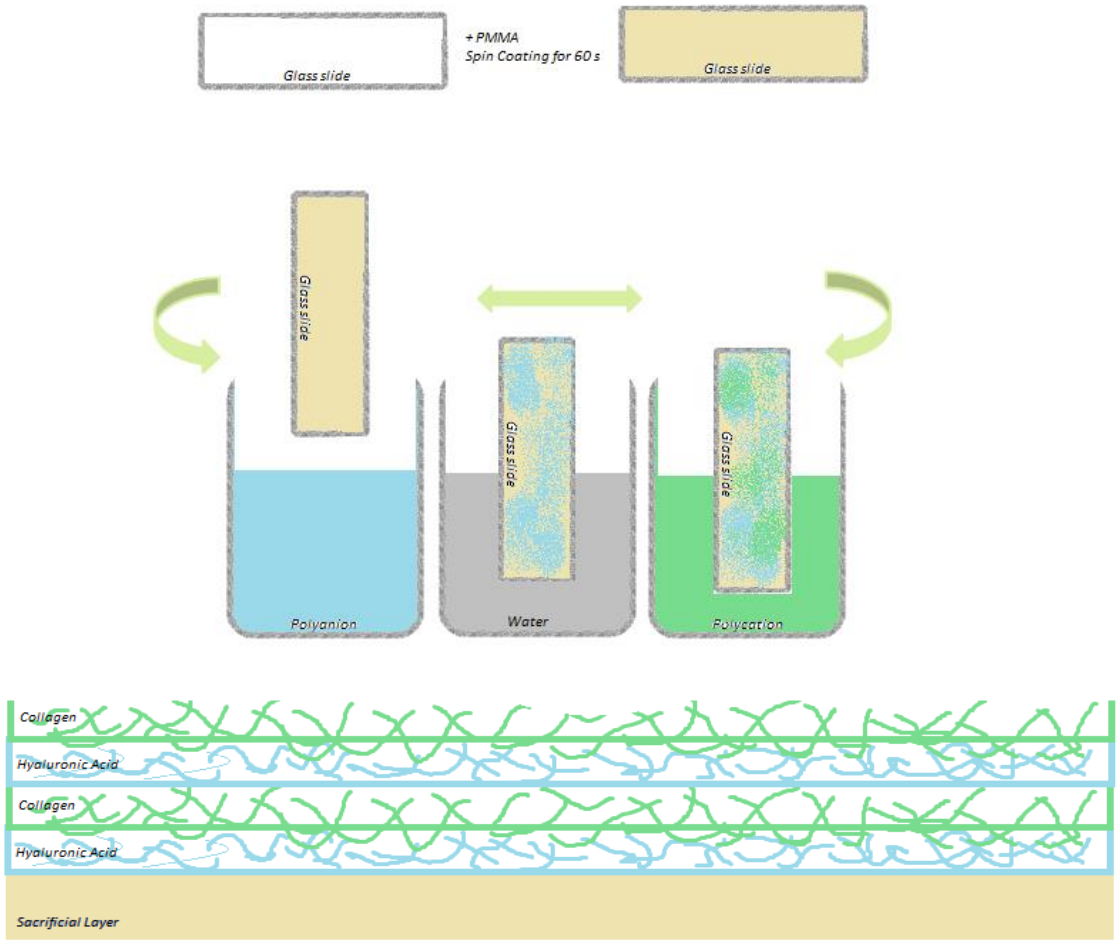

Figure 4.2. Schematic displaying the set-up used to prepare the PEM multilayer on a spin-coated PMMA substrate using a manual dip-coating method for initial experimentation.

4.7.2. Dip coating

The composite films were produced by a conventional dipping processes (figure 4.2) with the assistance of an automated dipping robot.

The following method has been implemented and formed the basic experimental technique in order to produce more complex designed multilayers with both synthetic and biological polymers in the following chapters. All samples synthesized were produced with the same processing technique, layout and deposition time parameters.

The system was set up, as displayed in figure 4.2, the numbers on the turntable correspond to the position at which the beaker is placed. It is crucial to get this element synchronized as it can determine the time and solution in which the substrate will be exposed to. The protocol began with dipping a positively charged substrate (using polymer (PMMA) to produce a sacrificial layer, the sacrificial layer was prepared treating a PMMA sacrificial substrate in PEI solution to charge the substrate surface) into a solution containing an anionic polyelectrolyte sodium poly (styrene sulfonate), (PSS) followed by a rinsing step. During the dipping process the PEM was rinsed in Milli Q water prior to being put into contact with the polymer solution, the reason for this is to desorb weakly adsorbed polymers from the surface of the PEM and to eliminate cross contamination of the polymer solution which has already made contact with the topmost layer of the polyelectrolyte, multilayer structure (175).

In order to cast each layer, an automated dipping robot was used for multilayer assembly. This results in the poly anion and poly cation being alternately adsorbed onto the substrate surface to build PMMA/ (a/b) n thin films, where a and b refer to the cationic and anionic polymer (figure 4.3). The substrate is then dipped into a solution of cationic solution. The electrostatic attraction between the polyions results in the surface charge being restored back to negative. Once the monolayer of anionic polyelectrolytes have formed, the intermediate rinsing steps use Milli Q water to remove excess polyelectrolytes after each deposition. The protocol for this experiment will contain 3 beakers of deionized Milli Q water.

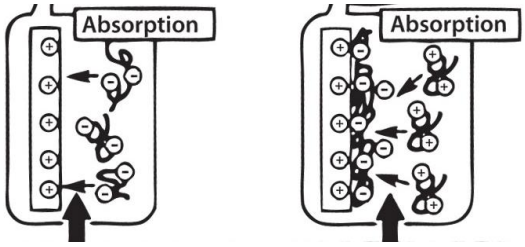

Figure 4.3. Schematic displaying the charge attraction on the multilayer, the charge is neutralised and then overcompensated which results in a charge reversal prior to deposition of the next layer.

The time and beaker position was programmed into a LabView program and this controlled the full functionality of the experimental procedure. It is an automated system and therefore the dipping speed was pre-programmed within the software. In addition to this, the exposure time and the co-ordinates for positioning the sample set according to the size of the substrate. The number of deposition cycles-bilayer (n) were also programmed. This can vary from one deposition cycle to infinite. The solutions were periodically refreshed after each 3 cycles, this will prevent any contamination of the solution (figure 4.4). The water-rinsing beakers were also refreshed for consistency and good practice.

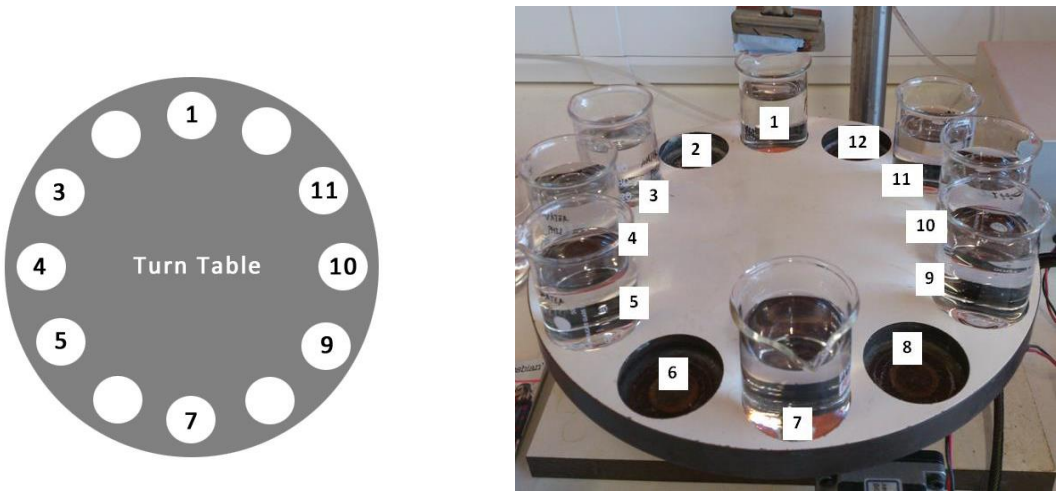

Figure 4.4. Schematics of the turntable design configuration, in addition to the set-up of the dip coating machine used for sample preparation (Queen Mary University of London).

For each experimental set-up, the same configuration was used, the table below identifies the solutions, corresponding position on the robot and deposition time. The variable in this system, was the number of deposition cycles, and this was determined by the desired thickness of the PEM multilayer, where n= 1, 10, 20, 40, 50 etc.

Table 2. Identifying the beaker position, beaker contents and deposition time for the experimental set-up used to synthesise the PEM multilayer.

Beaker No.	Beaker Contents	Deposition Time / mins
1	**Poly-anion**	15
3	H_2O -1	1
4	H_2O - 2	1
5	H_2O - 3	1
7	**Poly-cation**	15
9	H_2O -1	1
10	H_2O -2	1
11	H_2O -3	1

The molecular interaction of the polyanions and polycations are dependent on the ionic strength and pH of the solution and these are important factors to consider when using weakly charged polyelectrolytes. Electrostatic repulsion in the charged polyions causes the swelling of the polymer, which is undesirable (176). Once the polyelectrolyte deposition has taken place, there is effectively an additional layer from the last deposition, an example of a film after deposition can be seen in figure 4.5 below.

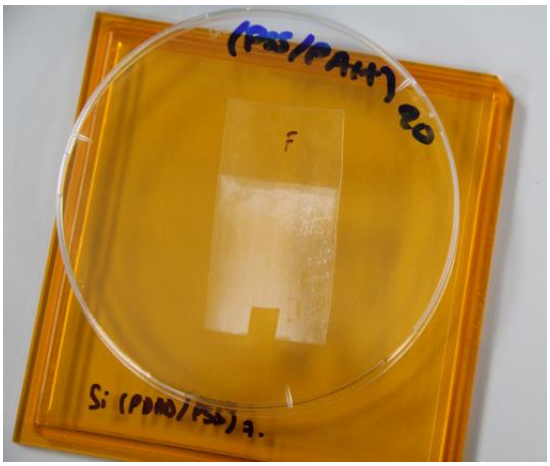

Figure 4.5. A photograph of the sample cast on to a PMMA substrate, and the resultant film.

It is clear from previous investigations that multilayer thickness increases linearly with the number of pairs of polyanion/polycation layers. Large film thicknesses are possible as the polyelectrolyte adsorbs at each layer therefore monitoring the number of layers at each stage and comparing results is elementary.

4.8. Fabrication of three dimensional assembly of PEM on PMMA substrate

A master silicon mould of periodic features of 2 μm width and 2 μm height respectively was used in the fabrication of the micro well design. The pattern mould was purchased from Kyodo (Japan) and traditional lithography and etching processes were used to design these moulds. The fabrication of the micro wells took place at the A Star Institute of Material Science and Engineering in Singapore.

Prior to application, all moulds were cleaned in standard piranha solution (3:1 mixture of 96 % sulphuric acid and 30 % hydrogen-peroxide) at 120 °C for 30 minutes. This was then rinsed thoroughly and with deionized water and dried with a stream of

nitrogen air to remove any impurities on the substrate. The PMMA film which had a thickness of 0.05 mm. This was cut into uniform rectangular 70 x 40 mm pieces and blown with a jet of nitrogen to remove any macroscopic dust particles. The substrate was then placed in a laboratory-standard oven at 100 °C for 1 hour for maximum cleansing.

The next step was to prepare the PMMA substrate for imprinting this was done by cutting out the PMMA sheets into rectangular shapes, slightly larger than the mould size and placing in between the mould and the atomically flat silicon wafer.

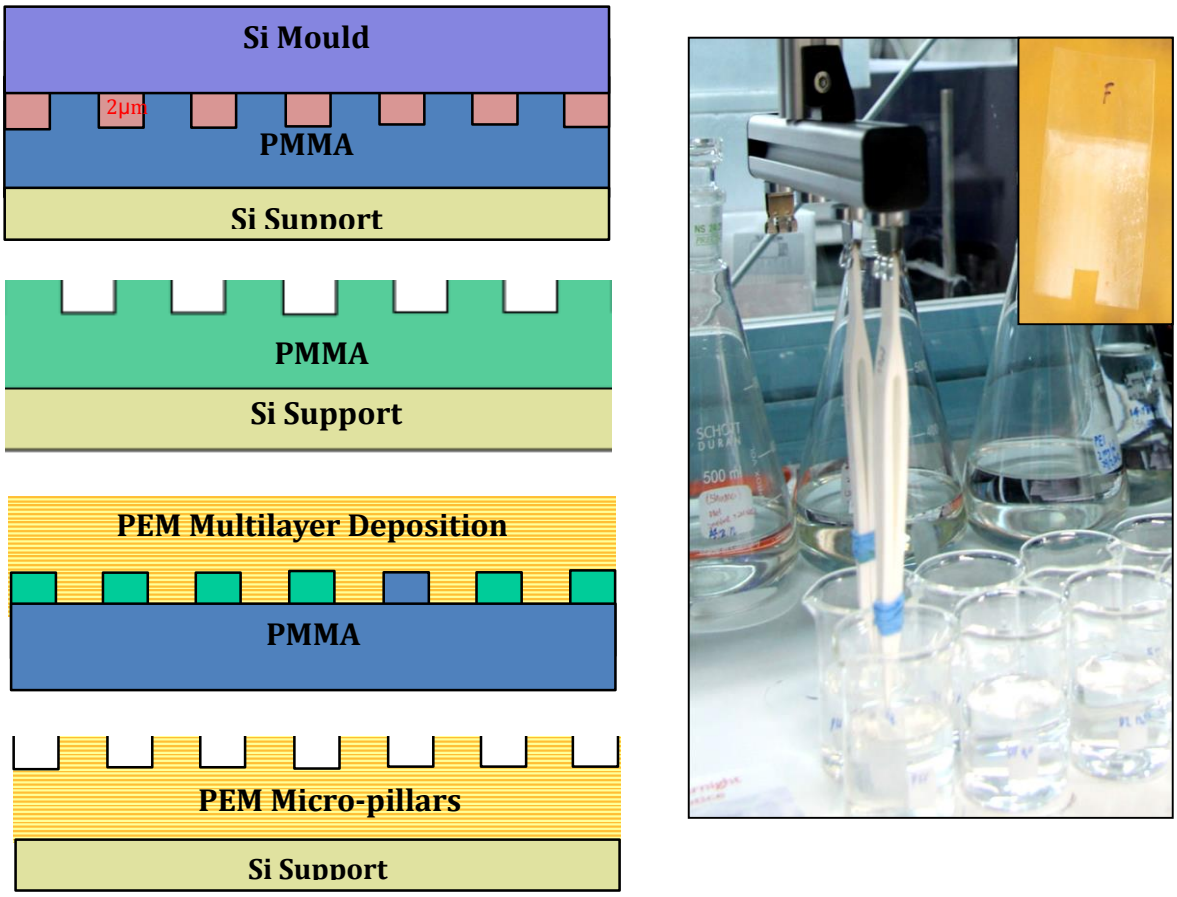

Figure 4.6. Schematic displaying the sandwich structure architected for nanoimprinting micro wells on a silicon substrate. Right: The dip coating robot and arrangement of solutions for automated layer-by-layer processing.

Upon doing this the micro imprinting process, as illustrated in figure 4.6 above was performed with an Obducat imprinter, using a temperature of 140 °C and a pressure of 4 MPa for a period of 5 minutes. This was then followed by releasing the pressure from the mould and a period of cooling at 80 °C.

This produced a negative replica of the pattern on the surface of the sandwiched PMMA- ultimately resulting in an array of micro wells.

4.9. Layer-by-layer assembly of PEM's on a patterned substrate

To avoid any air trapped inside of the wells, the PMMA was sonicated in a water bath for 5 minutes. The PMMA surface is negatively charged due to the presence of uniformly distributed ester groups. The PMMA was therefore first pre-coated with branched PEI hydrochloride solution of 2 g/L, whose pH was adjusted to pH 5 using 1 M HCl. This prepared the initial anchor layer with a high density of positive charges on the surface of PMMA. The PMMA was incubated in the PEI hydrochloride solution for 15 minutes and then rinsed three times for 1 minute in Milli-Q water to wash away any unadsorbed macromolecules from the surface.

Depending on the PEM composite being produced the below PE's were used for the dip-coating process:

1. PSS/PAH and
2. PDADMAC/PSS

Polymer concentration was 2 g/L, pH 5.5 using sodium-chloride solutions.

A commercial robotic dip-coating machine (Riegler & Kirstein GmbH, Germany) and a customized lab-developed version (Queen Mary University of London, H.G Gupta group) with similar functionality were used to create PEMs on the PMMA substrate. Once the PMMA is carefully secured in the dip coating machine the polyelectrolyte solutions were also put in alternating order. A standard procedure was used (20),

consisting of dip-coating the PMMA substrate with alternating layers of both PSS and PAH/PDADMAC from 2 g/L polymer solutions at pH 5.5 with a 2 M ionic strength adjusted by NaCl, resulting in formation of a PEM on a PMMA substrate. The polymer solutions were adsorbed onto the surface for 15 minutes at a time, and after each adsorption step a series of three 1 minute washing steps with Milli Q water was applied in order to remove any non-adsorbed macromolecules from the surface. Each cycle of adsorption and rinsing would contribute a single PE layer to the PEM formation. Finally, the polymer multilayer was formed on the sacrificial PMMA template, the terminal layer was always PSS.

4.10. Chemical infiltration

Chemical infiltration is the process of allowing ions to penetrate an area in order to interact with an inorganic phase of an otherwise organic field. In the dipping process, this is conducted by fully immersing the substrate into a salt solution whereby negatively charged ions infiltrate the area by attraction to the positively charged segments of the polycation. The film can then be immersed into a secondary solution which will in turn react with the first deposition layer, leading to the deposition of an inorganic material.

Chemical infiltration is conducted using the same method, but with different solutions, this is identified in the table below. Once again the sodium carbonate and calcium chloride are positioned in between the water-washing steps, the only variable here is the number of cycles for infiltration and this is determined by the desired nature of the sample.

The infiltration solutions, in this case are calcium chloride and sodium carbonate, the resultant deposition is calcium carbonate, this is the primary component of naturally occurring nacre.

Table 3. Identifying the beaker position, beaker contents and deposition time for the experimental set-up used to synthesise the PEM multilayer.

Beaker No.	Beaker Contents	Deposition Time / min
1	**Na_2CO_3**	15
3	H_2O -1	1
4	H_2O - 2	1
5	H_2O - 3	1
7	**$CaCl_2$**	15
9	H_2O -1	1
10	H_2O -2	1
11	H_2O -3	1

The content and growth of this nacre will be investigated further chapters.

Upon formation of the multilayer on the sacrificial PMMA, the multilayer is kept hydrated in deionized water upon the final stage of washing.

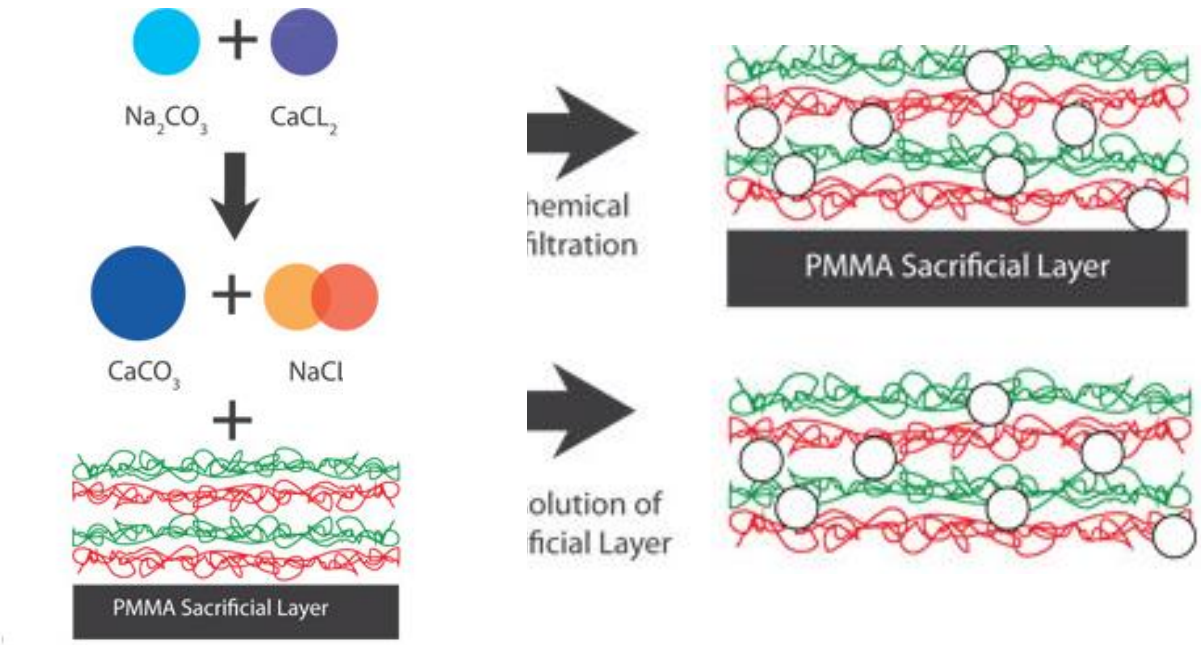

Figure 4.7. Illustration of the infiltration process using $CaCO_3$ inorganic particles.

Calcium chloride ($CaCl_2$) and sodium carbonate (Na_2CO_3) solutions at 1M concentration are prepared separately using DI water. The automated dip coater was again utilised to dip the formed PEM composite into the calcium chloride and sodium carbonate solutions alternately (figure 4.7); between each dip into either $CaCl_2$ or Na_2CO_3 solution, a washing step where the PEM was dipped into Milli-Q-water was used, and this prevented cross contamination of ions.

Removal of the sacrificial template

Once the PEM multilayer was constructed, the sacrificial PMMA substrate was removed, and the PEM multilayer transferred onto a silicon wafer, as follows.

A silicon wafer was washed with piranha solution (2:1 mixture of 96 % sulphuric acid and 30 % hydrogen peroxide) at 140 °C for 30 minutes. The wafer was then rinsed with deionized water, dried with a stream of nitrogen and heated in an oven at 100 °C for 1 hour. Eight alternating layers of PSS and PDADMAC are then formulated on the

silicon wafer using the robotic dip-coating apparatus as described above. Once the polyelectrolyte multilayer has been established on the PMMA substrate it can then be transferred onto PDADMAC/PSS, coated silicon pre-wetted with a droplet of water. As part of the nanoimprinting technique, sealing the multilayer on the wafer was performed at 24 °C for 1 hour under a pressure of 10 bar.

The entire multilayer was then placed in a bath of toluene for 1 hour to dissolve the PMMA. The wafers were removed from the solvent with the PEM present on the surface. Two types of polyelectrolyte multilayer composites were produced via the automated layer-by-layer dip coating process; $(PDADMAC/PSS)_n$ and $(PAH/PSS)_n$. The number of bilayers (n) in polyelectrolyte multilayer composites produced via the automated layer-by-layer dip coating process was varied, and included 8, 14, 20, 40 and 60 bilayers for (PDADMAC/PSS)n and 20, 40 and 60 bilayers for (PAH/PSS)n. The effect of altering the number of infiltration cycles in the inorganic precursors (Na_2CO_3 and $CaCl_2$) was also monitored (1, 20, 40 and 60) while keeping the number of polyelectrolyte bilayers constant (177).

4.11. Instruments for characterisation

4.11.1. Microscopic optical imaging

Measuring the size and scale of the films produced using the layer-by-layer method is necessary. Optical spectroscopy has been used as a classic method for probing the thickness of polyelectrolyte multilayers. Ideally the layers should be developed on a glass substrate with a moiety which absorbs light at the desired wavelength of interest.

The optical absorption hence gives estimation as to the deposition of the materials on the surface of the substrate as depicted in figure 4.8.

Optical microscopy can be used to analyse a sample surface. This is beneficial as it can give a good idea about the sample geometry and characterisation. Optical microscopes function by magnifying the original specimen by large factors.

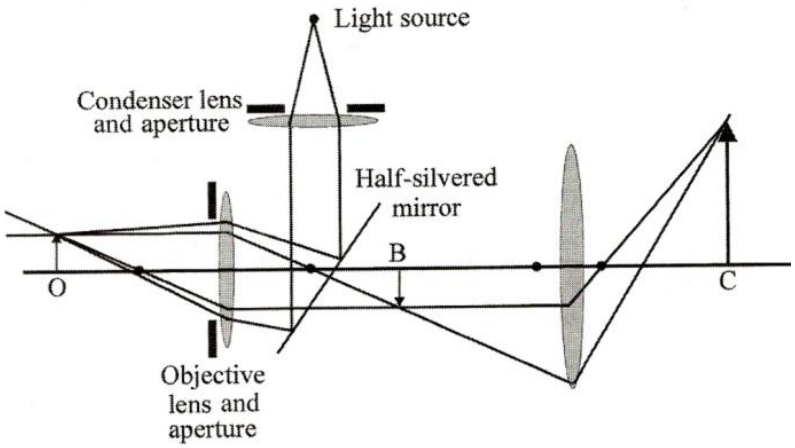

Figure 4.8. Schematic of microscopic lens set up (178)

Images are formed by the combination of picture elements whereby each pixel is coded for a separate brightness level and hence converted into digital form for analysis. For this reason, parameters including resolution, magnification, and depth of field are very important in electron microscopy as they can determine the final resolution of the image and these are controlled according to each specimen.

The simple optical microscope has evolved since the 17th century when a simple convex lens was used; focal length and magnification are the key considerations for the optical microscope. A multiple lens system is used to reach higher levels of magnification through a multiple stage process. The objective lens primarily allows for the production of an inverted image at a set magnification, it also controls the angular spread of the light on the surface. Subsequently the projector lens is combined

to produce a greater magnified, upright image of the specimen. A light source is also applied to the specimen surface to illuminate it; an opaque object is illuminated from the front to obtain a better quality image and at the same time improving contrast levels. The optical microscope only allows a limited set of fixed magnifications, the magnification can be changed by the addition of a different lens which has a separate focal length, and the magnification is then manipulated by the movement of various components of the microscope to define the image. The resolution of the optical microscope is the point between two separate entities. The resolution is often affected by diffraction as the light passes through a series of channels via an aperture, this may be overcome by the use of an ultraviolet beam (178-179).

To produce sharp, high quality images it is preferential for the specimen to lay flat, however in some cases this is not possible, therefore resulting in a change in depth of field where the sample is not in a relevant plane causing the production of an image which is out of focus. The objective aperture controls the convergence angle; by decreasing the depth of field this can be improved. The wavelength of microscopy in an optical microscope is much lower than that of an electron microscope which shall be explored further; it is also much more difficult to scatter light on a sample which is not uniform. Fortunately a light microscope has the ability to correct chromatic and achromatic aberrations by the association and combination of different lenses. It is important to avoid the formation of aberrations as it can result in an image with bad resolution.

Ellipsometry is an alternative method which uses polarized light in order to probe the dielectric properties of a thin film which can effectively determine the film thickness, refractive index, molecular orientation and surface roughness. A change in

polarization will ultimately allow the measurement of layers thinner than the wavelength of light, ultimately allowing the analysis of atomic layer formation (180).

4.12. Scanning Electron Microscopy

A beam of electrons is passed onto the surface of the specimen; the scanning electron microscope is most effectively used in the analysis of surface morphology of bulk specimens. The electron beam is generated via an electron gun formed of a tungsten filament, field emission guns are also commonly used in the beaming of electrons (190).

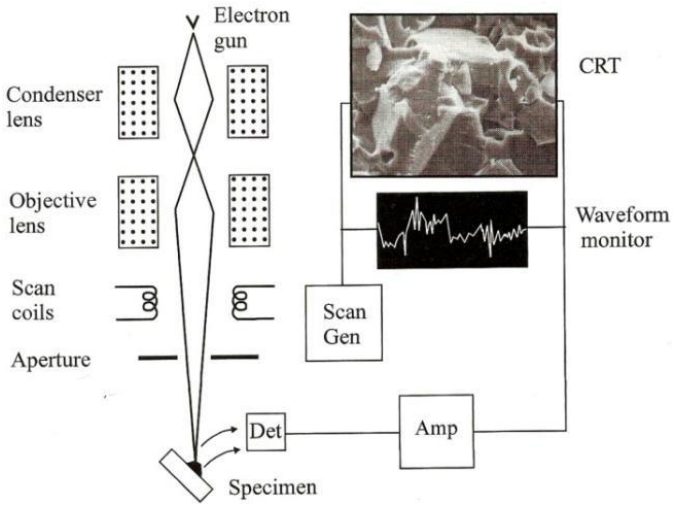

Figure 4.9. Schematic of scanning electron microscope lens set up in relation to image construction and specimen interaction (178).

The electrons are excited to a high energy level (1 keV-30 keV) whereby the beam is then reduced (with a diameter of 2-10 mm) as depicted in figure 4.9. The detecting component then counts the number of secondary electrons which are given off at each ordinate of the sample surface. In conjunction with the electron beam, the cathode ray

tube produces signals which are displayed on a projection screen, these raster images increase in clarity as the scans are continuously passing along the sample. Radiation caused by the interaction of incident electrons and the specimen can lead to emission from the sample surface, this results in a modulated signal change which allows for contrast of the image (180-182).

Secondary electrons and backscattered electrons are produced within the SEM (figure 4.10) and penetrate the specimen. This results in loss of energy, only radiation produced from the specimen volume is detected. Due to this X- rays are not easily absorbed and hence escape easily from the specimen. Once the electrons penetrate more than 1 μm they are no longer able to backscatter again. Backscattered electrons have a broad energy spread and electrons with the highest energy scatter fewer times, these primarily occur at near the incident beam and result in high spatial resolution and crystallographic information of the sample.

The most common signal used in the SEM involves the detection of secondary electrons they are detected by the scintillator-photomultiplier component more commonly referred to as the Everhart-Thornely detector.

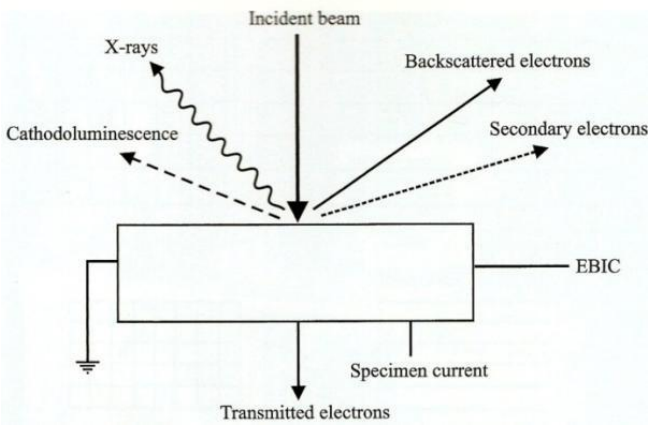

Figure 4.10. Schematic displaying the incident beam and the interaction range of electrons on the sample specimen (178)

As the secondary electrons collide with the scintillator, light is emitted and transformed into photons which in turn are converted into an electron pulse. The performance of the SEM depends on several factors including; Pixel formation, resolution, probe size and beam current. The pixel size in particular is important as it enhances the quality of the image, within a digital SEM the images are recorded onto a computer. Each spot is located by a pixel on the image. If the electron probe is greater than the pixel size then the signals become merged therefore control is required with regards to the specimen.

As electrons are significantly scattered along the surface of the specimen within a gas chamber, this allows for a better quality image to be produced. Other functions of the SEM include chemical analysis of the sample using X-rays and low energy electrons. The SEM primarily focuses on topographic characterization by the use of secondary and backscattered electrons.

When preparing a sample for analysis in the SEM it is necessary for it to be conductive, this allows for detection by the electron beam and as the high energy electron beam is bombarded on the specimen this is necessary to avoid charging effects from taking

place. If the specimen being analysed is of a metallic nature is it vital for it to be mounted onto a conducting specimen platform for it to be earthed within the chamber. Semi- or non- conducting specimens including biological specimens, polymers and ceramics need to be gold coated (~10 nm) using a sputtering technique. Porous structures need to also be coated effectively in order to ensure a positive surface conductivity of the sample.

SEM samples were prepared adequately prior to sample analysis, the sample was air dried prior to mounting on a sample stub. The samples were individually secured onto the sample holder using conductive carbon tape to provide an improved conductive path for electrons. The samples were gold coated prior to analysis in the SEM.
Scanning electron microscopy was used to obtain topographical images of the surface and cross sections of the composites. Secondary electron imaging at 5 keV using a JEOL JSM 5600 was used to image the PEM samples along their planar axis. A higher resolution FE SEM JSM-6700F was used to image the PEM samples transverse to their planar axis, in order to analyse the internal cross-section of the PEM.

4.13. Transmission electron microscope

Ernst Ruska obtained the Nobel Prize in Physics, 1986 in relation to the development of his work on microscopy and the transmission electron microscope (TEM). The TEM operates on the same basic principles as the light microscope; light is limited by wavelength and so using electrons instead allows the TEM to analyse at lower wavelength regions thus resulting in a high resolution image which is not possible to achieve with a regular light microscope (183)

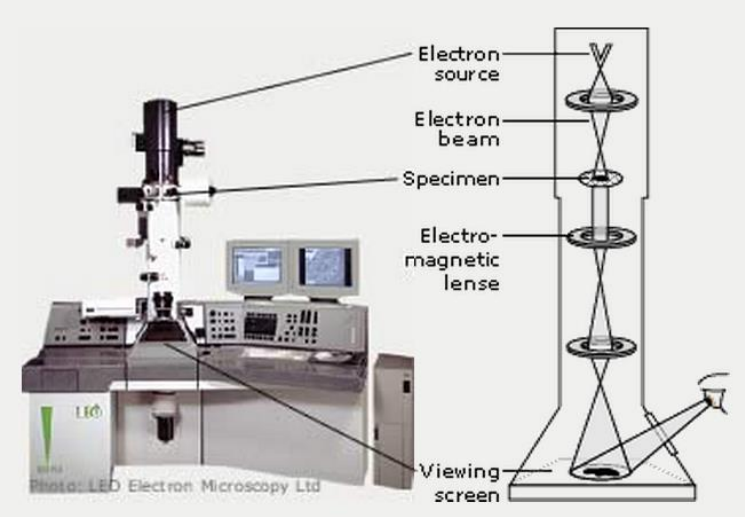

Figure 4.11. Schematic displaying the interaction of the electron beam and sample specimen in relation to viewing the image on microscope (64).

The electron source emits electrons which travel through a vacuum filled column as depicted in the schematic in figure 4.11; of the microscope. Electromagnetic lenses are used to focus a thin electron beam. The beam travels directly through the specimen and once they reach the sample surface the density of the sample will scatter the beam of electrons (184). The un-scattered electrons which remain part of the beam reach a fluorescent screen resulting in a 'shadow image'. Using this shadow image it is possible to navigate around the sample and this gives an indication to the variation of density around the sample.

4.14. Atomic force microscopy

Atomic force microscopy (AFM) can show a significant amount of information about surface features with unprecedented clarity. It is versatile as it can analyse samples in both a dry and liquid environment at the atomic scale. For this reason the samples do not necessarily need to be hydrated or coated with additional conductive layers. However depending on the nature of the sample resolution may be enhanced with sample hydration (185).

AFM can directly be used to identify surface topography of ‘rough’ samples in order to determine the characteristic features of the landscape.

In comparison to scanning-electron microscopy, AFM provides an excellent level of topographic contrast with direct measurements of surface features and quantitative height information and statistics. The three-dimensional image construction using the AFM is also economically viable in terms of sample preparation and is often a desired analytical technique when characterising the films surface as it gives an informative characterisation of the sample.

The AFM is composed of a tip which is mounted on the end of a cantilever. This construction is bought into close proximity of the sample and results in a raster image formation through interaction with the sample surface.

The tip has to also be chosen in relation to the sample characteristics, a sharp tip can yields a more detailed image and can be used at the atomic scale. The radius of curvature and aspect ratio are essential parameters which are influenced by the AFM tip.

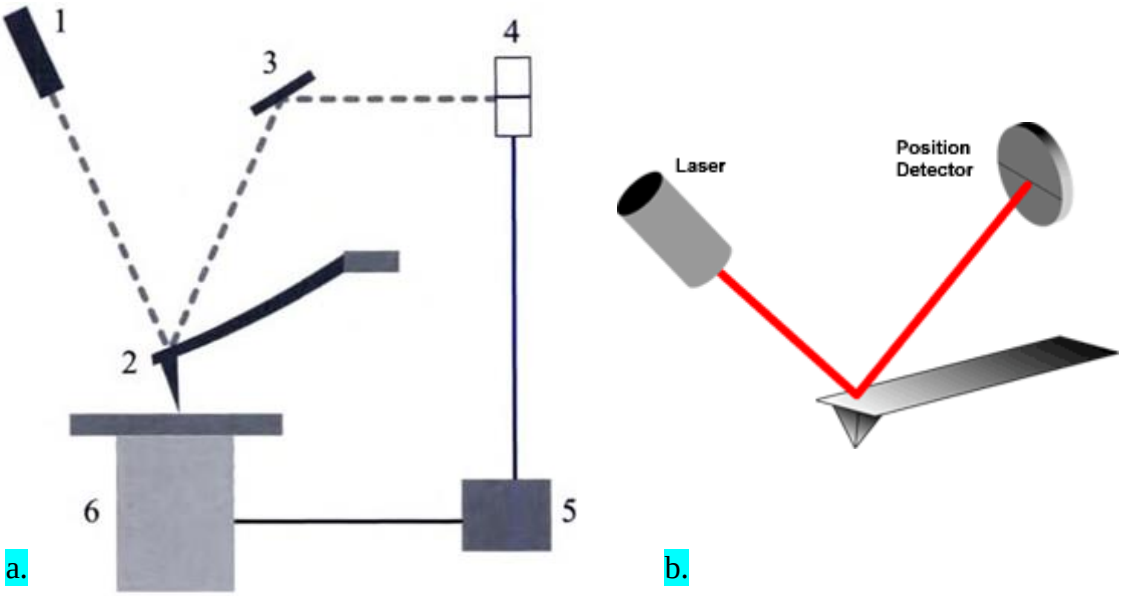

Figure 4.12. a. Schematic diagram of an atomic force microscope set up. 1. Laser diode 2. Cantilever 3. Mirror 4. Position sensitive photodetector 5. Electronics and 6. Scanner with sample (185) b. Beam deflection system using a laser and position detector which is implemented in order to obtain feedback (185).

The AFM relies on the forces between the tip and the sample as seen in figure 4.12 (185). The force is calculated according to the deflection the cantilever experiences during imaging. The stiffness of the cantilever can be identified and Hook's law can identify the relationship between deflection and stiffness of the lever. The modification of the AFM has allowed various parameters to be controlled depending on the nature of the sample.

Contact mode AFM is used expansively whereby the tip is deflected and adjusted in order to maintain a constant interaction with the sample surface. This is ideal for high speed and atomic resolution scanning.

In comparison; non-contact mode AFM makes use of an oscillating cantilever, the forces between the tip and sample surface are low and on the order of pN (10^{-12} N). The resonance frequency and amplitude of the cantilever can be manipulated in order to obtain an image.

4.15. Thermogravimetric analysis

Thermo gravimetric Analysis (TGA) is a destructive technique involving the thermal degradation of a sample. A precise balance within the furnace chamber weighs the sample at short intervals with changing temperature and the results are depicted as a graph. The sample can be tested in a controlled environment either as a function of temperature or time. The furnace is usually purged with an inert gas (nitrogen or helium) to help maintain the controlled environment. A typical graph is illustrated in figure 4.13 below.

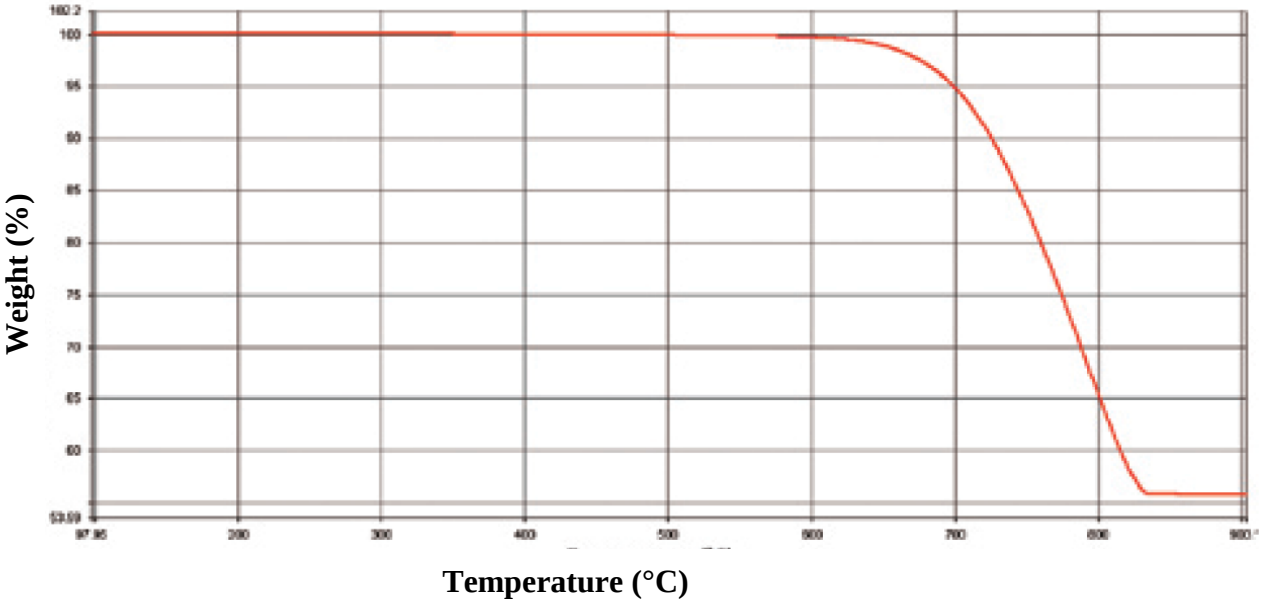

Figure 4.13. Depicts the thermal degradation of $CaCO_3$. The weight loss begins to occur at approximately 600 °C and finishes at 825 °C.

The peaks produced are compared to literature to distinguish what they are. TGA not only tells us what is present but it also shows intensity of each component within the sample. This technique is ideal for compounds such as $CaCO_3$ because the weight lost in the sample will be a result of its degradation into CaO and CO_2. The weight left

minus the total weight of the sample will equate to how much organic component and inorganic component ($CaCO_3$) is present.

The objective of TGA is to obtain results that reveal high density of $CaCO_3$ to prove that it has penetrated more than just the surface.

Figure 4.14. Displaying the wire coil prepared to support the TGA sample whilst testing.

One major benefit for the TGA is its versatility in the parameters to test with. The protocol is quite simple with most of the setting computerised. The gas and air must both be set to 20 Pa. The next step involves cleaning the sample pan with nitric acid. The sample should be placed on the mount, an example is demonstrated in figure 4.14 above, followed by tearing the balance. One cycle takes approximately 90 minutes to complete.

Table 4. Displays the settings programmed for the film analysis

Parameter	Setting
Sample size	10 mg
Sample pan	Platinum
Temperature range	10 °C to 900 °C
Scanning rate	10 °C per minute
Purge gas	Nitrogen
Purge gas rate	20 ml / min

The weight percentage of the inorganic phase formed inside the PEM was determined by thermogravimetric analysis (TGA; Perkin Elmer). TGA sample were deposited on PMMA substrates and peeled off from the substrates to avoid dissolution of the glass or PMMA substrate as well as contamination from the dissolved substrate the sample was then put onto the TGA sample pan. The original component, PSS/PDADMAC polyelectrolytes film and pure calcium carbonate, were analysed to use as a reference.

TGA was carried out by weighing 2mg of the PEM film and placing in a platinum pan, followed by heating to 900 °C at a scanning rate of 10 °C / minute. Prior to doing this, the sample was mounted on a wire coil, for ease of use in handling and transferring into the machine. The sample was purged with nitrogen gas at 29 ml / minute. The percentage of calcium carbonate was calculated from the loss of mass of completely dried samples assuming the remains at 900 °C are attributed to calcium oxide left after

elimination of organic component and thermal decomposition of calcium carbonate (186).

4.16. Time-of-flight secondary ion mass spectrometry

Elemental characterisation was conducted using Time-of-flight Secondary Ion Mass Spectrometry (TOF-SIMS) (ION-TOF GmbH, Germany). The analysis beam was 25 keV Bi+ with 1 pA average current scanned over a 200 μm × 200 μm area. Positive secondary ions were detected for the PEM multilayers infiltrated with $CaCO_3$, since Ca has a high yield of positive ions. The second beam of 1 keV Ar+ with 12 nA current scanned over a 200 μm x 200 μm area was used to etch the multilayer film and get cross-sectional elemental profile of the samples. In the spectra, peaks of relevant ions (S^+, Ca^+) were identified and their integrated intensities of the ions present in each sample were used for subsequent analysis (187).

Secondary ion mass spectrometry has been used to successfully analyse polymer films, the process involves bombarding the surface of the sample with primary ions. The process can depict a detailed trace molecular analysis of the surface of a sample at a shallow sub-micron level. It is an efficient method, which detects the presence of low concentrations of molecules and elements (188-189).

The method allows:

- Characterisation of surfaces in organic and inorganic coatings
- Can identify the presence of any impurities on a sample
- Can determine the composition of a sample
- Provide elemental mapping

These can in turn supply information on the chemical structure and composition of the films. Typically the primary ion beam has an energy which can be between 10 keV to the MeV range.

Primary ions are bombarded onto the sample surface. Typically argon is used, whereby ion pulses with lengths of 10-15 ns are generated from a continuous beam. Argon also has the ability to produce high intensity, short primary ion pulses. Secondary particles are released via a sputtering process from the surface of the sample. In addition to electrons, atoms and molecules which can be partially positively or negatively charged are also emitted. As the molecular ions are emitted they are separated and detected within a time-of-flight mass spectrometer as depicted in figure 4.14 below (187).

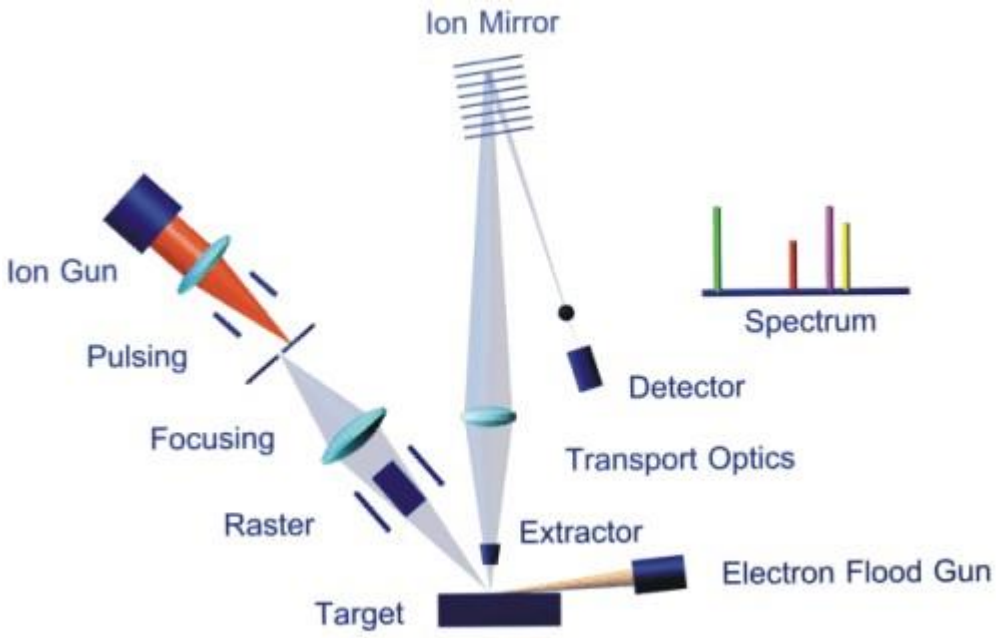

Figure 4.14. Displaying the components which determine the pathway of the electrons as a spectrum is obtained via the TOF-SIMS analysis (187).

For amorphous and polycrystalline samples the sputtering process creates a series of atomic collisions. Atoms with sufficient energy undergo secondary collisions and this propagates further with the energy of the atoms decreasing upon each collision.

A known problem which occurs with thick polymer samples, when the surface becomes charged as a result of the incident beam of positive ions or local charging of the nuclear track region. This results in a wider array of mass lines and again is related to the conductivity of the polymer itself. The analytical process is destructive but this can be minimized through the use of a pulsating beam. As a result the sample can change during the sputtering process. The secondary ions can be detected quasi-simultaneously, thus the analytical technique is highly useful for smaller samples. All the secondary ions are accelerated within an electric field with potential U and separated in a field free drift tube Particles which have a different mass-to-charge ratio m/q reach the detector after the time of flight t. The effective flight path is s and this corresponds to the drift present in the tube itself.

$$\mathrm{m/q} = \frac{2eU}{s^2} t^2 \qquad (5)$$

The secondary ion sensitivity for each element is calculated from the standard relative to a reference element E_0, usually silicon. Using the relative sensitivity values the element ratios E/E_0 in the sample can be identified from the secondary ion sensitivities SI:

$$(E/E_0)_{Sample} = \frac{[SI(E)/\,SI(E0)]\ Sample}{[SI(E)/SI(E0]\ Standard} (E/E_0)_{\ Standard} \qquad (6)$$

Hence the relative sensitivity is found below and it is determined by the nature of the sample, ionic species, matrix material and analytical conditions.

$$RS\ (E,E_0) = \frac{SI(E)/\ SI(E0)}{E/E0} \qquad (7)$$

It is pertinent to say that the velocity of an ion with a given kinetic energy depends on its mass. As the ions enter the drift tube they are separated according to their velocity prior to reaching the detector. A reflector is used in order to focus the energy to make up for the difference in flight entrance times. Ions with a higher energy are able to penetrate the electric field deeper and by adjusting the electric fields with precision all the secondary ions of one species are able to reach the detector simultaneously. The schematic depicts the route the ions traverse through prior to reaching the detector where the fraction discriminator converts the incoming signal to a normalized signal.

4.17. *Nano-indentation*

The layer-by-layer technique is used to prepare multilayer polymer thin films. The films can then be characterised through nano-indentation. Nano-indentation is a way to monitor the performance of a material through its elastic properties and characterise its response to deformation (190-191).

Mechanical properties, indentation modulus of the PEM multilayers were investigated using a nano-indentation system (Agilent Nanoindeter XP). A sharp diamond Berkovich indenter tip with a diameter of ~50 nm was positioned over the surface of the film and the force was applied and held at a peak and unloaded at the same rate of loading.

The indentation modulus was obtained. The samples were tested with a maximum load of 600 mN at a maximum depth of 2 μm and harmonic displacement of 2 nm at a

frequency of 45 Hz using a Poissons ratio of 0.35. Upon correction of the tip modulus the sample modulus is recorded.

Nano-indentation was carried out at multiple points on the samples in order to determine how uniform the PEMs were, mechanically. An average was taken of the peaks obtained. The graph below in figure 4.15 displays a typical force penetration curve which illustrates the elastic and plastic recovery of a polymeric sample.

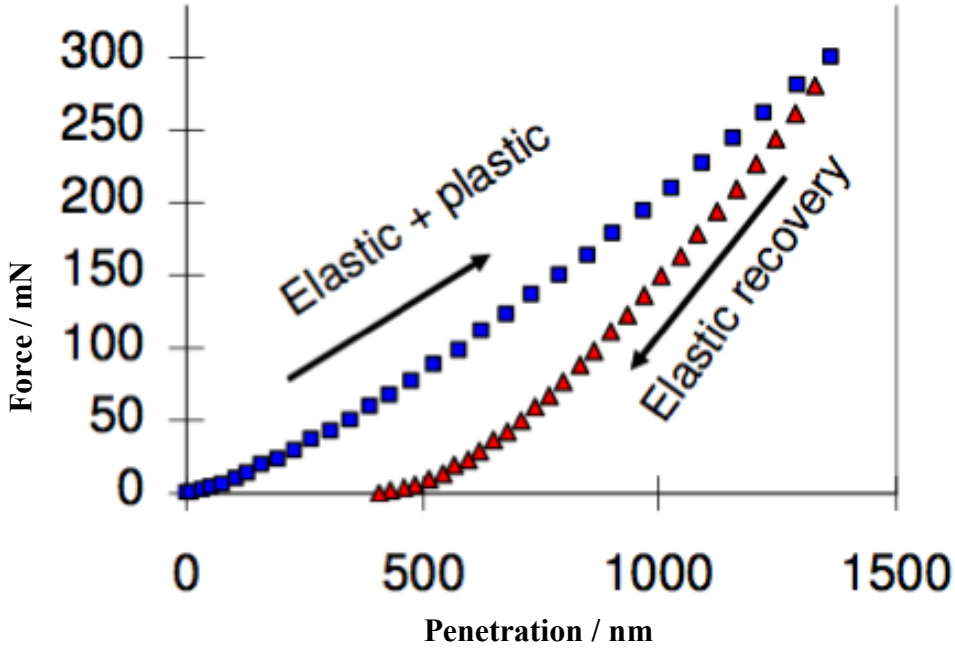

Figure 4.15. Typical graph displaying the elastic recovery of a polymeric sample on application of a force and the change in depth as it is applied.

The machine can record small load and displacement with a high level of accuracy and precision. Load-displacement data can be used to determine modulus, hardness and other mechanical properties. A prescribed load is applied to the indenter in contact with the sample surface. As the load is applied, the depth of penetration is measured as depicted in figure 4.16. The area of contact at full load is determined by the depth of impression and the known angle or radius of the indenter.

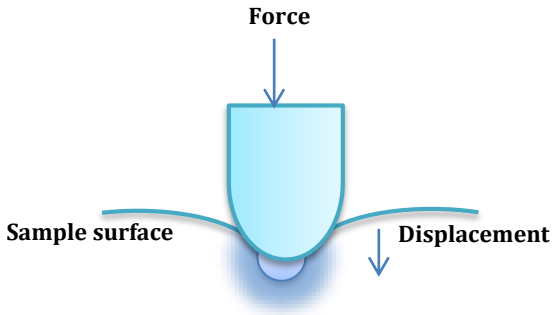

Figure 4.16. Schematic displaying the sample displacement which takes place when the indenter tip comes into contact with the sample surface.

Instrumented nano-indentation is a special type of characterization approach and is well suited to give a high throughput investigation of mechanical properties of a material. This is primarily down to the force and displacement control when conducting tests on highly sensitive samples.

Combination of the below testing parameters and contact mechanics will enable the characterization of material properties of the film:

- Force (controlled), identifying the relative force on the sample surface.
- Displacement (nm range) of the material on application of the force.
- Contact area and Time, influences the deformation mechanics of the material.
- The sample should be supported on a substrate when testing, this will prevent the sample from sliding under application of force.

Figure 4.17 displays a schematic diagram identifying the generation of the force via the force springs in the indenter, in combination with the displacement sensor, the tip comes into contact with the surface of the sample through a negative feedback mechanism. This is a highly controlled system and therefore should avoid any external stimuli during the experimental technique.

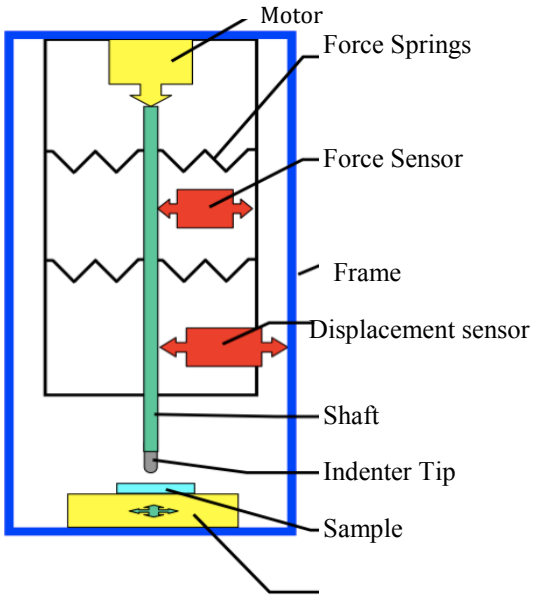

Figure 4.17. Schematic displaying the sample displacement which takes place when the indenter tip comes into contact with the sample surface.

In addition to obtaining the Young's modulus of the sample, the hardness of the sample was also measured. The hardness of a sample is a measure of the resistance to local deformation of a material and is a combination of the Young's modulus, yield strength and strain hardening capacity of the material (192-193).

4.18. X-ray diffraction

X-ray diffraction was conducted using X-ray diffractometer (Bruker D8) with Cu Kα radiation (40 kV, 120 mA) and 0.02 ^{0} step and 2θ range of 20-60 ^{0} was used to analyse crystal structure.

Essentially XRD is a method used to identify the atomic and molecular structure of a crystal whereby crystalline atoms cause beams of incident X-rays to diffract into various directions. The measurement of the angles and intensities from a

crystallographer can give an indication of the three-dimensional presence of the density of electrons within the crystal structure and this is illustrated in figure 4.18.

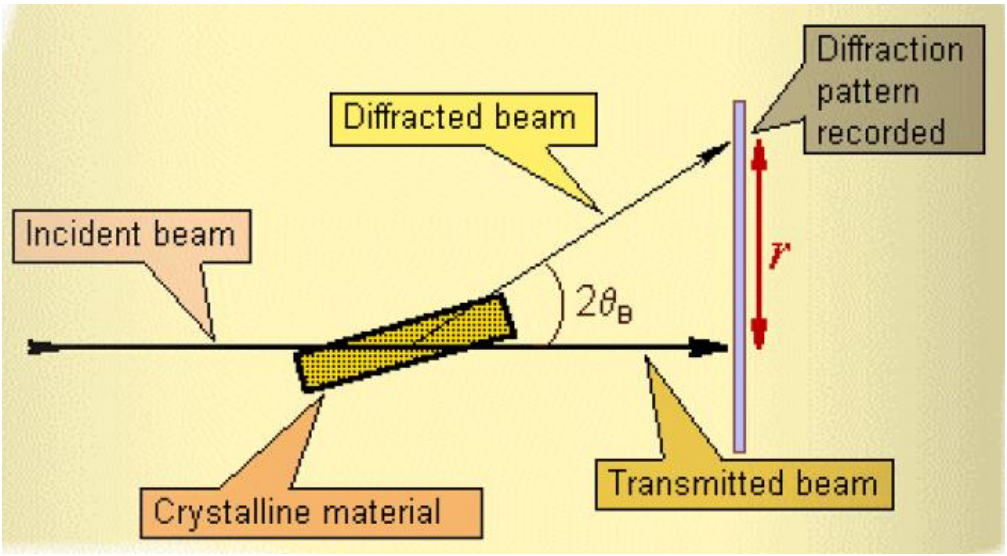

Figure 4.18. Illustration of the incident beam and diffraction whilst conducting XRD (178).

This rapid diffraction technique is primarily used for phase identification of a crystalline material. The diffractometer generates X-rays and these are bombarded on the target material with electrons. As the electrons gain sufficient energy to dislodge the inner shell electrons of the target material, this ultimately results in a characteristic X-ray spectra.

5. Naturally inspired polyelectrolyte multilayer composite films synthesised through layer-by-layer assembly and chemically infiltrated with calcium carbonate

5.1. Introduction

Over the past decade, research in the field of nanotechnology and nanocomposites has experienced a significant explosion. A variety of methods have been implemented to synthesise biomolecular patterns in combination with thin films and surface chemistry (118). The layer-by-layer (LBL) assembly of polymer multilayer thin films has been widely used with a combination of nanoparticle constituents in order to obtain high performance and high quality thin film composite materials (196). This architecture is achieved through the cyclic deposition and charge overcompensation phenomenon where high molecular weight species are adsorbed on a solid-liquid interface. This makes the layer-by-layer method an appealing alternative to other thin film deposition techniques including Langmuir Blodgett deposition, electrophoresis, spin and spray coating (197-198).

The sequential organisation of stabilized nanoparticles through the electrostatic adsorption onto oppositely charged layers of polyelectrolytes makes layer-by-layer especially suitable for the production of stratified thin films where hierarchical organisation can be achieved by controlling the vertical distribution of layers at the nanometre level in a specific pre-determined order. If combined with micro patterning techniques, a material with three-dimensional control of nanoscale architecture can be synthesised with control over the lateral distribution of layers, their shape, dimensions and composition. Control at this level creates a route for application in the photonic,

electronic and medical fields (199), which has already been extensively exploited. However, the area of mechanically strong layer-by-layer composites formed by inorganic/organic constituents mimicking natural bio mineralized composites has received relatively less attention. In this area, several proof-of-principle studies have demonstrated that layer-by-layer templating can create small volumes of layered nanoparticle-polyelectrolyte multilayers which have properties similar to tough high performance biological ceramics like nacre (200-202)

The overall exceptional mechanical performance of natural bio mineralized composites like the abalone nacre in shells, or the mineralized collagen matrix in bone, arises more due to the microstructure and hierarchical organization (203), rather than due to any exceptional mechanical properties of the individual components themselves. This hierarchical architecture in bio mineralized composites is strongly influenced by interactions, barrier properties and basic biomimetic concepts. In nearly all bio mineralized composites, a precursor organic matrix comprising proteins and polysaccharides plays a crucial role in controlling the growth of the inorganic phase, as first proposed by Lowenstam in his theory of organic matrix mediated mineralization. The main types of majority of bio minerals include calcium carbonate, variants of calcium phosphate such as the carbonated apatites in bone, calcium oxalates and silica or iron oxides (204).

The nucleation kinetics is believed to play an important role in the development of these structures. The primary concept is that charged groups on the organic molecules, together with aspects of their secondary and tertiary structure, can control the nucleation, growth and form of inorganic materials within a porous network of such molecules, generating the hierarchical composite structures (205). It is possible to exploit the principles of bio mineralization (206-207) to prepare novel

materials as can be seen in the classical nacre model (208) and here we explore the ability of polyelectrolyte multilayer films to nucleate inorganic crystallites in a biomimetic manner.

Herein, we report the results of synthesis of polyelectrolyte multilayer (PEM) films on sacrificial Polymethylmethacralate (PMMA) substrates by layer-by-layer templating, followed by an infiltration of an inorganic phase with the goal of nucleating crystallites of calcium carbonate, to form a hybrid bio mineralized nanocomposite. The PEMs have been synthesised using poly (sodium 4-styrenesulfonate) (PSS), poly (diallyldimethylammonium chloride) (PDADMAC) and poly (allyl amine hydrochloride) (PAH). For each system (PSS-PAH and PSS-PDADMAC) the growth of calcium carbonate through chemical infiltration was monitored. The content, composition, local mechanical properties and microstructure of the ensuing organic/inorganic LAYER-BY-LAYER multilayer was determined and discussed towards to natural biological composites like bone and nacre.

5.2. Aims and objectives

The general aim here is to fabricate nanoporous charged polyelectrolyte multilayers made from the following configurations:

1. PAH/PSS
2. PDADMAC/PSS

These polymers were chosen as PAH/PSS is a well-studied polyelectrolyte complex and has a high level of polymeric interaction between the anion and cation. Similarly PDADMAC/PSS was utilized for the similarity the polymer complex displays to biological polymers like collagen and hyaluronic acid. For this reason these polymers were most suitable for this investigation (209).

The PEM's will then be infiltrated with calcium and carbonate ions, the growth of an inorganic phase will be investigated within the nanoporous multilayer and compared to the growth occurring in naturally occurring structures like bio mineralized composites like nacre.

In addition to this, the effect of the multilayer thickness and number of infiltration cycles will also be controlled and investigated to determine any yield of calcium carbonate within the PEM film. The mineralized content will then be determined through TGA analysis and nano-indentation testing will determine the Young's modulus of the nanocomposite material.

5.3. *Visual inspection of PEM multilayers*

From visual inspection, it was straightforward to distinguish the PDADMAC/PSS multilayers from the PAH/PSS. The latter were found to be much clearer in colour, making it difficult to distinguish between the layers and the PMMA with a naked eye. The former samples were much more vivid and exhibited a milky white colour on the substrate. The colour intensified with increasing number of layers. This behaviour for the PDADMAC/PSS samples initiated from factors such as film roughness or polyelectrolyte diffusion that promote exponential growth (210).

We will first describe results on PAH/PSS/ PEMs, followed by PDADMAC/PSS PEMs.

SEM on (PAH/PSS)/$CaCO_3$: The cross section of the (PAH/PSS) n films built in 2 M NaCl were analysed with SEM after being transferred onto a PDADMAC/PSS-coated silicon wafer. Prior to chemical infiltration it was seen in Figure 5.1-a that the (PAH/PSS) 20 film had an average thickness of ~550 nm. Upon 20 cycles of chemical infiltration the thickness had increased to ~2 microns (Figure 5.1-b). The increase in

thickness within the 20 bilayer PEM was attributed to the growth of calcium carbonate particles within the multilayer.

In the same manner, the multilayer film was synthesised with 20 bilayers, upon achieving this, infiltration cycles of the same number were applied to the multilayer. The composite after 20 cycles of $CaCO_3$ infiltration consisted of a relatively dense upper layer having nearly the same thickness as (PAH/PSS) 20 before infiltration (Figure. 5.1-a) and comparatively porous bottom layer with many voids. Note that the film is shown upside down after sealing, so the upper layer has initially been assembled on PMMA template and bottom layer has been formed after infiltration and can be attributed to the calcium carbonate shell.

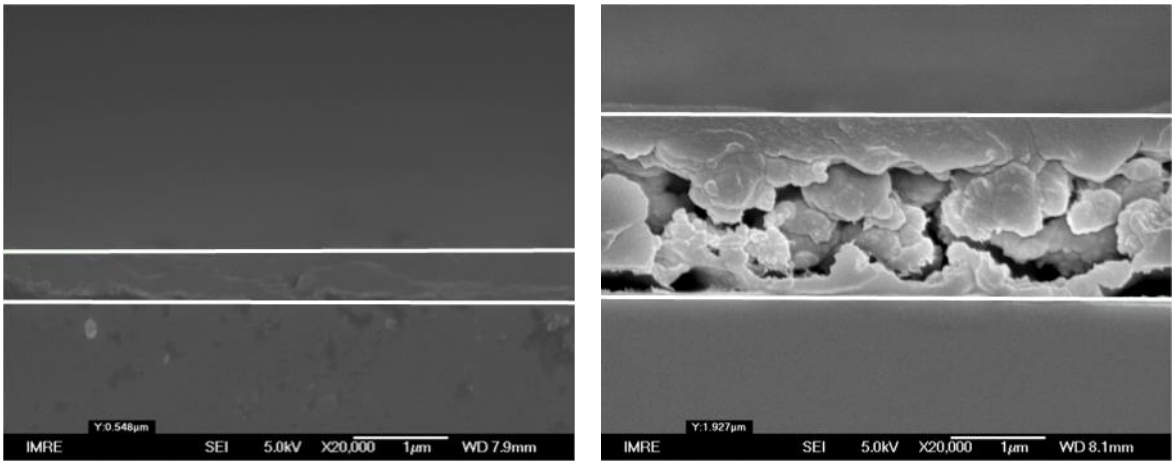

a **b**

Figure 5.1. Cross-sectional SEM images of (PAH/PSS)20 films formed at 2 M NaCl before (a) and after 20 cycles of infiltration with calcium carbonate (b); scale bar: 1 µm. The infiltrated calcium carbonate is visible in (b) whereby a porous film is displayed.

Topography of the samples also demonstrates a significant change. The (PAH/PSS) 40 film had a smooth surface with no visible voids (see Figure 5.2-a). Upon 40 cycles of infiltration, the surface appeared to be covered with comparatively porous

calcium carbonate shell as seen in the Figure 5.2-b, in good agreement with cross-sectional data shown above.

As the number of PAH/PSS bilayers was increased to 60, the surface appeared to become very rough (see Figure 5.2-c). Similar increase of the PAH-PSS film roughness upon multilayer build-up has been shown before (20, 24). However the surface of sample after 60 cycles of infiltration was much smoother with several cracks (see Figure 5.2-d), which another indication of calcium carbonate shell formation was on top of PAH/PSS multilayer.

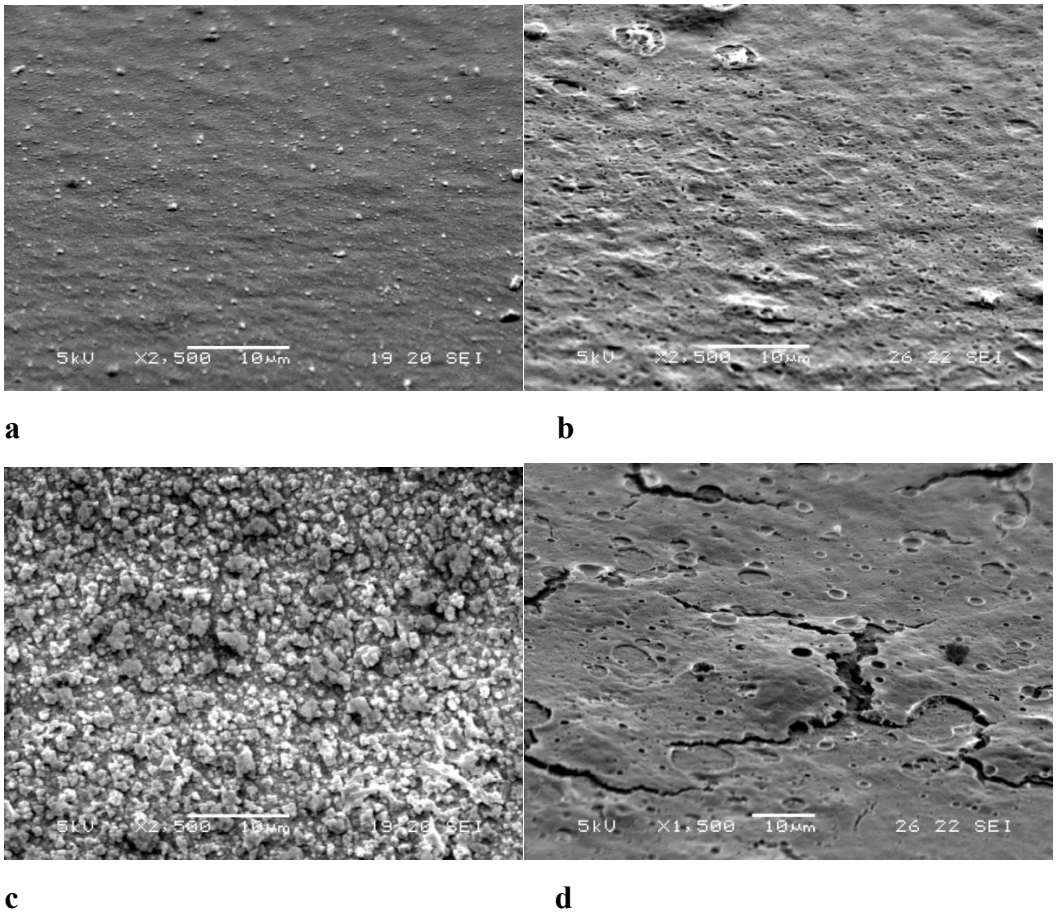

a **b**

c **d**

Figure 5.2. SEM images of (PAH/PSS) 40 (a, b) and (PAH/PSS) 60 (c, d) films formed at 2M NaCl before (a, c) and after (b, d) 40 and 60 cycles of infiltration with $CaCO_3$, correspondingly; scale bar: 10 µm, x 2500 magnification. Surface topography significantly changes as there is an increase in the number of bilayers.

At the same time, infiltration resulted in the $(PAH/PSS)_{60}$ film lifting off the surface of the PMMA sacrificial template, probably due to a compressive force generated between stiff $CaCO_3$ layer forming on a thick elastic foundation that exceeds at some point a relatively weak adhesion of PAH/PSS multilayer towards the PMMA substrate.

5.4. *TOF SIMS on (PAH/PSS)/$CaCO_3$*

Investigations of the change in the morphology of the surface of the samples and of whether the calcium carbonate had penetrated within the multilayer are important to understand the structure of the formed PEM composites. In order to do this, TOF-SIMS was used. The PAH/PSS samples before and after calcium carbonate infiltration were etched with Ar^+ ions. Cross-sectional elemental profiles (as a function of etching time) and maps of spatial distribution of corresponding elements were created as shown in Figure 5.3. The ions of two elements: Ca^{2+} attributed to $CaCO_3$ and S^+ attributed to the PSS in the (PAH/PSS) polyelectrolyte multilayer film.

It was seen that the S^+ ions were evenly distributed in the sample prior to infiltration (see Figure 5.3b, image 1), and these ions were attributed to the PSS layer. The intensity decreased to nearly zero after ~400 s of etching (Figure 5.3a, line 1) that could be an indication of the complete etching of the $(PAH/PSS)_{20}$ film. After 20 cycles of $CaCO_3$ infiltration just traces of sulphur were detected (see Figure 5.3-a, line 2 and Figure 5.3-b, image 2), probably due to a thick layer of $CaCO_3$ formed on top of the PEM film which cannot be etched upon the time of experiment. This result was in good agreement with the SEM data discussed above, which showed formation of a $CaCO_3$ layer on the surface of PEM upon infiltration.

The overall number of Ca^{2+} counts in all tested samples was much higher than for S^+ because of the high yield of ionisation for calcium.

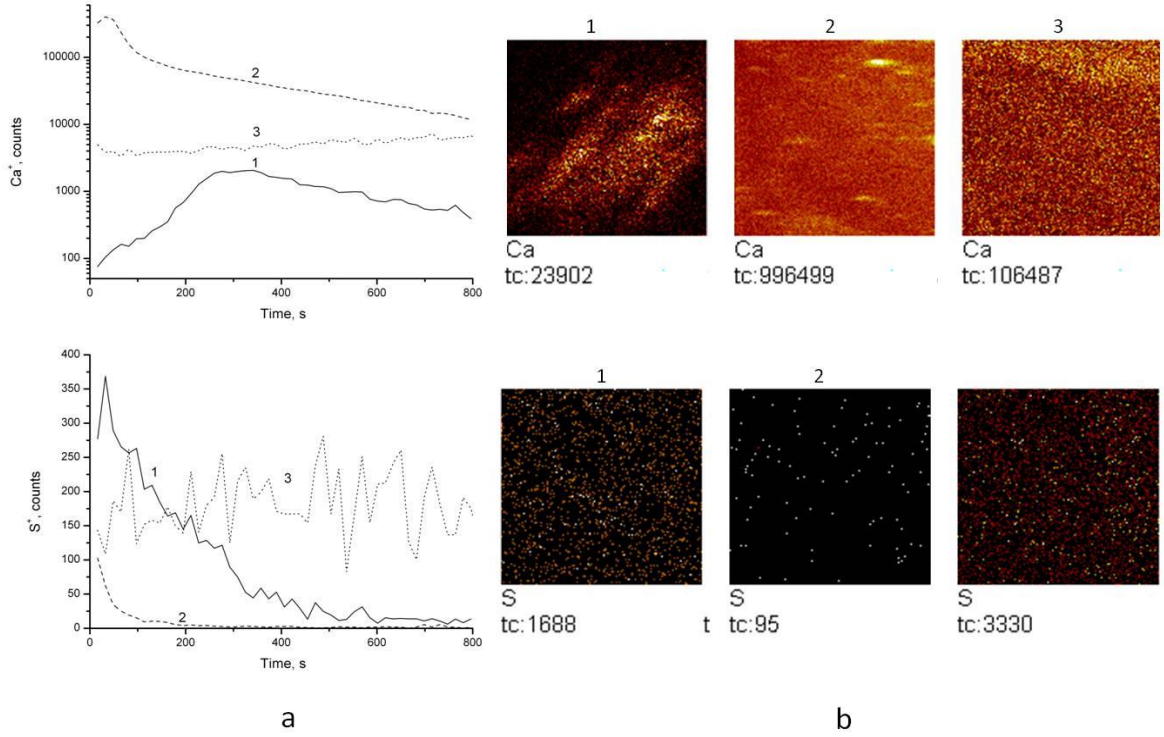

Figure 5.3. TOF-SIMS data on Ca^+ and S^+ counts depending on etching time (a) and mass resolved images (chemical maps) of positive ions, scan size 200x200 µm (b) for $(PAH/PSS)_{20}$ film before (1) and after (2) 20 cycles of infiltration with $CaCO_3$ and for $(PAH/PSS)_{40}$ film after 40 cycles of $CaCO_3$ infiltration, scanned from the back of the film (after PMMA dissolution and sealing towards Si) (3).

It makes TOF-SIMS a very sensitive method for this element. Even before $CaCO_3$ infiltration, TOF-SIMS detected some unevenly distributed Ca (see Figure 5.3-b, image 1). The profile shows that calcium appears in TOF-SIMS spectra only after 400 s of etching (see Figure 5.3-a, line 1). As discussed above, the PSS/PAH film was nearly completely etched by this time, thus detected calcium could be attributed to some dust particles on the PMMA template. After infiltration, Ca^{2+} counts increase by more than two orders of magnitude, calcium distribution becomes even and covers the

whole sample (see Figure 5.3-a, line 2 and Figure 5.3-b, image 2). The counts decrease slowly with etching time.

However, the key question was whether $CaCO_3$ just formed a shell on the surface of PEM film, or penetrated into the multilayer. As it was not possible to etch away the $CaCO_3$ shell and reach the multilayer within the time duration of the experiment, as evidenced from the absence of the sulphur signal, the sample was sealed onto Si, dissolved PMMA and scanned it from the back. In this case, calcium evenly distributed across the sample was detected from the very beginning (see Figure 5.3-b, image 3), and Ca^{2+} counts were two orders of magnitude lower than in the top of the composite, and in this case not decreased but increased slowly upon etching (see Figure 5.3-a, line 3). As for sulphur, it was homogenously distributed and at about the same content as in PSS-PAH multilayer film, but this content did not change with etching time. Probably, etching rate of PEMs is affected upon calcium carbonate infiltration. Taken together, the SEM and TOF-SIMs results confirmed the change in morphology and infiltration of calcium carbonate within the PEM.

5.5. *XRD on (PAH/PSS)/$CaCO_3$*

It is of interest to identify whether the calcium carbonate phase formed in the PEM is a crystalline phase or amorphous. Crystalline polymorphs of calcium carbonate include calcite, vaterite, aragonite and other types. To distinguish if a crystalline form of calcium carbonate is present in the infiltrated PEM, the samples were analysed with XRD as shown in Figure 5.4. It was observed that no clear reflections corresponding to the presence of any crystalline phase were present for any of the samples analysed, with the exception of two very low intensity peaks at $2\theta = 29.4°$ ((104) peak in calcite) and at $2\theta = 21°$ ((004) peak in vaterite).

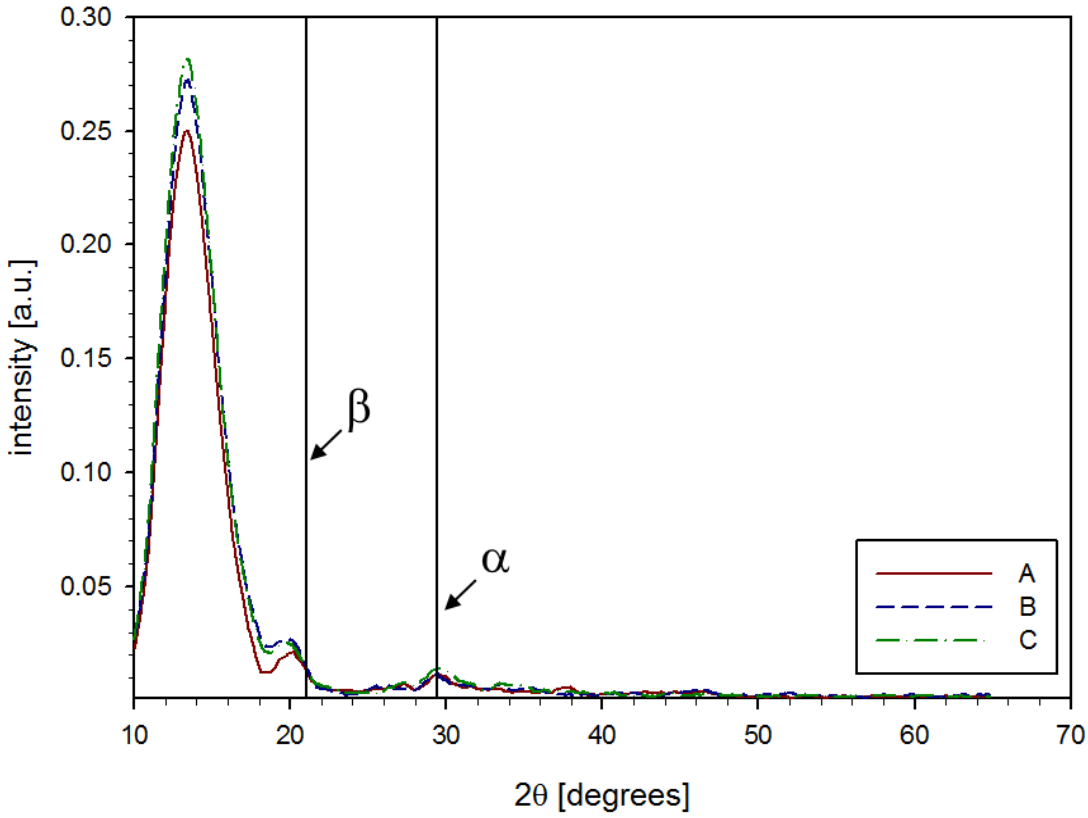

Figure 5.4. X-ray diffraction profiles of PMMA-(PAH/PSS) 20 with no $CaCO_3$ (A), PMMA-(PAH/PSS) 40 after 40 cycles of infiltration with $CaCO_3$ (B), and PMMA-(PAH/PSS) 60 after 60 cycles of infiltration with $CaCO_3$ (C). No clear X-ray peaks are observed, except a weak intensity peak at 29.4° (α; calcite: (104) and a peak near 21° (β; vaterite: (004).

These small peaks present in all the samples including sample A with no infiltrated $CaCO_3$ and could be attributed to dust particles presented on the surface of PMMA prior to layer-by-layer assembly of PEMs (see discussion of TOF-SIMS results in the previous section).

(PDADMAC/PSS) 40 films, comparison with a material with higher porosity: Figure 5.5 displays the (PDADMAC/PSS) 40 after chemical infiltration as there is a significant change in surface topography. In this set of images the multilayer number

is kept constant but the infiltration cycles are varied to 1, 20 and 40 respectively. Each PEM is kept hydrated before being exposed to the calcium chloride and sodium carbonate solutions with a washing step in between. Figure 5.5a below shows the nature of the PEM with only one infiltration cycle. The surface is rough with a lot more pores. These sites act as regions where the calcium ions can diffuse within to stimulate growth of the inorganic phase. As the infiltration cycles are increased to 20 the surface becomes saturated and smooth, see Figure 5.5b. There is visible difference in topography with Figure 5.5a and completing full 40 infiltration cycles results in a complete change in topography again, as seen in Figure 5.5c. This is due to the nucleation and crystal growth which is prevalent in the (PAH/PSS) n.

The PDADMAC/PSS films exhibit swollen, gel like properties [28, 29]. This is influenced by the ionic strength of polymers solutions upon multilayer build-up. This is necessary to demonstrate a synergistic toughening mechanism which is biologically inspired (211-212).

The difference between the PAH/PSS and PDADMAC/PSS films can also be attributed to the change in chain mobility, the diffusion coefficient within the PDADMAC/PSS matrix is significantly higher than in PAH/PSS, this is due to the lower density of complex sites as confirmed also by other groups [24, 30]. When debating the film thickness and growth of films exponentially or linearly we can look into different parameters as to why the films will grow in either direction. They can be attributed to whether there is an exact charge compensation in the film between the positive and negative charges carried by the polyanion and polycation then diffusion is still probable, as a result of the change in chemical potential of the free polyelectrolytes within the film and those in the solution.

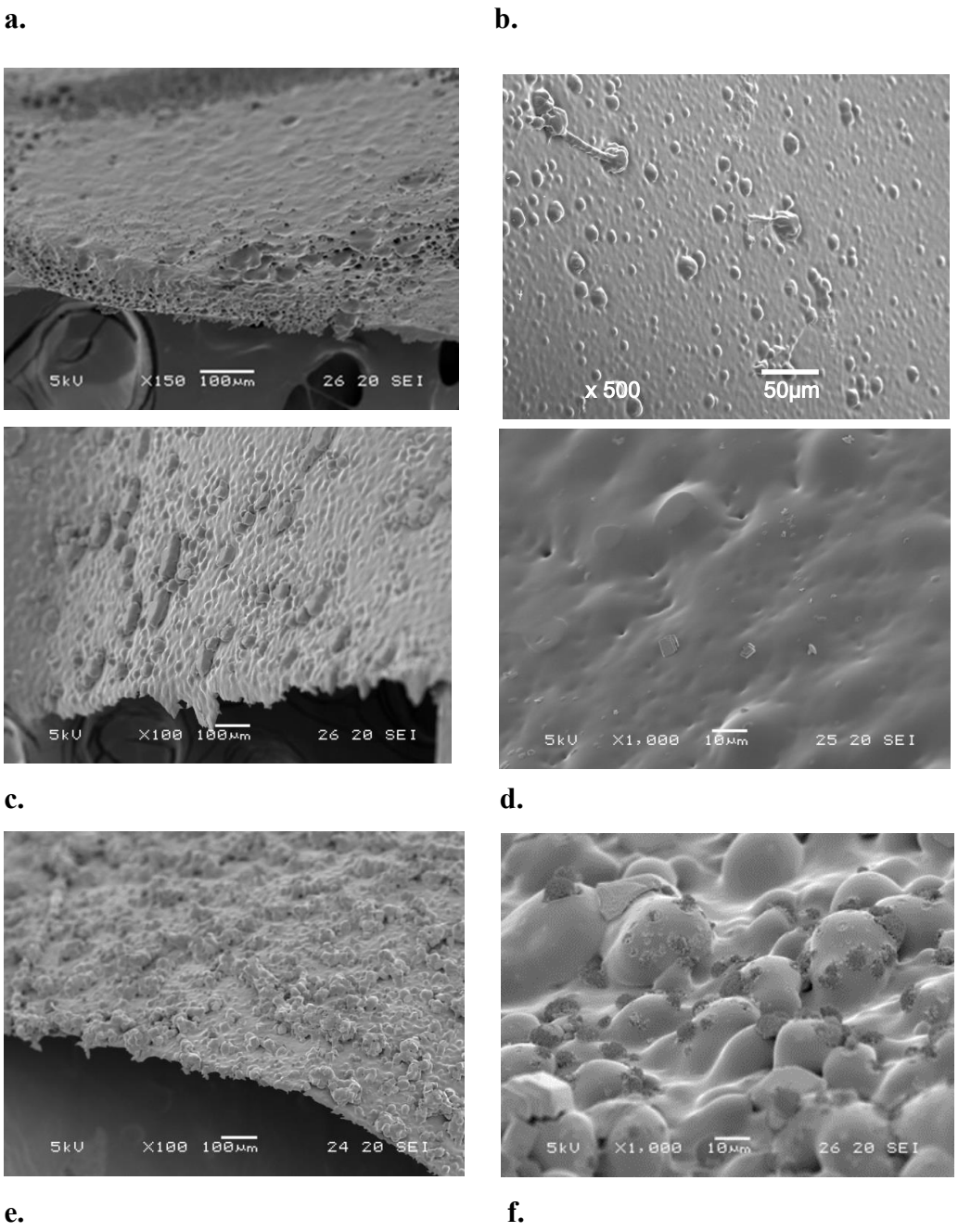

Figure 5.5. Monitoring the effect of infiltration cycles on the polymer composite multilayer in the (PDADMAC/PSS) composite system by Scanning Electron Microscopy: (PDADMAC/PSS) 40 – 1 infiltration cycle (a), 20 infiltration cycles (b), and 40 infiltration cycles (c).

(Figure a,c,e, x 100 magnification –scale bar 100 µm and Figure b,d,f , x1000 magnification-scale bar 10 µm)

5.6. *TOF-SIMS on (PDADMAC/PSS)/$CaCO_3$*

As with the (PAH/PSS) n PEM's, TOF-SIMS was also conducted to analyse the growth and presence of calcium carbonate beyond the surface of the (PDADMAC/PSS)14 / $CaCO_3$ multilayer (see Figure 5.6). This was analysed from the back after sealing on to silicon wafer. From this analysis there is an increase in calcium intensity in the calcified sample as it is etched further into the sample, this is positive as it indicates the depth of penetration of calcium within the bilayers.

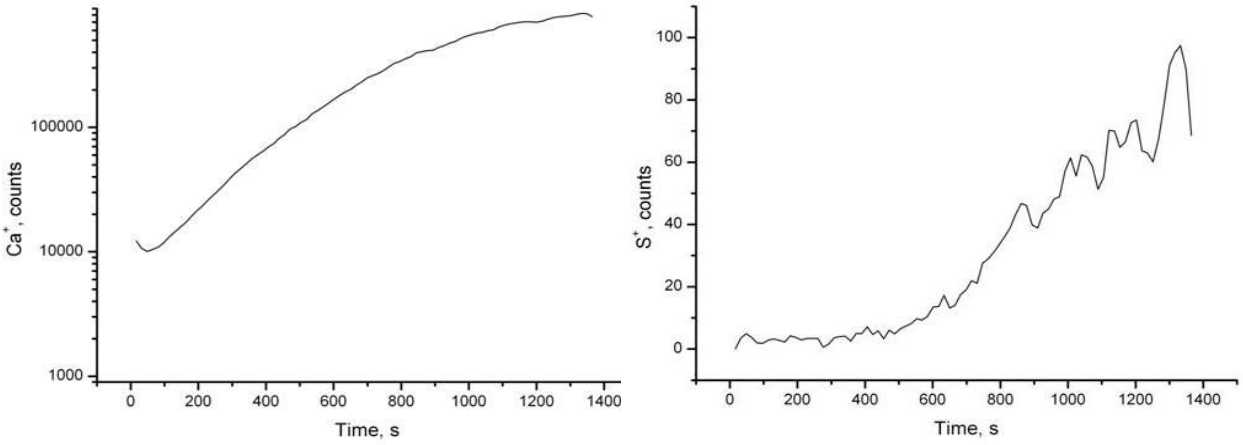

Figure 5.6. . TOF-SIMS data on Ca^{2+} and S^{+} counts depending on etching time for (PDADMAC/PSS) 14 /$CaCO_3$. The Ca^{2+} count increases as the sample is etched demonstrating the presence of Ca^{2+} and S^{+} within the multilayer.

The sulphur indicates presence of the PSS contribution within the PEM and this continues to increase as the sample is etched, demonstrating the presence across the bilayer and confirming that it is not only in high intensity across a single top-most region as part of a crust.

5.7. *TGA on (PAH/PSS)/$CaCO_3$ and (PDADMA/PSS) $CaCO_3$*

Upon identifying the presence of calcium carbonate within the fabricated PEMs its overall content was of interest to characterise infiltration process. TGA profiles for (PAH/PSS) 40 and (PDADMA/PSS) 40 are shown in Figure 5.7 a and b.

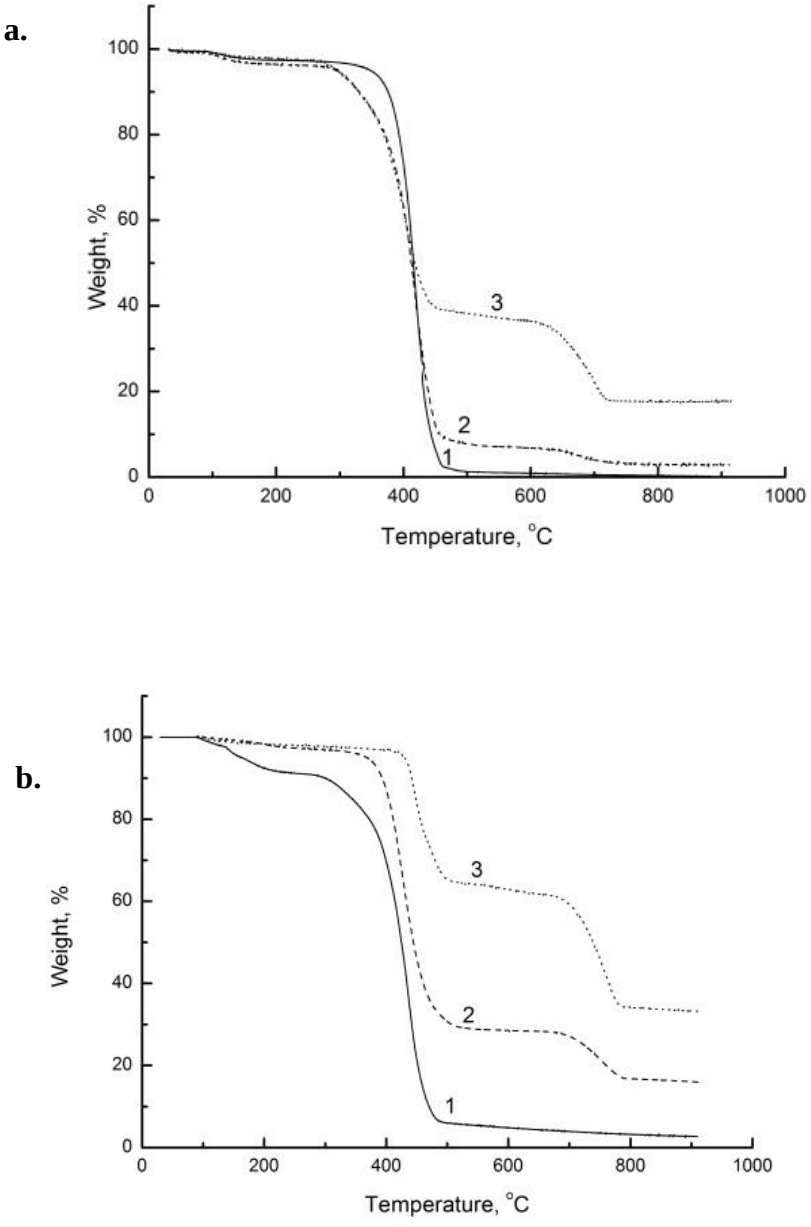

Figure 5.7. Thermogravimetric analysis profiles of (PAH/PSS) 40 (a) and (PDADMAC/PSS) 40 (b) films after their infiltration with $CaCO_3$ in 1 (1), 20 (2), 40 (3b) and 60 (3a) cycles. As the number of bilayers increases the wt. % evolved at final decomposition increases, thus resulting in a greater volume of calcium carbonate present in the sample.

(PAH/PSS)40 film after 1 infiltration cycle losses 100% of its weight at one step from ~ 300 to ~500 °C due to decomposition of organic matter. It doesn't contain any measurable amount of calcium carbonate. An additional weight loss step happening from 610 to 720 °C appears in TGA of the sample after 20 cycles of infiltration. At this step sample weight decreases from 6.71 to 3.53% (53% weight loss) that could be assigned to thermal decomposition of $CaCO_3$ and formation of CaO (100 and 56 Da, correspondingly). The sample after 60 infiltration cycles demonstrates more pronounced weight loss step in this temperature range, from 36.15 to 18.02 wt. % (50% weight loss). Thus the weight percentage of $CaCO_3$ in (PAH/PSS) 40 multilayer film increases with number of infiltration cycles. In (PDADMA/PSS)40 films after 1 infiltration cycle, organic matter also decomposed in one step from ~ 300 to ~ 500 °C, but it didn't degrade completely and sample still had ~ 2.8 wt. % at 900 °C.

These residues could be carbon-rich substances formed upon sample calcination in N_2 atmosphere. The samples obtained after 20 and 40 cycles of infiltration have another weight loss step happening from 680 to 800 °C due to $CaCO_3$ decomposition. The wt. % of $CaCO_3$ and CaO (after subtraction of the weight of carbon-rich organic residues) were 24.0 and 13.5 (56% weight loss) for sample after 20 infiltration cycles and 57.2 and 30.9 (54 % weight loss) for sample after 40 infiltration cycles. Thus, $CaCO_3$ weight percentage in the PDADMA/PSS films was much higher in comparison to the PAH/PSS. This difference was attributed to the nature of the polymer and the way in which the electrostatic bonding played a role within the multilayer reflecting the higher interaction energy between PAH and PSS compared to that between PDADMAC and PSS.

5.8. *Nano-indentation on (PAH/PSS)/$CaCO_3$*

All samples were sealed onto a silicon wafer which had an adhesive film made of (PSS/PDADMAC) 8 multilayer as discussed (in Section 4.0) to increase adhesion of the PEM film. Nano-indentation of (PAH/PSS) 40 PEM's was conducted in order to determine the Young modulus and hardness of the polyelectrolyte multilayer before and after chemical infiltration. Prior to chemical infiltration, the Young modulus for (PAH/PSS) 40 film was measured to be 3.8 ± 0.3 GPa with an average hardness of 0.16 GPa. This is in good agreement with the Young's modulus of 4 ± 1 GPa calculated from elastic deformation of shells made of (PAH/PSS) 40 multilayer and 4.7 ± 0.7 GPa determined via stress-induced mechanical buckling instabilities (152).

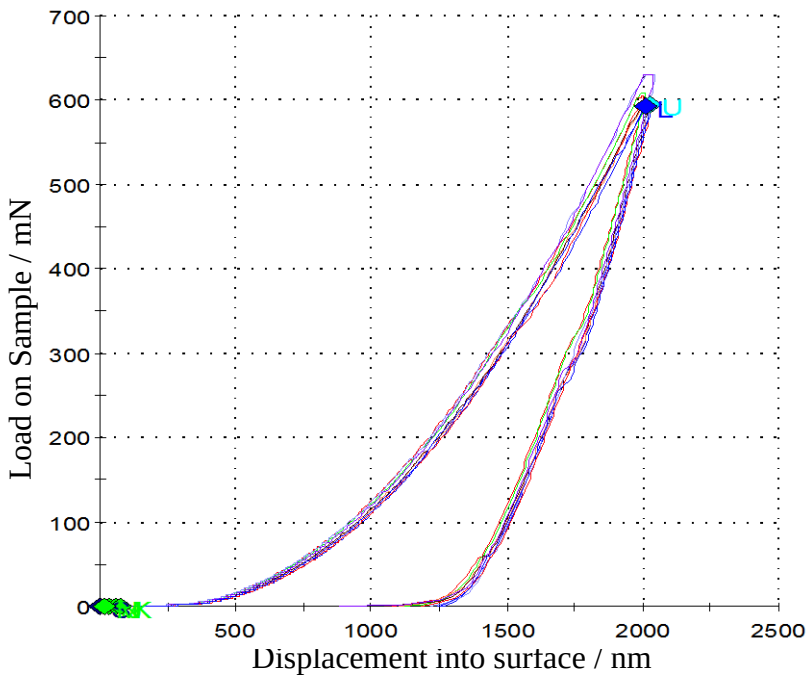

Figure 5.8. Force-displacement curves obtained from nano-indentation of PEMs from ((PAH/PSS)40/$CaCO_3$)40 measured at 10 unique sample points. There is not much deviation with the curves, demonstrating a uniform sample surface.

After 20 cycles of infiltration, the average modulus for (PAH/PSS) was determined to be 10.0 ± 0.3 GPa and an average hardness of 6.3 ± 0.3 GPa.

Thus the increase in modulus is 2.6 times and in hardness nearly 60 times after mineralisation. This is a significant enhancement of mechanical properties and can be comparable to the natural materials like bone and nacre. The elastic modulus of un mineralized bone collagen is ~1-2 GPa, which increases to ~10-20 GPa on mineralization to ~ 50% volume fraction of carbonated apatite [13], a factor of about 10-20.

5.9. Non-infiltrated vs infiltrated

Observations under the SEM display a clear distinction in morphology between the planar and infiltrated samples. The PSS/PDADMAC polyelectrolyte samples are porous and grainy in nature, this is evident in figure 5.9 a and b. There are a large number of grooves and the irregular morphology demonstrates the versatility in deposition and synthesis of this film. Although no highly organised composite has been formed, The images certainly suggest the successful precipitation of $CaCO_3$ within the polyelectrolyte multilayer. The infiltrated samples show the calcium carbonate diffusing within the porous areas of the film and growing within these regions. It has greater surface roughness compared to the planar samples.

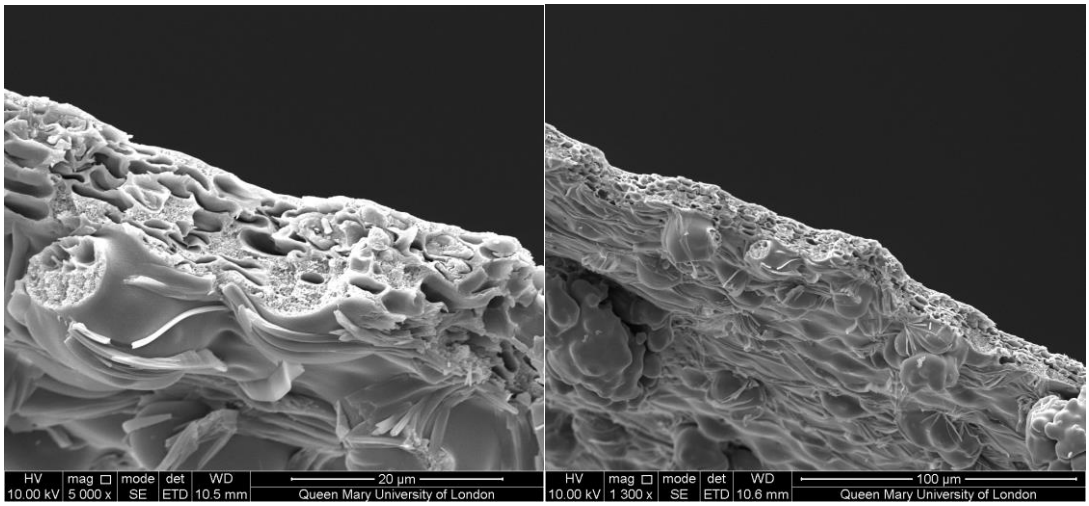

a. **b.**

Figure 5.9. Displaying cross sections of (PSS/PDADMAC) 60 at 5000x (a) and 1300x (b) magnifications respectively.

The planar samples have less of a smoother textured surface which becomes more uniform upon further precipitation of calcium carbonate within the multilayer.

The planar sample for (PDADMAC/PSS) 60 shown in figure 5.9, displays a number of voids, which are no longer visible after infiltration. The only reasonable explanation for this is simply that it has been filled by the inorganic particles after the infiltration process. These particles are homogenously distributed a surface. It may be suggested that sufficient time was not allocated to allow two solutions to mix however evidence from (PDADMAC/PSS) suggests otherwise. Previously analysed samples demonstrated the compact nature of PSS/PAH multilayers. The surface is not as porous with very few voids to allow the inorganic particles to enter the preceding layers. A void at one particular point is likely to be covered by the under lying layer that could be an underlying obstacle for full infiltration in that cycle. So in conclusion, it can be seen that the PSS/PDADMAC favours the infiltration process compared to PSS/PAH multilayers.

5.10. Conclusion

In this work, nanoporous charged polyelectrolyte multilayers (PEMs) were made from PAH/PSS and PDADMAC/PSS. The PEMs were then infiltrated with calcium and carbonate ions to nucleate and grow an inorganic phase inside the nanoporous polyelectrolyte multilayer, in analogy to the nucleation of calcium carbonate phases in prototypical bio mineralized layered composites like nacre. The effect of multilayer thickness and also of the number of infiltration cycles was investigated. It was found that the yield of calcium carbonate within the PEM film increased with the number of infiltration cycles. Calcium carbonate penetrated through the organic multilayer film and then formed an amorphous shell on its surface. Mineralization of the PEM with the fraction of inorganic component (over 8 wt. %) caused a 263 % increase of the Young modulus reaching an average modulus value of 10.0 GPa. Even more drastic effect has been observed on hardness where mineralisation increases it 60 times. These results show the promise of using layer-by-layer, PEM multilayers as mesoscale scaffolds to form mineralized composites in a biomimetic manner. As a next step, the use of natural polymers (instead of synthetic PEs) to mimic natural mineralization, and the effects of including complex microscale modulations in topology appear as promising lines of investigation.

6. Synthesis of biological PEM's via Layer-by-Layer Assembly with Collagen and Hyaluronic Acid

6.1. Introduction

Mimicking natural composites which show exceptional mechanical properties due to their hierarchical organization is an excellent starting point for the design of a new generation of synthetic materials. There have been numerous attempts in the field of materials engineering and design in the past decade to develop strategies based on materials containing collagen, mainly in the field of tissue engineering for the purposes of biomedical applications in wound healing and skin grafting techniques as collagen is a material which has a slow and infinite growth rate in the human body (213-214). Naturally occurring polymers including chitosan and hyaluronic acid have been used as gels or scaffold in the preparation of these materials. When working on the nanoscale for these applications, the physical properties and architectural design can be highly controlled and development occurs through a bottom-up assembly approach. Owing to its excellent mechanical properties and its comparatively simple morphology, nacre has attracted considerable attention also. The high level of toughness and strength in nacre result from its hierarchical structure. The challenge remains in controlling the internal structures of these architectural designs, and it is extremely challenging to adjust the structural parameters like thickness, porosity and surface charge without manipulating the entire architecture.

In an attempt to control the material design at this level the layer-by-layer approach of self-assembly of polyanions and polycations has been identified as a successful method to build film on a solid substrate with a high level of precision and control over the thickness of the film, hydration, viscoelasticity and mechanical integrity of

the films seen in hierarchal, self-assembled systems (215-219). These factors can be manipulated by changing some of the parameters controlling the synthesis of the film, the polyelectrolyte solutions, concentration of the solutions, pH, deposition cycles on the substrate are all parameters which can be adjusted to manipulate the characteristics of the composite multilayer (220). Through the deposition of the polyelectrolyte multilayer the film begins to grow, this is attributed to the charge overcompensation phenomena, the method has been widely adopted for designs featuring DNA, proteins and structural nanoparticles. This overcompensation has been confirmed by zeta-potential measurements. The adsorption of one of the oppositely charged polyelectrolytes occurs by the cooperative effects of the many ion pairs that are created. Its counter ions are then replaced with an oppositely charged polyelectrolyte. This replacement is entropically favoured.

In this chapter, the synthesis of polyelectrolyte multilayer assemblies based on the layer-by-layer approach is considered using a naturally occurring polysaccharide, hyaluronic acid (HA) and collagen. HA is a linear, unbranched polymer composed of repeating disaccharide units, glucuronic acid, β-1-3-and β-1-4 linked N-acetyl-glucosamine. HA is a major component of the extracellular matrix and of the synovial fluid. It is implicated in joint lubrication, water homeostasis of tissues, cell motility and inflammation (220).

In addition to this type-I-collagen will be utilized, collagen is a structural protein which is found in animal connective tissue within the body, collagen is also present in the skin, bone, tendon, dentin and cartilage in its most abundant type-I-collagen form. In this investigation, type-I-collagen from rat's tail is used to synthesis the (HA-Coll) multilayer films (221-222). The PEM is constructed entirely out of natural materials

which are present in the extra-cellular matrix of biological organisms, as a contrast from previous chapters where synthetic polymers have been used.

This investigation further infiltrates calcium carbonate within the film to provide a reinforcement mechanism within the PEM and the samples is then characterized from a physicochemical perspective, SEM and TGA in particular is used to identify the growth of calcium carbonate within this naturally occurring multilayer.

6.2. Aims and objectives

The aim of this work is to assemble a layer-by-layer composite structure with naturally occurring biological polyelectrolytes using the layer-by-layer assembly method. The polyelectrolyte multilayer films are constructed with collagen-type I and hyaluronic acid. By alternating the deposition of the films the polyelectrolyte film should increase in thickness and integrity. In addition, to this, the film will then be infiltrated with calcium chloride and sodium carbonate- again through layer-by-layer deposition in order to produce and inorganic reinforcement phase within the film.

Due to the nature of the collagen it is found from previous research (223) that collagen cannot diffuse into the film but only reacts with the outer layer of the structure. The architecture is functionalized through the growth of the inorganic phase, this is then quantified in order to identify the relationship between the growth of the multilayer and the mineralization process.

6.1.1. Growth and fibrillogenisis of collagen

Using collagen and hyaluronic acid in a layer-by layer system and then treating with chemical infiltration to mimic materials like bone and nacre which are present in nature. Collagen has the ability to precipitate into collagen fibrils, this process is called

fibrillogenesis of collagen (224). Collagen fibrillation is a strong function of external pH. At a low pH 3 no fibrillation of collagen occurs compared to higher pH's where collagen reaches near its isoelectric point of 9.3. Charged amino acids are balanced and molecules tend to favour the elongation configuration resulting in fibrillation. The three main steps in collagen fibrillation include initiation, linear growth and lateral assembly.

Collagen fibril formation is greatly influenced by complex molecules and small ions. Research has reported that collagen fibril formation is mainly controlled by the presence of mucopolysaccharides (polyanionic in nature) demonstrating a two phase- nucleation and growth process. In the same period researchers (225) published Cl^-, F^-, $HCO3^-$, Br^-, I^-, SCN^- ions as the major accelerators on collagen fibril formation. Arginine, ornithine, citrulline, aspartic, glutamic and ascorbic acid histamine, creatine, acetamide, asparagines, glutamine, guanidine were reported as major components delaying collagen fibril formation in accordance to their concentration (225). These studies made up the foundation of collagen fibril formation in-vitro environment on low molecular weight electrolytes.

In this investigation type-I-collagen was used to synthesise collagen fibrils, the layer-by-layer technique was used to deposit the collagen on the surface of a sacrificial substrate (PMMA), this would allow for investigation of collagen fibril growth. The image below displays a SEM micrograph, magnification x 30 000 with a scale bar of 5 microns displays of a single layer of collagen, this shows the dense network of collagen fibrils present on the surface of the substrate.

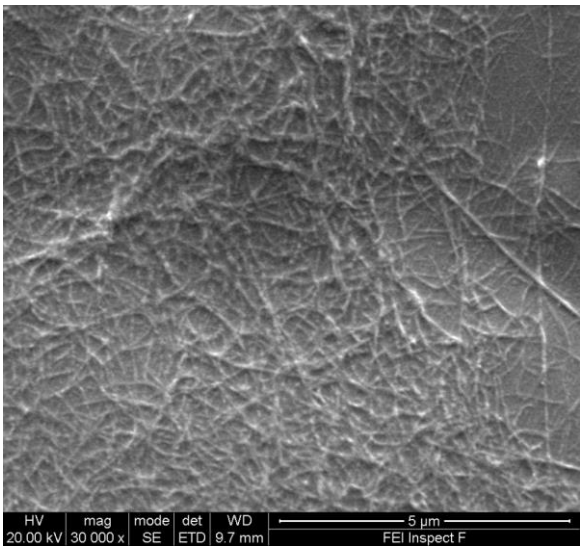

Figure 6.1. SEM micrograph a substrate with collagen fibrils deposited via the Layer-by-layer technique via dip coating.

In this case the collagen fibrils appear to be overlapping and spread across the surface of the substrate as depicted in figure 6.1, in some region the density of collagen is thicker. The top right hand side of the image shows a very low density of collagen fibrils and this could be due to the dipping process. The adhesion of collagen evenly on the surface of the substrate continues to remain a challenge and this can be seen in the image with the large spaces between the fibrils.

6.3. TEM on (HA-Coll)-one bilayer

In addition to this a TEM micrograph image was taken of (Ha-Coll)- single bilayer, when imaging samples in the TEM it is necessary to have an atomically thin and flat sample as this gives the ideal, optimum conditions for imaging. For this reason the l-b-l technique was used to create a single layer directly on the surface of the TEM imaging grid. From the TEM micrograph the translucent imagery displays the cross network of collagen fibrils within the hyaluronic acid, this gives the bilayer a spongy effect and the network of fibrils and can continue to grow within the HA. The layer-by-layer multilayer structure of the (HA-Coll) film is clearly displayed in TEM

images. The regions with a high contrast show the change in layers. The darker the images, the higher the electron density, therefore suggesting that there are more layers present for the electron beam to penetrate. The lighter area of the image shows a reduction in the thickness of the film and this is due to the lower electron density. The collagen fibrils are nanometres in diameter while the lengths range from nanometres to micrometres in length.

The TEM analysis on the single bilayers confirm the growth of the collagen fibres and this in turn confirms the effect of fibrillogenesis of the bilayer.

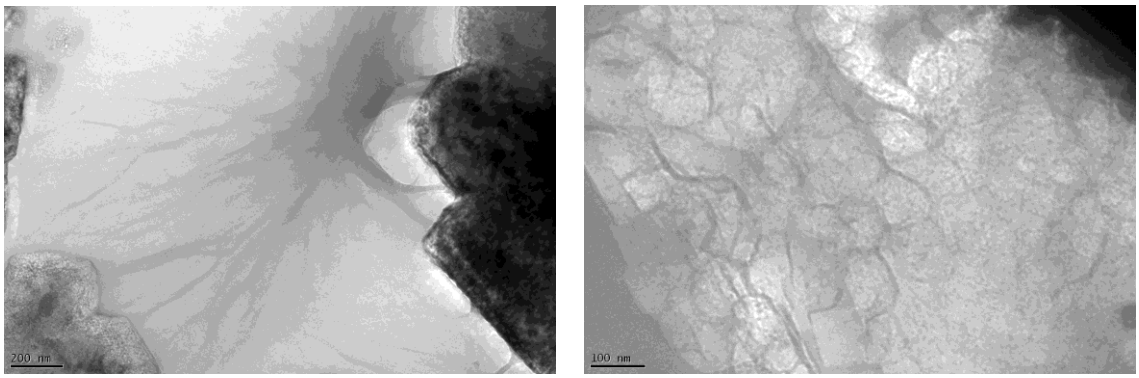

a. **b.**

Figure 6.2. TEM micrograph a substrate with collagen fibrils deposited via the Layer-by-layer technique via dip coating when combined with hyaluronic acid in a single bilayer.

From the previous section it was evident that collagen fibrillation took place on the surface of the single bilayer, the TEM now also confirm that the fibrillation is within the single bilayer and the HA forms a gel-like environment, together they aim to provide a dense network with great potential. In this investigation the growth of calcium carbonate is monitored within this dense network of collagen and HA and this is closer to what is present in naturally occurring materials.

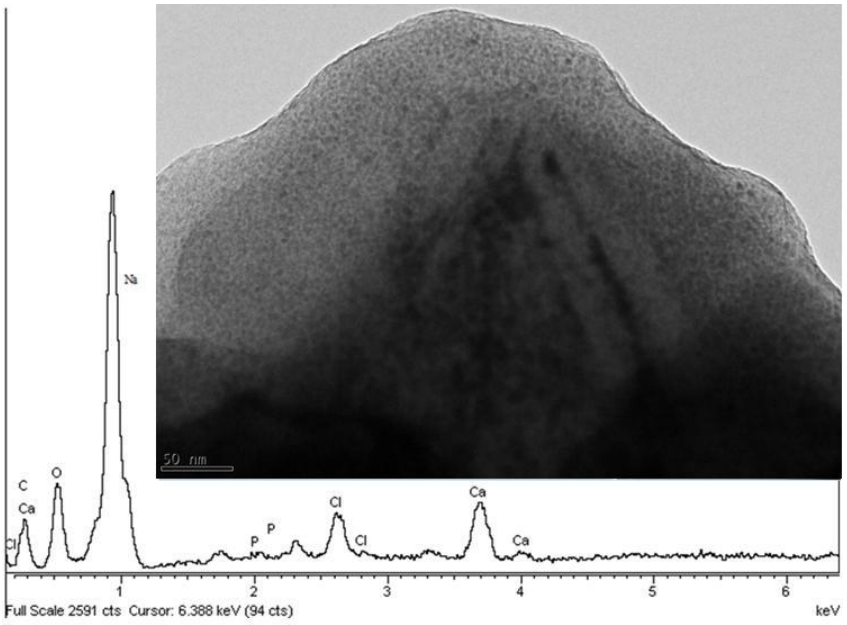

Figure 6.2. EDX spectra of PMMA(HA/coll $_5$ multilayer build using alternate deposition in $NaCO_3$ and $CaCl_2$, inset TEM characterization of thin film shows mineralisation to have occurred, 50 nm scale bar.

The EDX spectrum is an analysis of the bio composite PEM of the mineralised collagen and hyaluronic acid via layer-by-layer deposition into $NaCO_3$ and $CaCl_2$ solutions, the resultant film is depicted in the inset in figure 6.2.

The sample surface was analysed in the region where there appeared to be a higher density of mineralized collagen fibrils. The peaks corresponding to carbon and oxygen are present and this confirms the presence of collagen and $CaCO_3$, although this cannot be conclusive due to the presence of other material residue on the sample. There are also peaks related to phosphorus which could be assigned to contamination. There are peaks corresponding to sodium and chloride ions which are associated with residue from incomplete dissolution or exchange of counter ions during the layer-by-layer assembly processing method. The peak from calcium confirms mineralisation and the high electron dense areas produced in the TEM. No other elements were recorded apart from small copper peaks which arise from the sample grid. There is a high contribution that arises from calcium and carbon, and largely from oxygen. These values are similar

as those found in the studies (97) which recorded a similar contribution of elements when synthesizing HA-Collagen structures.

6.4. Visual inspection- SEM on (HA-Coll)

6.4.1. Controlling the number of bilayers in the PEM

Now that the growth of collagen fibrils has been established on a single bilayer, the layer-by-layer technique was used to continuously grow the film. The (HA-Coll) films were grown with 1, 20 and 40 bilayers. This was a continuous process. The SEM images below display the (HA-Coll) films. The PEM films were then kept in a hydrated state and, as described in previous sections, the film was infiltrated with calcium-chloride and sodium carbonate. This was a lengthy process as it was necessary to investigate growth within a natural polymer complex. The results can then be compared to that which exists in nature, in this case nacre, as discussed in the literature review (Section 2.0). Reinforcing the (HA-Coll) in theory should increase the mechanical stability of the film.

Figure 6.3a displays a planar cross section of the (HA-Coll) film, the film has been deposited on a PMMA substrate. This image displays only a single bilayer on the substrate of the PMMA, it is evident that the surface of the PMMA has been covered in a gel like coating. This is attributed to the hyaluronic acid in the PEM multilayer. In addition to this figure 6.3.b displays the film after infiltration of calcium carbonate, again there is no significant difference in the topography when comparing both the infiltrated and the non-infiltrated samples. The thickness of the film does not change, this can be associated with the fact that the sample was exposed to only one cycle of

calcium-chloride and sodium-carbonate, this would imply that there was not enough ionic transfer for mineralization to take place.

The collagen itself will have been dispersed randomly across the surface of the substrate; this was also recognized in studies conducted on collagen fibrillation (197) where it was established that the collagen molecules randomly distributed within the film and therefore had to undergo uniaxial stretching to produce a more regular pattern of distribution. This however was required for them to achieve crystallisation and for hydroxyapatite crystals to preferentially orient themselves along the collagen molecule. In this experiment, however, it was possible to produce the crystallisation along the collagen fibril which was found to occur in biological tissue. They earlier found that the inorganic material appears to be distributed all along the fibres or in patches extending over more than one fibre, and this was found to occur with the use of apatite crystals (197). The structure of the fibrils is also more apparent than that displayed in the cross sectional images of the TEM (figure 6.2). As the collagen and hyaluronic acid multilayer is formed, the collagen is embedded within the layer. As collagen only attaches to the surface of the multilayer it cannot be characterised when the multilayer exceeds one. This could also be down to the fact that the mineralization process exceeds the network.

It can therefore be concluded that the mineral has deposited within the fibrils. These SEM images are found to be similar to those in previous studies (198) which demonstrate the natural bone surface of canine femur which is described as loosely packed fibres of collagen. The infiltration process could also have created a thicker film as a result of a high concentration of collagen fibrillation locally, therefore creating larger surfaces for mineralisation. There appear to be nanoscale horizontal crack-like features in the collagen fibril that were observed at high

magnifications and this may suggest that there are crystals mineralising into the collagen fibril in the location of the gap zones.

In addition to this, the single bilayer thickness in this case is on average 1.5 μm in thickness. The single bilayer covers the surface of the film and this could be attributed to the nature of the biopolymer. The collagen fibrils are not visible here in these SEM micrographs, this could be a result of the small concentration of the collagen film that was used to make the solution. Studies (199), found that the thickness of the PEM is increased upon the deposition of collagen layers however it is decreased with the addition of hyaluronic acid therefore having the opposite affect and this is cause by the diffusion of the HA into the porous collagen structure adsorbed on the substrate.

The PEM structure was found to be affected by pH's nearing physiological pH from 4.0 - 7.0. They also found that the rinsing steps of the PEM also had an effect on the adsorption of a newly deposited layer and the thickness of the PEM was increased by rinsing the film less vigorously and consistently, with constant flow of a buffer solution- not water (199). This however does not agree with the findings of other research groups (200). It has been reported that the washing step may not be essential as it is "impossible to break the few bonds by simple washing". Unless, there is repulsion from electrostatic forces where all binding sites to the previously adsorbed layer are saturated, the bonds cannot be broken and the process is irreversible (200).

a. **b.**

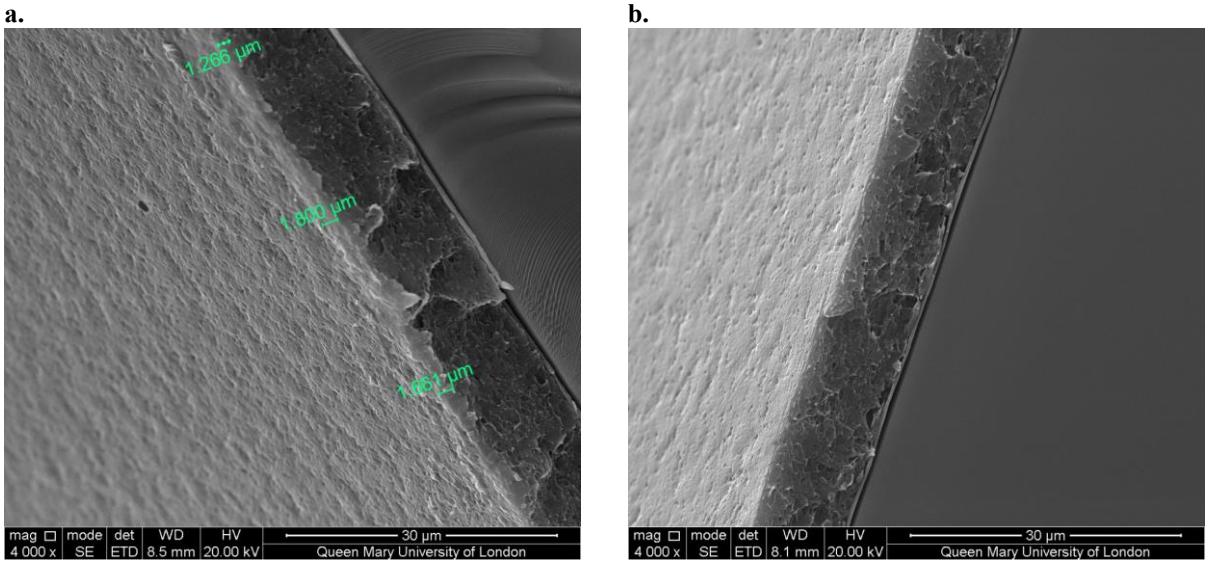

Figure 6.3. SEM micrograph of (HA-Coll)1 with a single bilayer, a. displays a single bilayer with no chemical infiltration at a magnification of magnification x4000 and scale bar of 30 microns. b. Displays (Ha-Coll-$CaCO_3$)1- 1 bilayer with chemical infiltration, magnification x4000, scale bar is 30 microns.

The build-up of multilayer films exhibits a linear growth regime with the successive layer depositions, leading to a uniform and dense fibre network, fully coating the supporting substrate. This phenomena has also been observed by other researchers (223) in this field. This can be further demonstrated as the number of bilayers are built up further.

Figure 6.4.a displays (HA-Coll) 20 bilayers, collagen and hyaluronic acid complex displays gel like properties. From this image it can be seen that the film is thicker than the single bilayer, on average the thickness can be calculated to 2.8 µm. Previous investigations on the film growth of hyaluronic acid indicated that the adsorbed amount of hyaluronic acid is generally smaller than the adsorbed amount of collagen in the PEM matrix even if it varies with the layers. There are many reasons that may attribute towards the growth of the film thickness, HA most likely forms networks composed of double stranded helices that are one or two helices in width. Since the molecular dimension for an HA helix is approximately 5 Å, the notion supported is that HA is adsorbed in the form of flat sheets of HA double helices. The collagen,

however, has notably higher molecular dimensions, and its lowest structural unit is the micro fibril that has a width of 4 nm and approximate length of 500 nm. It might therefore adsorb with the micro fibrils lying in a side-by-side configuration. Thus leading to a continuous growth of the multilayer. During the layer by layer process the substrate is exposed to the collagen and the hyaluronic acid for the time. This exposure time may affect the diffusion rate of the molecules. This in turn can hinder the aggregation of the molecules and thus the density of the PEM, common adsorption times for polyelectrolytes range from 5 to 20 min.

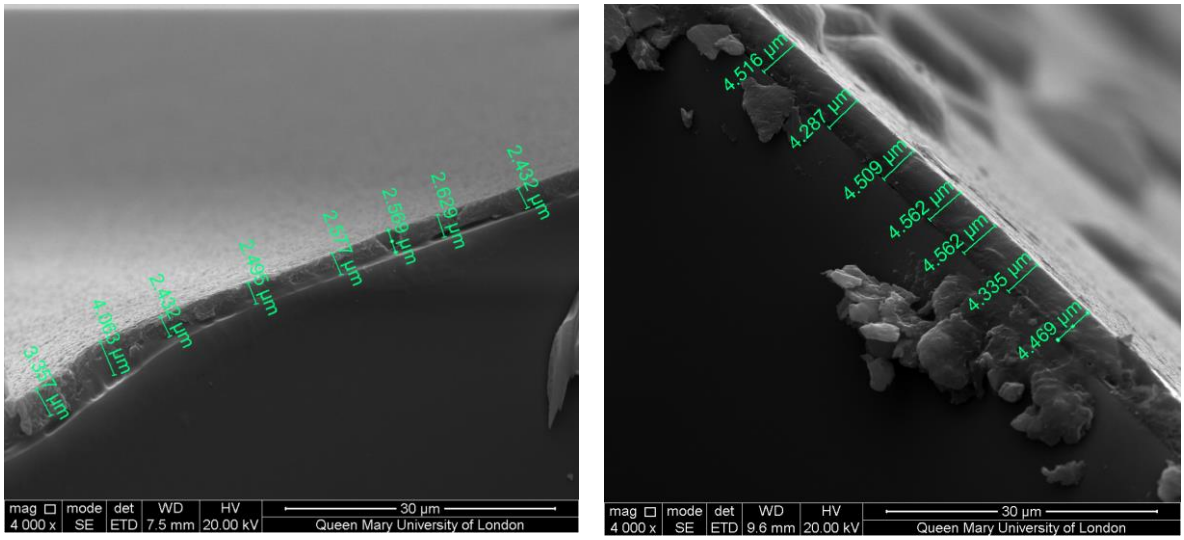

a. **b.**

Figure 6.4 . SEM micrograph of (HA-Coll) 20 with a 20 bilayers, a. displays a single bilayer with no chemical infiltration at a magnification of x4000 and scale bar of 30 microns. b. Displays (Ha-Coll-$CaCO_3$) 20- 20 bilayers with chemical infiltration, magnification x4000, scale bar is 30 microns.

Figure 6.5 a and b display the (HA-Coll) multilayer produced at 40 bilayers through the automated layer-by-layer mechanism. From this it may be seen in figure 6.5a that the film appears to be mechanically stable in its form. The bonding between the collagen and hyaluronic acid multilayer is relatively strong compared to the bonding between the film and the substrate. This can be deduced from this image because the film is intensely pulling away from the substrate surface.

Figure 6.5a. is purely the 40 bilayers of collagen and hyaluronic acid with no other infiltration, the film exhibits an extremely smooth surface with a uniform cross section to illustrate its consistent nature. The uniform thickness can be attributed to the synthesis and processing mechanism of layer-by-layer assembly. In addition to this, the average thickness of the 40 bilayer sample is calculated to be 3 μm in thickness. Surprisingly this is not hugely different to the 20 bilayer PEM, in fact the film thickness is practically the same. However, the massive difference in morphology is clearly exhibited in the infiltrated sample. The PEM can clearly be distinguished from the substrate which is atomically flat. Comparatively the topography of the sample is also radically different. The infiltrated sample has a rougher surface, there are no particles protruding from the surface, so potentially the diffusion and growth of calcium carbonate has taken place beyond the surface of the film. The cross section displays a regular structure and there is no outer crust on the surface of the film. This indicates uniform homogeneity of the film. There are globular deposits on the surface of the film which result in a rough surface and this could be due to the growth of calcium carbonate within the multilayer and on the surface of the film.

In addition to this, the surface roughness may also be a result of high flexibility and polymer entanglement of the polymeric chains. Research in this field (226) concluded that as a result of the conservation of the inner interface widths that occur during layer-by-layer deposition from the polyelectrolyte solutions the surface of the PEM is often left with a collapsed dry surface. Research also concluded that the polymers' internal interfaces interpenetrate as new layers adsorb onto the previous layer and the chains are said to be in a swollen state (201). The collagen fibrils are embedded within the PEM while the rest of the substrate maintains its smooth morphology. This sample cannot be imaged at a higher magnification due to the

sensitivity of the substrate under higher temperature and focus of the electron beam which results in damage to the collagen fibrils.

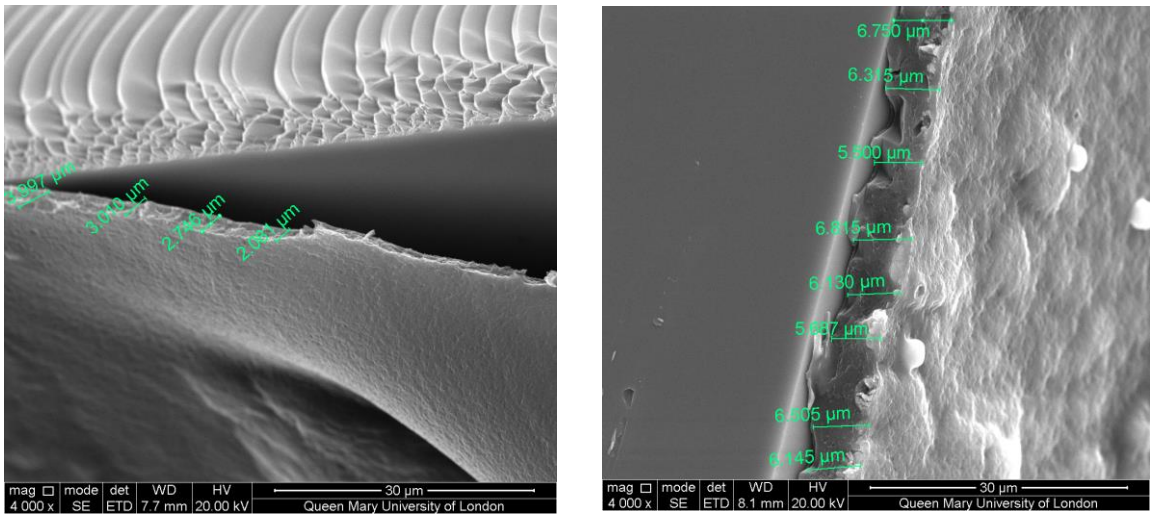

a. **b.**

Figure 6.5 . SEM micrograph of (HA-Coll)40 with a 40 bilayers, a. displays a single bilayer with no chemical infiltration at a magnification of x4000 and scale bar of 30 microns. b. Displays (Ha-Coll-$CaCO_3$)40- 40 bilayers with chemical infiltration, magnification x4000, scale bar is 30 microns.

It is possible that a non-linear increase in the thickness of the film is present. The reasons for a non-linear increase can be described by the biopolymer interactions. The nature of their compact stacking means more layers can be alternately formed with decreasing space in-between each layer. Results showed that collagen and HA have a random order arrangement resulting in a more irregular formation and this increases the distance between each layer due to the presence of particles. The lack of compact stacking of a substantial amount of layers i.e. 60 means that the overall thickness for (HA-Coll) 20 will be significantly lower when compared with (HA-Coll) 40.

The increase in thickness of the 40-bilayer composite can also be described according to the nature of polymer and inorganic component matrix. The matrix plays a huge role in the nanoscale construction of a material. The image clearly demonstrates all the layers are uniform and within a compact matrix system, this functionality

adequately allows the inorganic particles to fill any voids present. within the porous material. The organic matrix is critical as it regulates the precipitation in biological materials. As the self-assembly aspect is not a possibility, it is important that organic films are fabricated in an ordered manner and this is deduced clearly from the layer-by-layer phenomena. The polyelectrolytes were formed separately before infiltration to allow good integration of $CaCO_3$ within the ordered matrix and solutions were refreshed at regular interval to prevent contamination and impurities.

As the bilayer number has been increased, the PEM structure appears to separate from the substrate. This is due to the strong electrostatic interaction between the polyelectrolyte layers. There are also the charge interactions that arise as a result of the negative charge of PAH and the positive charge of PSS. These interactions create a structure that can stand separate from the substrate as these forces are stronger than the charge interactions and van der Waals forces between the PMMA and the first polyelectrolyte layer.

Comparing these bio-composites again with naturally occurring materials like nacre, where the bioorganic polymers (chitin and proteins, 10 to 50 nm in thickness) and aragonite platelets (200-900 nm in thickness) form an ordered, “brick and mortar”-like structure. The polymeric part provides elasticity and adhesion while the aragonite tablets act as rigid building blocks. For this reason, nacre is 3000 times tougher than its main component, namely aragonite. Various mechanisms have been proposed for this high toughness, in particular, organic material adhesion, presence of asperities and importantly, the patterned surface of the aragonite surface which generate a locking mechanism, hardening and spreading of non-linear deformation around defects and cracks. In nacre, a crack cannot move through the platelets but has to travel around them, the resulting increased crack length then being responsible for an enhanced work of fracture. This may be attributed to the orientation of the

layered structure and also the reinforcing inorganic material which maintains the structural integrity of the architecture whilst increasing its surface area. The nanometre size of the mineral crystals in nacre is important to ensure optimum fracture strength and maximum tolerance of flaws. For nacre the calculations show that the mineral crystals should have a minimum thickness of 200 nm (202-204)

6.5. Mechanical performance of (HA-Coll-$CaCO_3$) PEM multilayers

The mechanical performance of (HA-Collagen) thin films was tested, the tests demonstrated a high level of mechanical integrity. As a continuation of the process, the mechanical performance of the films was measured using nano-indentation, the testing was conducted at IMRE A* Institute of Materials Science and Engineering. The table below identifies the Young's modulus of the biological polyelectrolyte multilayers.

There is a general trend indicating that upon increasing the number of multilayers the Young's modulus also increases. The modulus practically doubles from one single bilayer to 40 bilayers and this is an extraordinary indication of the strength of the (HA-Collagen) network, that which is present in nature. Considering the 40 bilayer structure further, it can also be seen that as the sample is infiltrated with calcium carbonate there is an increase in Young's modulus of 1 GPa. Supported by the SEM micrographs- which confirm the free-standing and highly compact films this can be recognized and the calcium carbonate effectively acts as a reinforcement mechanism in this composite material.

Table 5. Displaying the Young's modulus values attained for the various biological PEM's.

Sample	Young's Modulus / GPa
(HA-Coll) 1	3.9 ± 0.10
(HA-Coll-$CaCO_3$) 1	4.3 ± 0.23
(HA-Coll) 20	5.2 ± 0.07
(HA-Coll-$CaCO_3$) 20	5.3 ± 0.08
(HA-Coll) 40	6.5 ± 0.17
(HA-Coll-$CaCO_3$) 40	7.5 ± 0.42

Previous studies took into consideration the stability of an organic matrix. A uniform matrix was highly likely to produce an organized and self –assembled structure. This contributes to enhanced mechanical properties with compact integration of the multiple phases. Stress concentration points resulting from the pore density may lead to failure of the material at a much lower yield stress when conducting tests like nano-indentation. Conversely, having pores that span vertically across the whole length of the film may be an ideal design for the sufficient deposition of $CaCO_3$ throughout the film, as a uniform surface can potentially act as a barrier to the $CaCO_3$ particles and may prevent optimum infiltration conditions which explains the mechanical performance of the (HA-Coll-$CaCO_3$) 40 bio composite.

The mechanical integrity of the PEM may also be attributed to the mineralized collagen fibril network across the surface and penetrating within. This could be considered as evidence of intrafibrillar mineralisation according to studies (207-208) intrafibrillar mineralisation was prominent but instead of synthesizing a matrix a collagen sponge as the matrix for mineralization was used and produced the sub-fibres encased in mineral, which was shown in similar SEM images to those produced in the PEM biopolymers resulting in a compact high strength structural design.

The (HA-Coll) values before and after infiltration reflected a general trend and behaviour expected of the films, whereby an increase in strength was expected after infiltration. The Elastic modulus increased with the addition of an inorganic component. However for the 20 bilayer samples there was no significant increase in modulus, a feasible explanation could be that the inorganic particles may have caused swelling of the biopolymer films which may have reduced the density of the films that could be a cause for the reduction in stiffness. The modulus values gathered from (HA/Coll)$CaCO_3$) 40 were a much better reflection in the overall mechanical properties. Values up to 7 GPa were achieved.

This is reinforcing evidence that although the porous structure on its own does not contribute much in terms of its stiffness, it provides an effective matrix for small inorganic particles to precipitate and form a composite with enhanced mechanical properties. The results clearly show modulus values improved significantly. Although the results display a good basis for enhanced mechanical properties, a wide variation of modulus values across a small space of 50 μm is big cause for concern. The desired properties should show homogenous values across the whole bulk, which was not the case here. Further work needs to be conducted to improve the homogeneity of the mineralization process and compare this with the current methodology.

6.6. TGA Analysis on planar films (HA-Coll-$CaCO_3$)

The objective behind the chemical analysis of the film was to establish whether the carbonate particles had precipitated within the films. Samples were also quantified in terms of the inorganic component. All TGA plots show a similar degradation pattern during the initial stages. The general trend being that there is a 5 % mass loss during

the first 250 ºC. At 200 ºC over 95 % of the sample is still present. This shows that at this point any water or moisture that would have been present has been completely eliminated from the sample. It is common to expect a sharp peak only at 100 ºC instead of a gradual decline. This doesn't occur because of the presence of zeolitic water. The addition of minute minerals increases the boiling point of water and this can span anywhere between 100-250 °C.

Continuing on from 250 ºC there is a huge drop in weight percent. The mass being degraded here is predominantly organic compounds including hydroxides and hydrated oxides. The remaining degradation leading up to 500 ºC involves the dehydroxylation of hydroxyl groups. The resulting measurement curves for all planar samples undergo similar degradation patterns. Only one sharp drop in mass was exhibited that would correspond to the organic polymer. Polymers are made of different bonds, thus the input of heat and energy required to disintegrate each bond is different as each bond is associated with a critical dissociation to initiate depolymerisation. Depolymerisation is the reversal of free radical addition reactions, whereby the dissociation energy of each bond dictates the degradation behaviour. For example, a single C-C bond would be typically around 384 kJ/mol (varies depending on spatial environment).

Depolymerisation is more likely to occur if main chain scission is feasible or the dissociation energies are comparatively lower. The reaction usually begins with chain scission of the end groups as these bonds usually have the lowest dissociation energy. Elimination of side groups would occur at higher temperature because the bonds are more stable due to secondary and tertiary covalent bonding. Stronger bonding present such as crosslinking would hinder the depolymerisation process via stiffening but would eventually be broken at a higher temperature.

A typical TGA graph is shown, displaying the multi-stage decomposition behaviour which is characteristic of calcium carbonate. The final stage is where all moisture is removed and the sample has been already exposed to extreme temperatures and has been incinerated. In this case, for 40 bilayers, the final stage of decomposition takes place between 500-900 ^{o}C and this curve trend can be used to identify the remaining inorganic phase which remains as a residue in the sample.

The weight loss as a function of temperature was carried out in standardized settings as described in section 2. The sample was heated up from 30 ^{o}C to 900 ^{o}C at 10 ^{o}C per minute to allow complete degradation of the sample .The data gathered show five main distinctions for mass loss:

1. 25 ^{o}C-250 ^{o}C: Corresponds to loss in moisture and zeolitic water
2. 250 ^{o}C-400 ^{o}C: Loss of organic compounds, hydroxides and hydrated oxides
3. 400 ^{o}C-500 ^{o}C: Loss of combined water- dehydroxylation of hydroxyl groups
4. 500 ^{o}C-900 ^{o}C: Corresponding to the losses of carbonates from aragonite and calcite.

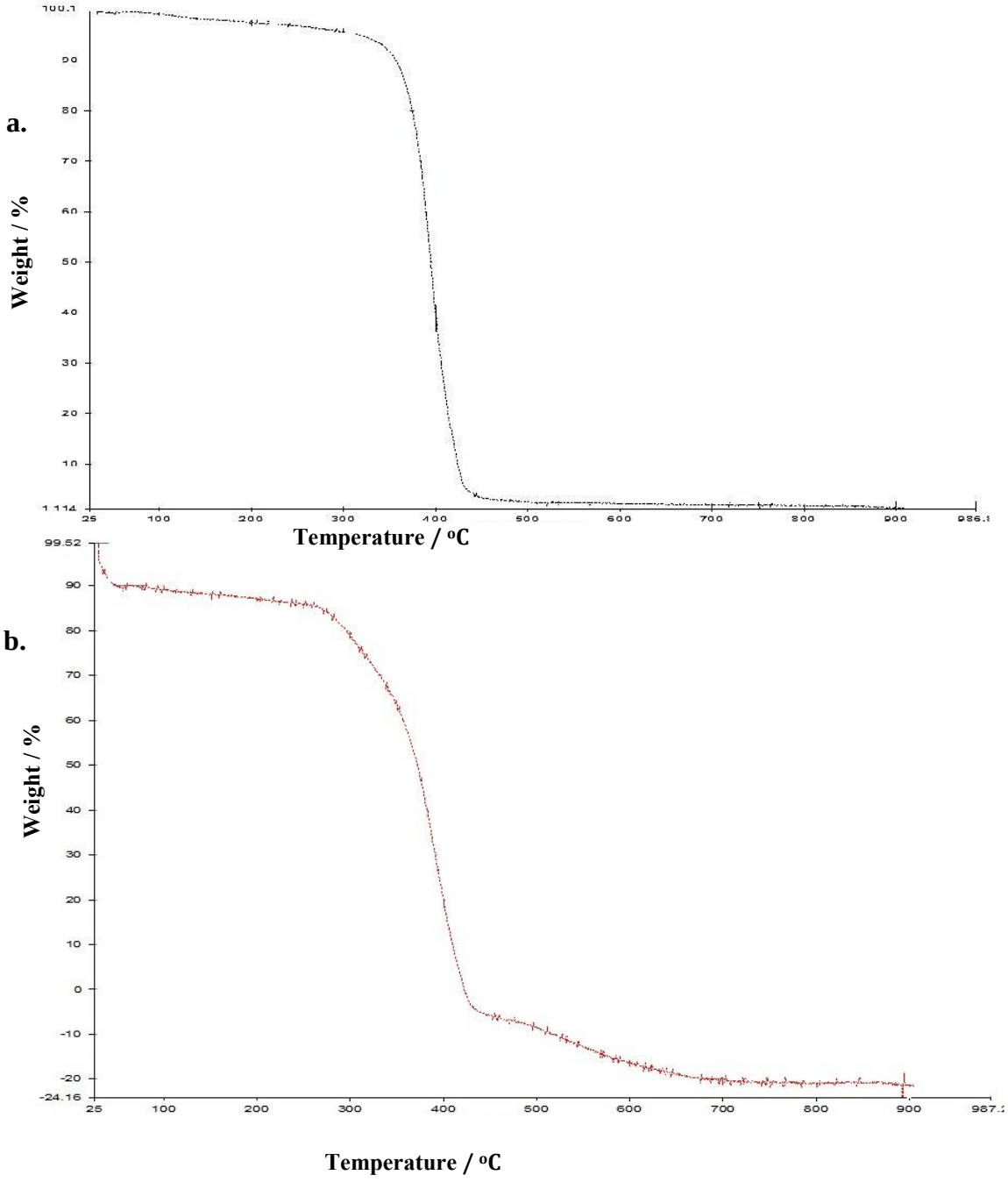

Figure 6.6. TGA curves displaying the degradation profiles where n= 0 (*a.)*, 1 (*b.)*, 20 (*c.)* and 40 bilayers (*d.)* with infiltration cycles synthesised using (HA-Coll) on planar 2-dimensional films.

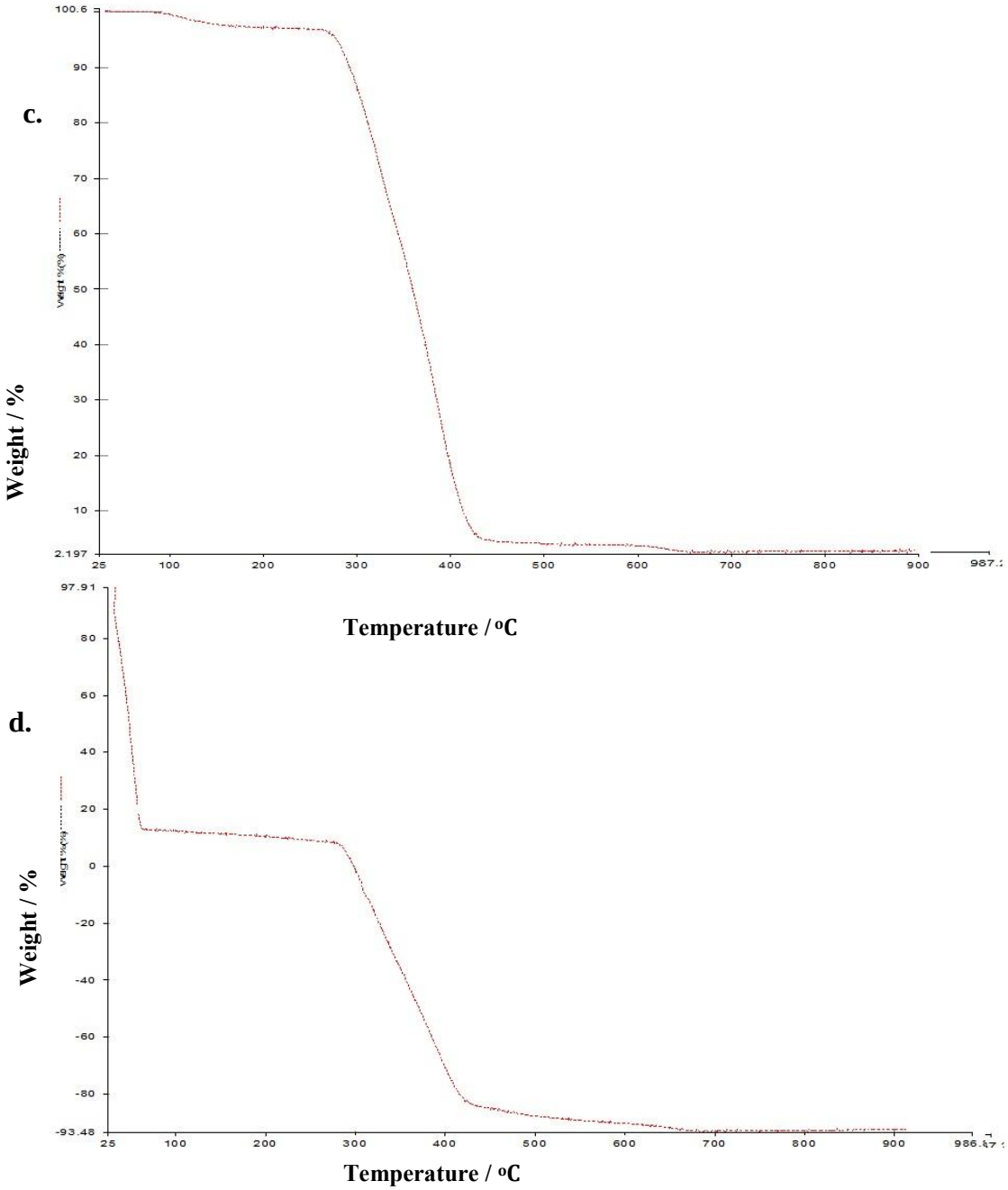

Figure 6.7. TGA curves displaying the degradation profiles where n= 0 (*a.)*, 1 (*b.)*, 20 (*c.)* and 40 bilayers (*d.)* with infiltration cycles synthesised using (HA-Coll) on planar 2-dimensional films.

From the SEM analysis and review of the film growth and mechanical properties of the planar film, the next step is to analyse the effect of the infiltration process on the film structure, both planar and modulated 3-dimensional surfaces.

The following table identifies the calcium carbonate content in each sample relative to the mass loss, which occurred at each of the stages, as described and depicted in figure 6.6, resulting in the decomposition process. TGA is a destructive testing process. Beginning with the planar samples, it may be seen that from the TGA results the single layer of (HA-Coll-$CaCO_3$) deposited was not sufficient enough to yield any calcium carbonate in the test. This does not mean that the sample did not contain any calcium carbonate, in fact from the SEM and the nano-indentation results it is evident that there is a change in properties and performance of the material. The lack of yield in the TGA may be attributed to the nature of the sample, the region of the sample which was tested, or even the fact that the sample was just too thin to give any conclusive data.

Table 6. Displaying the content of calcium carbonate present in the planar biological PEM's

Sample	Temperature Range ºC (mg weight loss in each range)				$CaCO_3$ (%)
	25-250	250-400	400-500	500-900	
(Ha-Coll- $CaCO_3$)1- Planar	-	-	-	-	-
(Ha-Coll- $CaCO_3$)20 - Planar	0.11	1.35	0.57	0.09	4
(Ha-Coll-$CaCO_3$) 40- Planar	0.14	1.09	0.23	0.06	16

As the number of multilayers are increased, (HA-Coll-$CaCO_3$) 20 bilayers, there is a 4% yield of calcium carbonate within the sample. Increasing the bilayers further, the inorganic content increases 3-fold. This is supported by the SEM micrograph images which displayed a significant increase in thickness and a high level of bonding between the multi-layer composite materials.

6.7. Conclusion

Although further investigations are necessary to clarify the reasons, it is apparent that the number of bilayers have a direct influence on the order of layer-by-layer assembly. The biological matrix is also an influencing factor on the growth of calcium carbonate during the infiltration process. The more pores and voids that are available within the matrix, the higher the likelihood of diffusion of ions and growth of the inorganic phase- thus having a direct effect on the strength of the material. These parameters were controlled during the investigative process in addition to the number of layer-by-layer cycles used for the preparation of each sample type. Furthermore from the experiments described above it becomes evident that the concentration of the solution influences the synthesis of the inorganic phase within the bio composite in addition to the number of deposition cycles and as number of bilayers are increased from 1 to 40, the percentage of calcium carbonate increases by up to 4 times, reflected by the mechanical integrity of the film.

7. Synthesis of biological PEM's via Layer-by- Layer Assembly with Collagen and Hyaluronic Acid on Modulated Surfaces

7.1. Introduction

When considering Biomimetics, all naturally occurring materials are present on a modulated surface, when considering abalone shell, bone and antler, all these naturally occurring materials are modulated, uneven and vary in thickness, shape and size (227). One thing they do have in common is their structural integrity and this can be clearly seen in the brick and-mortar complex structures as described in the introduction. All the materials have a functional matrix which is duly reinforced with an inorganic component. In nacre this is namely calcium carbonate.

7.1.1. (HA-Coll)n on a modulated three dimensional surface

Taking the above into consideration, the design features of a layer-by-layer polyelectrolyte assembly on a three-dimensional surface was investigated through a nano-patterning technique. A modulated surface was created and the behaviour of collagen and hyaluronic acid in the formation of modulated surfaces was analysed. Although in the early stages of research, this had never been attempted before and so using these biopolymers as a means to create fully biological vesicles was an interesting and innovative concept.

The samples were prepared as described in section 2 and the biological polymers were used in order to create the multilayer composite, using the same method and composition used to create the planar films previously. Prior to sealing these moulds and dissolving the sacrificial template the diameter of the wells was monitored.

The following samples were prepared in three dimensional arrays:

1. (HA-Coll)- 1 bilayer
2. (HA-Coll)- 1 bilayer- infiltrated with calcium carbonate
3. (HA-Coll)- 20 bilayers
4. (HA-Coll)- 20 bilayers- infiltrated with calcium carbonate
5. (HA-Coll)- 40 bilayer
6. (HA-Coll)- 40 bilayer- infiltrated with calcium carbonate

SEM analysis was conducted on the samples prior to sealing and dissolving the sacrificial template. Figure 7.1a displays the surface of the wells with only one deposition cycle of (HA-Collagen), prior to infiltration it can be see that the wells seem to have a slight film on the opening, comparatively 7.1b, displays the same sample after chemical infiltration, the wells are clear. In addition to this, the sample surface is also relatively smooth with no mixed depositions or surface roughness. The diameter of the original well is 2 μm. After one deposition cycle it was possible to measure the thickness of the deposition. After one deposition cycle the thickness was measured to be 0.26 ± 0.03μm. After infiltration this incrementally increased to 0.29 ± 0.04 μm.

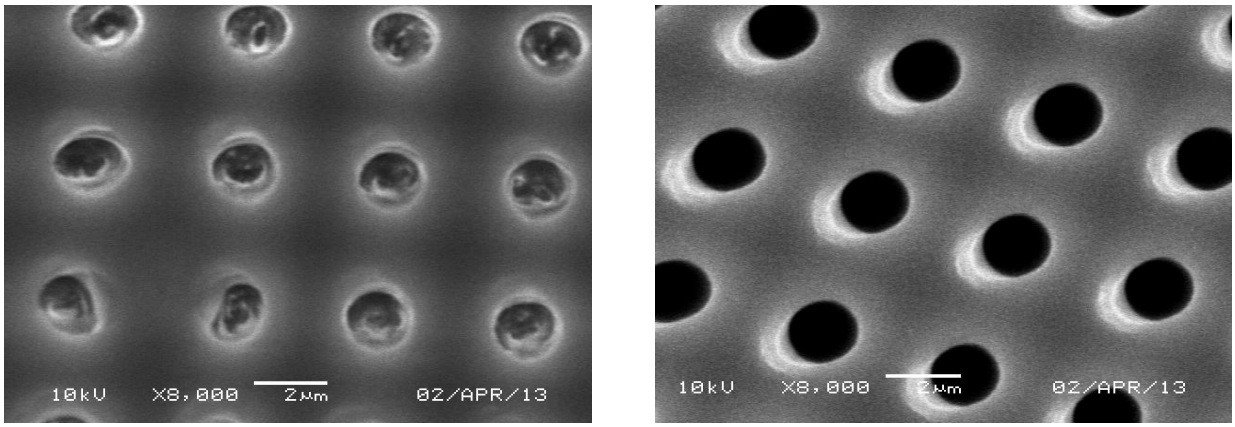

a. **b.**

Figure 7.1. (HA-Coll) 1 bilayer, top down view a. before sealing and b. after sealing.

As the deposition cycle was increased to 20 bilayers (figure 7.2) there was not much difference in the appearance of the non-infiltrated sample, the sample surface seemed slightly uneven, the film thickness on average was calculated to be 0.26 μm again. This was surprising considering on a planar surface the film thickness was also incrementally increasing. However once the sample was infiltrated with calcium carbonate there was a notable change in the diameter of the micro-wells. From the SEM image it can be seen that the wells seem to be shrinking in size, this is due to the film growth on the inside of the well. The film thickness after infiltration increased to 0.32 μm and this is notable. This follows the trend shown in the planar films and the thickness of the bio composite material continues to increase. There is no evidence of calcium carbonate crystals or deposition on the surface of the sample, this suggest that the infiltration is taking place in the film within the bilayers where there are pores in the structure and where crystallization can take place across a relatively constant diffusion gradient.

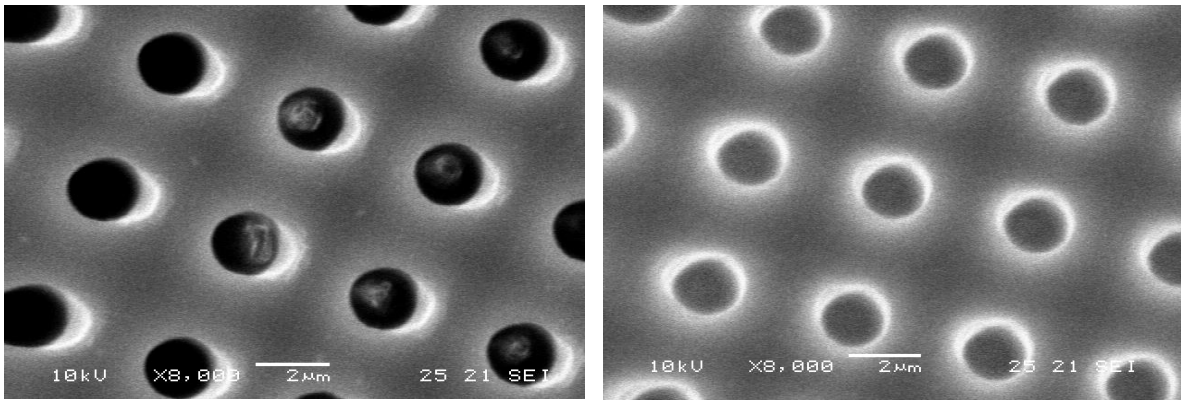

a. **b.**

Figure 7.2. (HA-Coll) 20 bilayer, top down before, a. infiltration and after infiltration b.

Finally, the number of multilayers was increased to 40 bilayers, the (HA-Collagen)-40 bilayer sample (figure 7.3) does not exhibit an extreme growth in thickness, this can be attributed to the fact that the strong intermolecular bonding between collagen

anh hyaluronic acid has created a strong, compact multilayer, whereby the film thickness in the well is 0.3 ± 0.01 μm. Once again infiltrating the sample meant that calcium chloride and sodium carbonate were diffused within the film and this significantly increased the thickness of the film to 0.41 μm**.**

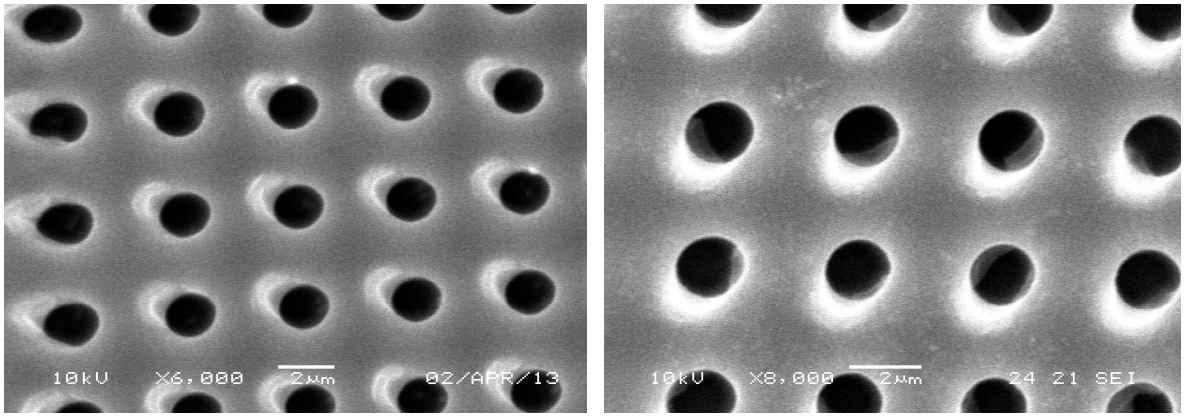

a. **b.**

Figure 7.3 (HA-Coll) 40 before sealing (a) and after infiltration, (b) (HA-Coll-$CaCO_3$)40.

7.2. Thickness of wells

The table below summarises the multilayers within the three dimensional assemblies corresponding to the sample type. The HA-Collagen films prior to infiltration are consistent in thickness however once infiltrating the samples they show a considerable change, this is in good agreement with the SEM images analysed.

Table 7. Displaying the sample type and the thickness of the micro well wall

Sample Type	Thickness depending on diameter of wells / μm
NO MULTILAYER	**2**
Coll- HA-1	**0.26 ± 0.03**
Coll- HA-1-1i	**0.29 ± 0.04**
Coll- HA-20	**0.26 ± 0.04**
Coll- HA-20-20i	**0.32 ± 0.01**
Coll- HA-40	**0.30 ± 0.01**
Coll- HA-40-40i	**0.41 ± 0.02**

Upon analysing the top-down images of the well, the next step was to seal the sample on a silicon wafer, this involved dissolving the substrate (the sacrificial PMMA) with toluene solvent. The (HA-Collagen) polymer complex displays gel like properties. This can be seen in the surface topography and dimension of the three-dimensional pillars created. It can be seen from the figure 7.4 below that the pillars have very low structural integrity with a single bilayer.

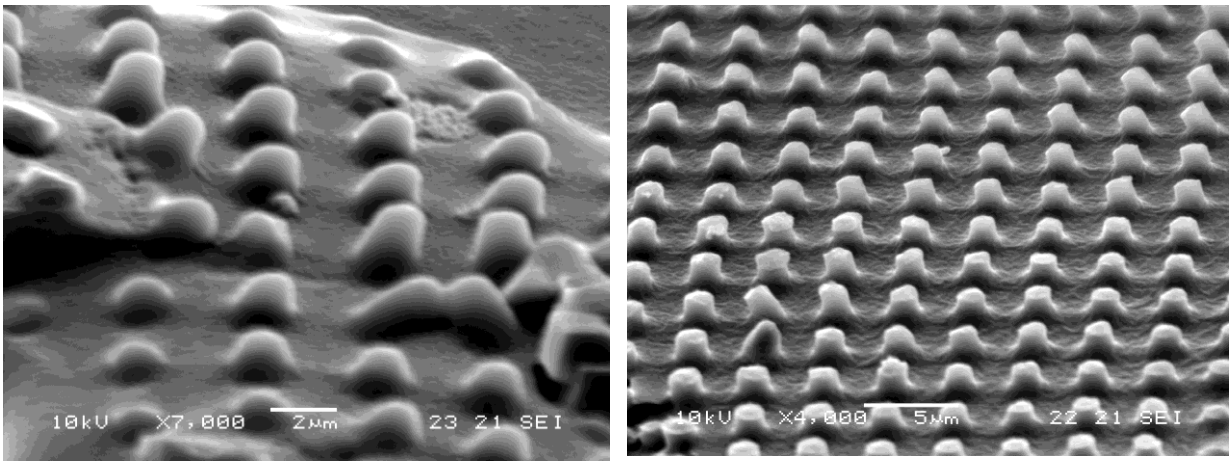

a. **b.**

Figure 7.4. (HA-Coll) 1 before infiltration (a) and after infiltration, (b) (HA-Coll-$CaCO_3$)1

The pillars are not a consistent shape and the bio-polymer did not manage to fulfil the mould. The mould size was 2 µm x 2 µm, from the image it is visible that at a higher magnification not all the pillars were formed and they are less than 2 µm in height and depth. The surface is also uneven and the film is not uniformly deposited. Prior to being infiltrated with sodium carbonate and calcium carbonate, the film displays poor surface topology and an uneven surface. This can potentially be attributed to the rinsing mechanism during the layer-by layer assembly procedure. If proper rinsing practices were not established between the individual layers, then this could have affected the film formation on the sample surface. and this is important when a PEM matrix is constructed. If a weakly adsorbed polyelectrolyte stays on the surface after

the rinsing step, the next layer of positively charged polyelectrolyte would be adsorbed to that layer. These layers can then detach during another rinsing step. Such detached areas were observed by visual inspection (no interference colours). It is essential to remove all weakly adsorbed polyelectrolytes.

As the film is infiltrated with one cycle of calcium carbonate, It is possible to see that the biopolymers covered the mould entirely as all of the moulds have a pillar protruding- seen on the lower magnification image. Although they appear swollen, it may also be deduced that that the single bilayer and single infiltration layer was not sufficient to cover the entire surface area of each micro well hence the appearance of the stumped well in figure 7.4b.

As the multilayers were increased to 20 bilayers (figure 7.5) the structure of the micro pillars once again changed, the pillars became more rounded on the top, gel-like in nature and appeared quite hollow. Upon infiltrating this same sample, the physical characteristics of the micro pillars changed further. The pillars appear to be strengthened and are less rounded on the top, the surface of the sample is also smooth in nature and the micro pillars have lengthened in size. The morphology of the pillars show consistency across the sample surface.

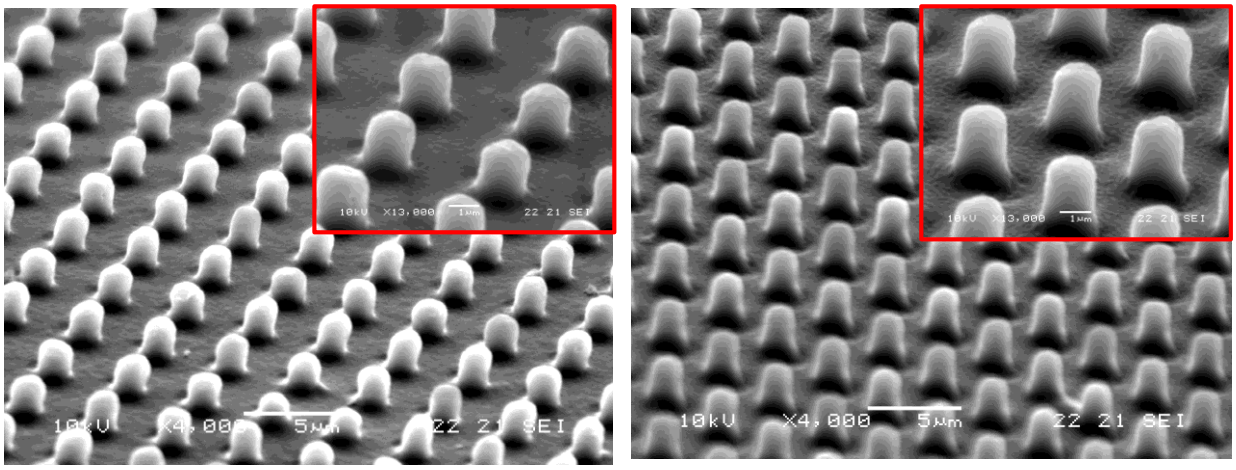

a. **b.**

Figure 7.5. (HA-Coll) 20 before infiltration (a) and after (b) (HA-Coll-$CaCO_3$) 20

To complete this study, the (HA-Coll) 40 bilayers (figure 7.6) was analysed, the sample displayed is contrasting compared with the previous samples, the surface of the sample appears to be layered and there are consistent wrinkles in the film. There is a possibility that like the planar counterpart the film was becoming independent of the substrate and this resulted in a compact formation of the array. The pillars appear to merge alongside each other in this sample and this could be down to the attraction taking place in between the micro chambers as well as beneath them. As the sample is infiltrated, there is a considerable change to the non-filtrated sample, the micro chambers appear to be heightened and fuller, each being independent of the other.

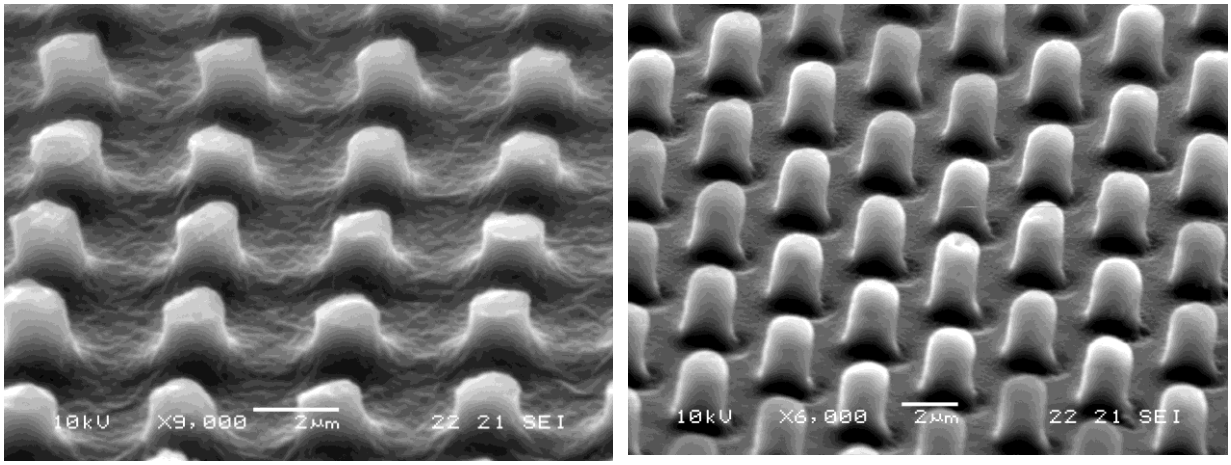

a. **b.**

Figure 7.6. (HA-Coll) 40 before infiltration (a) and after (b) (HA-COll-$CaCO_3$) 40

Considering the PEM sample is constructed first and then immediately infiltrated it is interesting to note the change in morphology of the micro chambers. This can be attributed to the growth and infiltration calcium carbonate within the micro chamber, thus resulting in a mechanically stable micro pillar which had been reinforced. The gel-like micro chambers have literally been transformed into solid, independent micro chambers upon infiltration and this illustrates the brick and mortar theory at the nano-scale.

7.3. TGA Analysis on three-dimensional arrays of (HA-Coll-$CaCO_3$)

Comparatively, assessing the yield of calcium-carbonate in the three-dimensional nanostructures also proves to be unattainable. This may be attributed to the nature of the sample taken, for 1 and 20 bilayers it was apparent that maybe the sample was not representative of the entire structure. However when increasing the bilayers to 40, the yield of calcium carbonate was found to be up to 30 -37% on average. This is depicted in the TGA curves displayed in figure 7.7 a. and b. respectively. The tests were repeated several times in order to attain consistency and reliability of results. A full comparison of sample types can be seen in Table 8.

The TGA content is supported by the SEM imaging as the nano-structures appear to be consistently different from the non-infiltrated samples. In addition to this the nano-indentation results also support the theory that the calcium carbonate reinforces the micro chambers, and calcium carbonate growth is occurring in the walls of the micro chambers through the chemical infiltration process rather than being deposited only on the surface of a sample.

There are several parameters which may have influenced the collection of TGA data. The heating was set to 10 °C per minute. This took approximately 90 minutes to go from 30 °C to 900 °C. Increasing the heating rate from 10 °C to 20 °C or possibly even higher rates requires shorter experiment times. The disadvantage of increasing the rate makes it increasing more difficult to approximate the mass loss from the graph because the process takes place too rapidly thus not allowing sufficient time for the TGA analyser to record the loss in mass.

Reducing the heating rate improves the accuracy of the reading but takes too long to complete, therefore selecting 10 °C is a feasible compromise and has been used commonly for calcium carbonate analysis.

It was noted that inorganic residue remained in the sample holder upon completion of the analysis. This was attributed to $CaCO_3$ which had not disintegrated. It was also observed that more residue was present in PSS/PDAMAC rather than PSS/PAH polymers complexes, indicating that a greater mass of calcium carbonate yielded from the (PSS-PDADMAC) polymers.

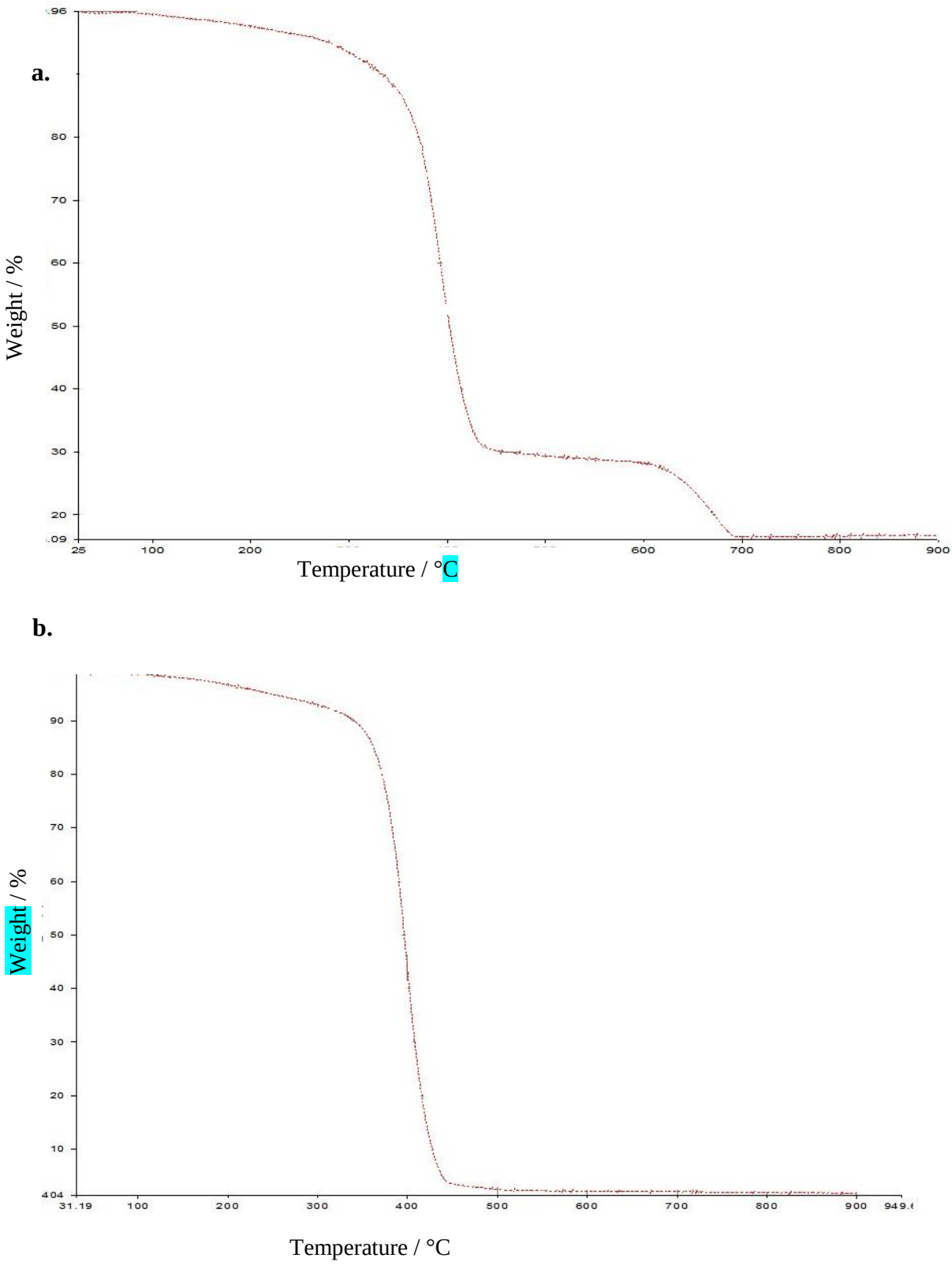

Figure 7.7 . TGA curves displaying the degradation profiles where n= 20 (*a.)* and 40 bilayers, (*b.)*, with infiltration cycles synthesised using (HA-Coll) on modulated surfaces with 3-dimensional assemblies.

Table 8. Displaying the content of calcium carbonate present in the planar biological PEM's and the three dimensional assemblies

Sample	Temperature Range °C (mg weight loss in each range)				$CaCO_3$ (%)
	25-250	250-400	400-500	500-900	
(Ha-Coll- $CaCO_3$)1- Planar	-	-	-	-	-
(Ha-Coll- $CaCO_3$)20 - Planar	0.11	1.35	0.57	0.09	4
(Ha-Coll-$CaCO_3$) 40- Planar	0.14	1.09	0.23	0.06	16
(Ha-Coll- $CaCO_3$)1- 3D Arrays	-	-	-	-	-
(Ha-Coll- $CaCO_3$)20 – 3D Arrays	-	-	-	-	-
(Ha-Coll-$CaCO_3$) 40- 3D Arrays	0.03	0.85	0.38	0.36	30
(Ha-Coll-$CaCO_3$) 40- 3D Arrays	0.07	0.52	0.60	0.39	37

A possible reason could be the failure to calibrate the sample using the microbalance simply because small sample size greatly increases the margin for error. It is therefore critical that the sample size meets the requirements. The sample size for the employed TGA machine had to be between 2-15 mg before running the test. Another factor may be temperature lag where the temperature in the furnace does not correlate with the temperature of the sample. This can result in lower ramp rates thus recording that the entire sample has been degraded (at a lower temperature) when in fact this is not the case. It could often be the case that some samples lack homogeneity that not consistent with the entire sample. Analysing a sample with impurities or one that has a composition that does not reflect the whole sample would produce varied results.

7.4. Conclusions

Overall, the successful fabrication of the (HA-Coll-$CaCO_3$) samples was achieved. The number of deposition cycles influenced the growth of the multilayer and variation between the infiltration processes achieved mineralization between the layering species.

Previous studies found that exponential growth is commonly accompanied by high surface roughness and high degree of diffusion but this wasn't seen to materialize for PEM's. It may be deduced that the type and combination of polyelectrolytes used have a significant effect on the composition of organic and inorganic components. A clear trend was established whereby the increased number of bilayers showed higher amounts of $CaCO_3$ around the polymer matrix as shown in SEM and TGA. The most conclusive results were found from the TGA investigation where values up to 160% inorganic mineral was attained from the 40-bilayer- mineralized sample. It was evident that these composites exhibited a higher degree of the desired 'brick and mortar' structure that showed improved mechanical stiffness.

Further work will be needed to control the overall mechanical properties of the nanocomposite. (HA-Coll-$CaCO_3$) demonstrated promising signs towards a highly structured composite via SEM. Chemical analysis and nano-indentation revealed that $CaCO_3$ was found to be dispersed in a well organised manner.

8. Three dimensional arrays of nanocomposite nano pillars via layer-by-layer assembly

8.1. Introduction

Nanotechnology has developed into an area of research with tremendous scientific and economic potential. Nanoscience is currently dominating the field with new, emerging materials being synthesized with a high level of control. This research continues to focus on the inorganic, organic, polymeric and biological fields of materials science with an outlook to identifying a relationship between structure and function at the nanoscale.

The technology transfer from nature to synthetic material is often called Biomimetics, biomimicry or bionics. An attempt to synthesise artificial nacre has been explored widely (228-229), in all approaches specific materials which are found in nature are reproduced, characteristics including; the architectural configurations and the materials characteristics are incorporated. The biggest hurdle lies in mimicking the architecture found at micro- and nano- scales in a way which allows the preparation of real, macro scale samples at a reasonable cost.

While there is still much work to be done in the creation and synthesis of these materials, attempts have been made to synthesise at the nanoscale by characterizing these basic building blocks. Further to the explosion of 'Nano' in the scientific field, nanomaterials are receiving much attention from a diverse number of disciplines, which can make use of these novel and highly architected systems.

This research focuses on the assembly of three-dimensional polyelectrolyte multilayers (PEM's) in an attempt to determine whether the chemically infiltrated nanostructures induce any resemblance to those found within biological composites. The three-dimensional structures are analysed in terms of their chemistry, topography and mechanical stiffness. There is much information on how PEM's work, however, the focus lies in acquiring a greater insight into the factors that influence PEM's during and after fabrication of these three dimensional structures and how these can be compared to naturally occurring inorganic materials like nacre and bone.

The bottom-up approach has been taken in order to synthesise materials at the nanoscale with complex architectural design. This approach involves the use of organic macromolecules as template for inorganic crystals to nucleate and grow from supersaturated solutions. Crystal growth is either accelerated or inhibited by the presence of an organic phase. This process is dependent on the functionality, molecular weight, concentration and density of functional groups on the polymer chains. Layered hybrid films showing high tensile strength and ductile behaviour have been synthesized based on a bottom up assembly and this was attempted in the following investigation.

Amongst the various approaches being explored in this field, layer-by-layer (LBL) assembly is highly recognized as one of the most simple, yet effective and versatile methods, whereby alternating deposition of oppositely charged components from dilute solutions or dispersions on a versatile, charged substrate material. The principles of layer-by-layer are effective, not only on bulk planar surfaces but also on micro/ Nano complex objects which may potentially have application in the field of biomedicine, efforts have been invested in improving and enhancing the propertied of

three dimensional structures to consistently gain a level of strength, permeability and structural integrity.

This part of the research will aim to describe the way in which hybrid nanostructures were synthesized using a controlled, automated system. The introduction of hybrid organic and inorganic films has further increased the scope of application for these films and their innovative and notable versatility has led to a number of novel designs and applications; biomimetic and bio-responsive materials, semiconductors, drug transfer systems and many more (113). The simple technique has thus led to an outbreak of research in this field which continues to evolve due to the limitless nature of the science.

8.2. Aims and objectives

The aim of this part of the research is to create a layer-by-layer composite arrangement taking into consideration the spatial arrangements of a structure. When partnering complementary groups of ions together, the layer-by-layer synthesis can result in complexes which can result in three dimensional structures when coupled with nano patterning techniques. In order to combine the multi functionality of these ultra-thin materials which have been previously investigated, it was essential to have precise control on the nanometre scale over the length, thickness and composition of the desired film.

For this reason, modulated surfaces were created and layer-by-layer films were fabricated via a direct-patterning route. The films were then lifted off the surface of

the substrate by solvent- assisted imprinting methods at room temperature described previously.

Previous work conducted in this area by Kiryukin et al. (157) focused on the modulated surface topography of the material in conjunction with the mechanical performance and buckling of the Nano structures, as depicted in the schematic in figure 8.1. Herein will be described the effect of layer-by-layer assembly and infiltration of inorganic calcium carbonate growth within the three dimensional arrays and the effect this has on the mechanical performance. This will be compared to the performance of naturally occurring materials like nacre, ultimately composites are formed in the lab on planar surface only, however exploration on a three dimensional array will give a significant insight on the growth mechanism of the multilayer in a simulated artificial environment.

Micro wells of 2 μm were imprinted on a PMMA substrate and prepared as described in the section 3. The PEM was constructed with two sets of polymers:

1. PSS/PAH and
2. PDADMAC/PSS

For these pairs of polyelectrolytes, two different regimes of PEM growth behaviour has been noticed and the growth of an inorganic phase- calcium carbonate has also been monitored through TGA analysis. The strengths of these materials were determined by nano-indentation of the arrays and compared with the mechanical performance of materials naturally present in nature- nacre and bone.

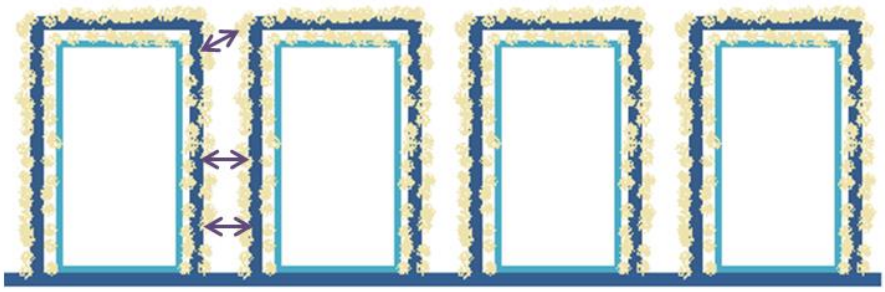

Figure 8.1. A schematic displaying the pillar structure and the infiltration process which will take place between the wells.

The investigation also aims to address the following:

1. Investigate how the three dimensional assembly will affect the morphology and growth of the film by performing optical imaging of the various conformations.
2. TGA analysis of the inorganic growth phase and determination of the quantity of the inorganic growth phase in relation to the number of cycles deposited in the multilayer during layer-by-layer assembly.
3. Nano-indentation- identifying the mechanical performance of the arrays of pillars and the comparison in relation to naturally occurring materials.
4. TOF-SIMS- To deduce the level of infiltration and to analyse whether the infiltration process was consistent throughout the length of the pillar itself.

In addition to the above, the imprint lithography process used to create the three-dimensional assemblies have yielded durable and consistent moulds patterns. However infiltrating the multilayer within a modulated PEM is still in in its infancy.

8.3. Structural characterization

The samples were analysed according to the techniques described in Section 2 of this report. Scanning electron microscopy (SEM) was carried out in secondary electron imaging mode at 5 keV with JEOL JSM 5600 (for planar images) and high-resolution FE SEM JSM-6700F (for cross sections) instruments. The cross sections of samples were analysed by freezing the PEM film transferred onto a Si support in liquid nitrogen followed by dicing the Si wafer abruptly. The thickness of PEM films was determined by analysing a minimum of five different regions of the cross section of the sample.

The following methods were used to analyse the samples:

- Visual Inspection of PEM Scanning Electron Microscopy (SEM)
- Thermogravimetric analysis (TGA)
- Nano-indentation
- Time-of-flight Secondary Ion Mass Spectrometry (TOF-SIMS)

8.4. Visual inspection of PEM multilayer

In order to address the effect of the multilayer on the structural properties of the three dimensional assembly the composite was made with a varying number of deposition cycles. For each configuration the following cycles were implemented to create a desired PEM for the given composition, n- is the number of deposition cycles.

1. (PSS/PAH)n – where n is: 10, 20, 40, 60 and 80 deposition cycles.
2. (PDADMAC/PSS)n – where n is: 8, 14, 20 and 40 deposition cycles.

Each PEM was infiltrated with $CaCO_3$ at the same number of deposition cycles for consistency and growth of the inorganic phase.

The fabrication of the patterned LAYER-BY-LAYER film is shown in figure 8.2, the spherical micro well arrangement is imprinted on the surface of the sacrificial PMMA

film. As PMMA is a thermal polymer, it can act as a resist component and works in conjunction with an established surface patterning technique. The imprinted PMMA can ultimately yield to a 100% yield and pattern fidelity. The PMMA also acts as a positive support for characterization, once the PMMA is transferred onto the PEI-coated silicon wafer it can be dissolved in toluene. The cross section of the film can then be analysed adequately.

8.5. Dimensions and growth

In addition to this, the images below reflect the relationship between the number of deposition cycles and the growth of the PEM multilayer. It may be seen that the number of multilayers increase, the film thickness also increases, the infiltration process follows this trend and although there is not an obvious change in the thickness before and after infiltration there is a change in the size of the diameter across the samples. This can be attributed to the fact that the calcium carbonate growth occurs within the pores in the multilayer rather than just building up on the top most layers.

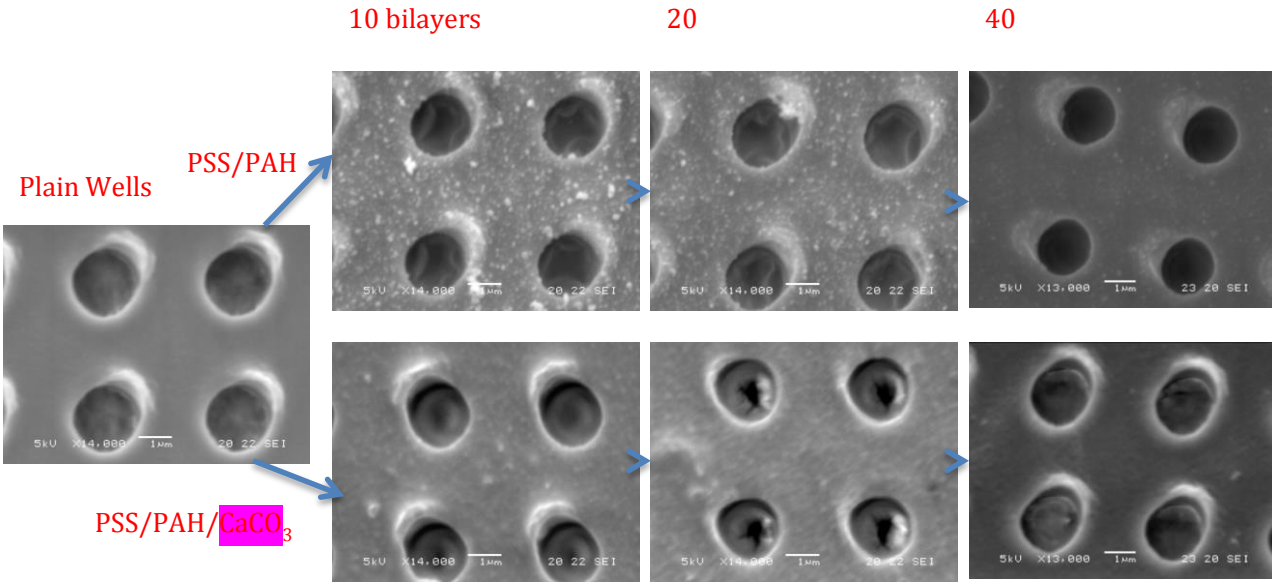

Figure 8.2. SEM- top down images displaying the (PSS-PAH) n deposition on the micro well template, top row- non infiltrated with calcium carbonate, bottom row, infiltrates with calcium carbonate, the diameter of the well continues to decrease as the deposition cycles increase.

It is also visible from the SEM images that at 10 deposition cycles, the surface of the substrate is rough as polymer deposits are visible, as the deposition number is increased, the surface of the substrates appears to be smoother, this is due to the nature of adhesion taking place on the surface of the sample and can be demonstrated consistently. When comparing with the infiltrated samples, the surface of the sample appears to have larger lumps which occur internally but appear to be pushing out of

the surface.

This can be seen in particular in the image corresponding to (PSS-PAH) 20 infiltrated with calcium carbonate, this suggests that any growth of calcium carbonate may be occurring beneath the surface, i.e. internally, within the film.

The chart demonstrates the evolution of (PSS-PAH)n thickness in accordance with the number of bilayers for the polyelectrolyte multilayer synthesized at 2M NaCl of the imprinted micro wells. The trend reflects the literature data on the linear growth behaviour of this polyelectrolyte multilayer on a flat substrate when the ionic strength is less than 0.3M.

The SEM images in figure 8.2 show an unsealed top-down image of the micro wells before and after chemical infiltration. It is visible that the well becomes more and more narrow as you increase the number of deposition cycles. This indicates that the PEM-walls of the well are beginning to grow. To further investigate this, the samples are sealed on to a silicon substrate and the PMMA is fully dissolved.

Table 9. Displaying the change in thickness with increasing level of multilayer deposition as in (PSS-PAH) polyelectrolyte multilayer, with and without chemical infiltration of calcium carbonate.

Sample	**Change in Thickness / nm**
Plain Well	**-**
PSS/PAH-10	41.0 ± 0.63
PSS/PAH 10 CO_3	7.00 ± 1.2
PSS/PAH-20	81.0 ± 0.17
PSS/PAH-20 CO_3	20.0 ± 0.15
PSS/PAH-40	104 ± 0.18
PSS/PAH-40 $C0_3$	27.0 ± 0.20

8.6. SEM on (PSS-PAH) three-dimensional pillars

Upon deposition of the PEM and chemical infiltration process the samples were sealed onto a silicon wafer and toluene was used to dissolve the remaining substrate. This gives the remaining three dimensional Nano pillars which are desirable in this investigation.

The samples were characterized by SEM, there main parameters that were manipulated as part of this investigation include the number of deposition cycles as mentioned previously. Looking at the SEM micrographs it is evident that the number of deposition cycles had a significant effect on the structural integrity of the samples. Figure 8.3a. displays the surface of (PSS-PAH) 20- sample with 20 bilayers used to synthesise the multilayer, at an angle it is possible to see the outcome of the sealing process and pillar density is still high, this sample has not been infiltrated with an inorganic phase and it may be seen upon closer inspection Figure 8.3b. that the pillars look flaccid in nature. The sample surface also looks relatively smooth in between the pillars. When infiltrating this same sample the pillars do not show any structural integrity (Figure 8.3 c and d). It may be observed that the sample surface is rough in nature and has protrusions on the surface. This can be attributed to a large number of reasons, the delamination process may have affected the integrity of the pillars, the nature of the polyelectrolyte meant that 20 bilayers of (PSS-PAH) are not enough to form free standing three dimensional pillars. It may also be that the calcium carbonate infiltration process did not take place adequately on the walls of the pillars as the PEM film was not thick enough and there were not enough pores for nucleation to take

place. In this case, the calcium carbonate may have infiltrated in the spaces between the pillars thus resulting in a rough looking surface.

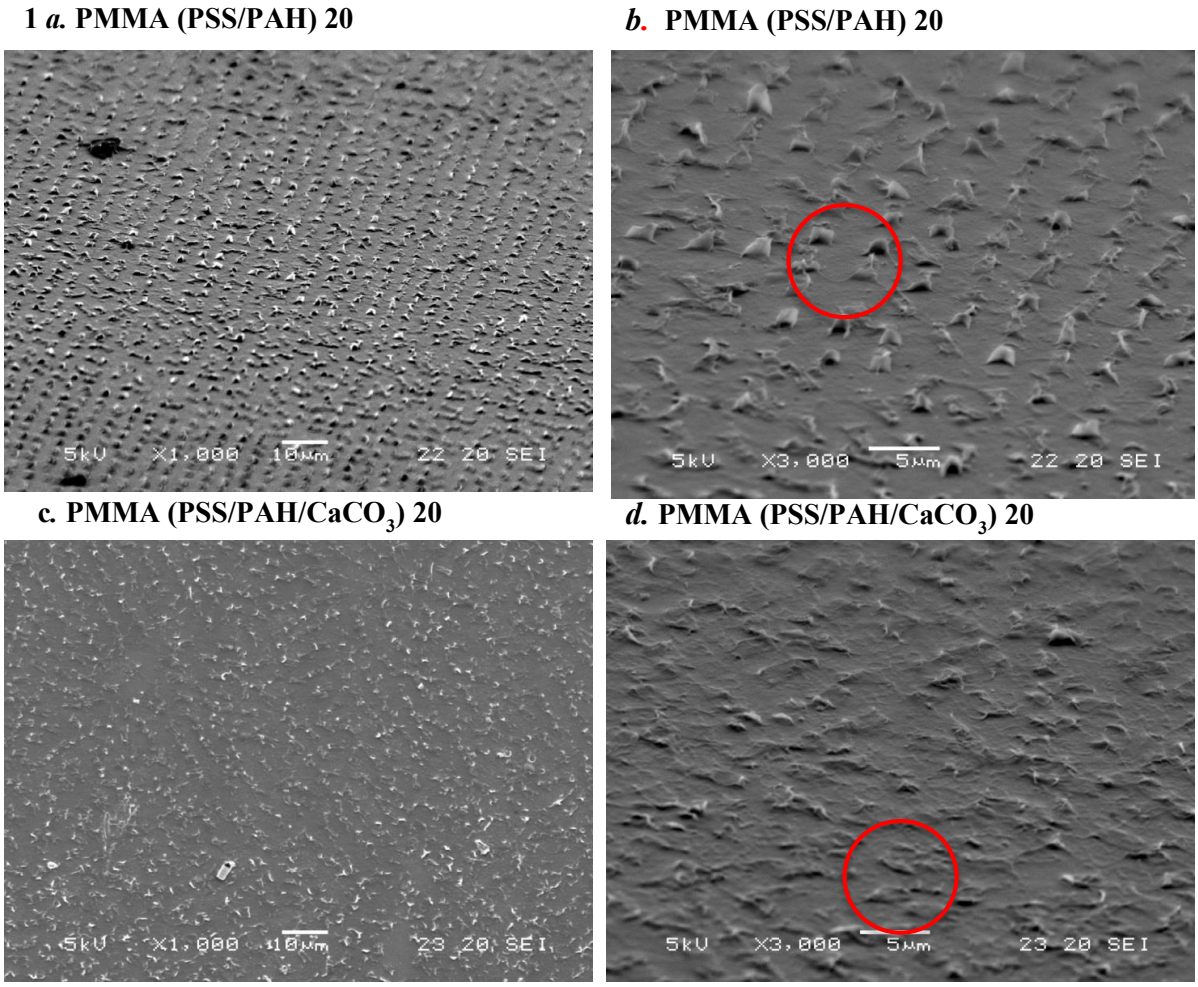

Figure 8.3. SEM micrograph displaying before (1a,b) and after (c,d) chemical infiltration of the sealed surface of (PSS-PAH)20 PEM micro chambers on a silicon substrate; 1a and 2a: x1000 magnification, 10 micron scale bar, 1b and 2b x3000 magnification and 5 micron scale bar.

Roughness on a substrate promotes high levels of polydispersity in polymer chains and the negative implication if this is an inhomogeneous film growth. Charge density of the substrate also determines how the chain conforms on the surface. The polymer chains should not coagulate, but instead lie flat against the surface. Coagulation, is the definition for when the polymer chains bulk up in a ball and is commonly caused by the overcompensation of polyelectrolytes through increased film roughness. A balance

must be achieved to ensure adequate roughness is present for sufficient wetting. This is not evident in these samples.

When the number of multilayers were increased in the (PSS-PAH) system to 40 bilayers there was a significant change in the integrity of the three dimensional arrays. It can be seen from Figure 8.4b that there were fewer areas of destruction on the sample if any at all. On closer inspection, the micro pillars are present in a three-dimensional format, however rounded on the edges where they taper off completely in some regions. This is a sample prior to infiltration, the pillars are comparatively shorter in length. The delamination process can elongate the polymeric structure as there is no stiffness. Upon delaminating it is important to analyse the samples rapidly, as polymers that have not been infiltrated can spread as the environment radiates heat and moisture.

When infiltrating this 40 bilayer sample the structure of the pillar completely changes, the pillars are more longitudinal in nature, they taper in the middle and are rounded on the top, this can be associated with two phenomena, primary being the delamination process which was due to handling and processing of the sample and the second is that there could be a high level of nucleation occurring at the tips of the pillars. This may be due to the reasoning that there is a greater degree of porosity in the 40 bilayer film and when combined with a chemical infiltration process the infiltration is occurring within the pillar head.

As the number of bilayer in the PEM increase to 60 (figure 8.4d) the three dimensional arrays are uniform, all intact and of an optimum height and width which was determined by the template used for synthesis. All the pillars in the SEM image appear to be uniform and there are no inhomogeneity's visible on the sample surface. As the

sample is infiltrated (figure 8.4c) it is clear to see the extreme change in structure of the pillars, once again, the pillars are tapered in the mid-section and larger on the ends, suggestive of the growth of calcium carbonate within the bilayer, due to growth concentrated in specific regions. The diameter of each pillar varies and although they are all in tact there is not a continuous uniform array of pillars present.

As the PEM layer is increased to 80- bilayers of (PSS-PAH-$CaCO_3$), figure 8.4e shows a top down image of the array, it is visible that the pillars do not retain their mechanical affinity as they did with 60 bilayers, many pillars have collapsed on the surface. This does qualify the strength of the PEM multilayer and the formation of the pillars are exclusively attributed to the PEM multilayer with infiltration in this image. As the (PSS-PAH)80 3-dimensional assembly is exposed to chemical infiltration there is a prominent change of appearance; the pillars continue to collapse, and this can be attributed to the calcium-carbonate, inorganic component of the film, which is brittle in nature and within naturally occurring materials like nacre.

Adhesion between the layers is highly dependent upon the ionic strength of between each charged polyelectrolyte. The PSS/PAH samples display rigid properties resulting in pact layer formation. It is therefore plausible to conclude that the electrostatic adhesion between PSS and PAH is strong but differs when compared with PSS/PDADMAC in the sense that they form more regularly. The stretching of each single polymer chain along the layers prevents any non-uniform and irregular conformations, hence setting the trend for the following layers.

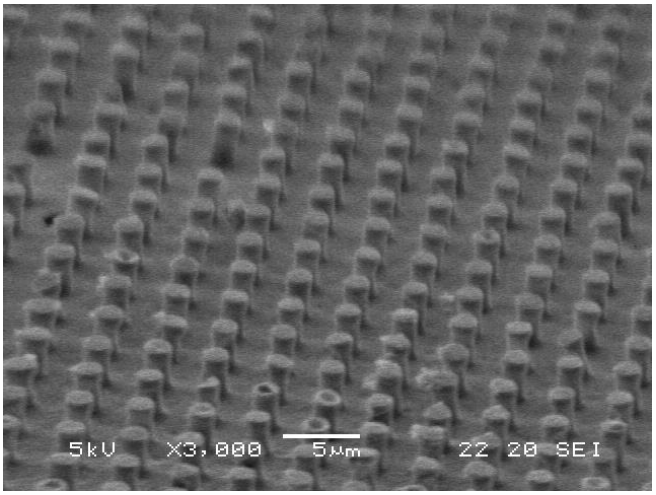

a. (PSS-PAH-$CaCO_3$)40

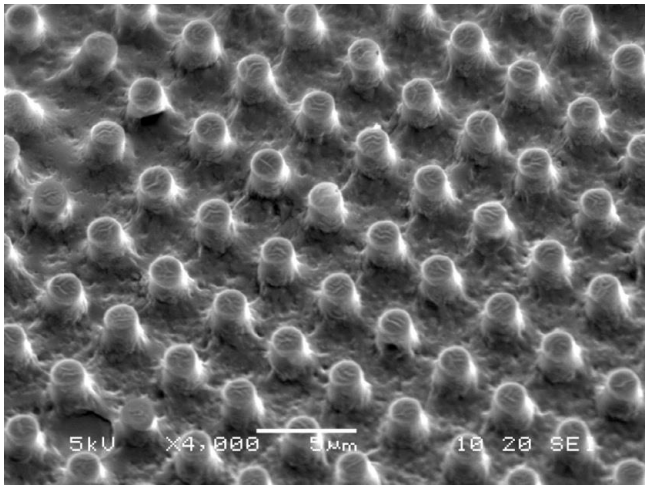

b. (PSS-PAH)40

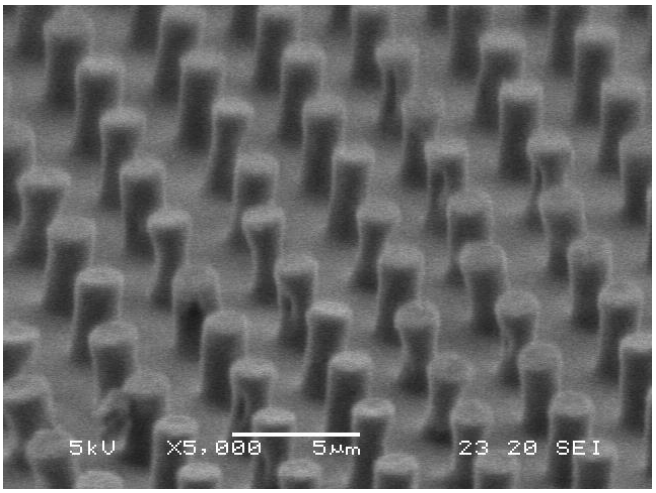

c. (PSS-PAH-$CaCO_3$)60

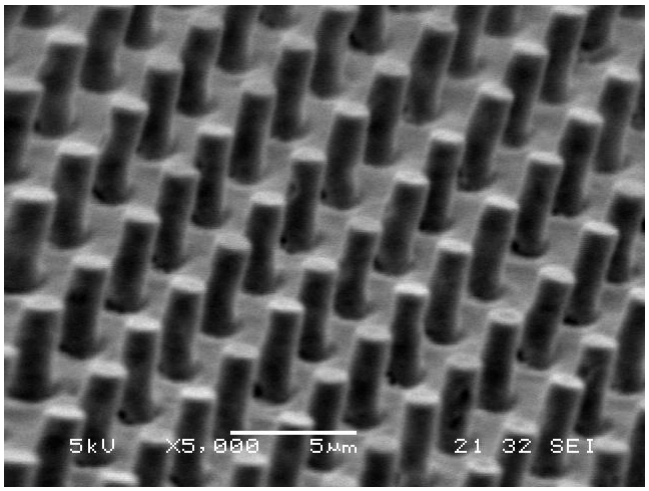

d. (PSS-PAH)60

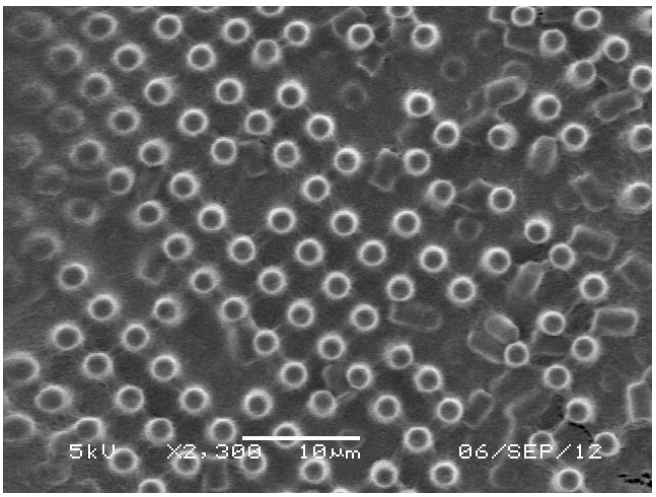

e. (PSS-PAH-$CaCO_3$)80

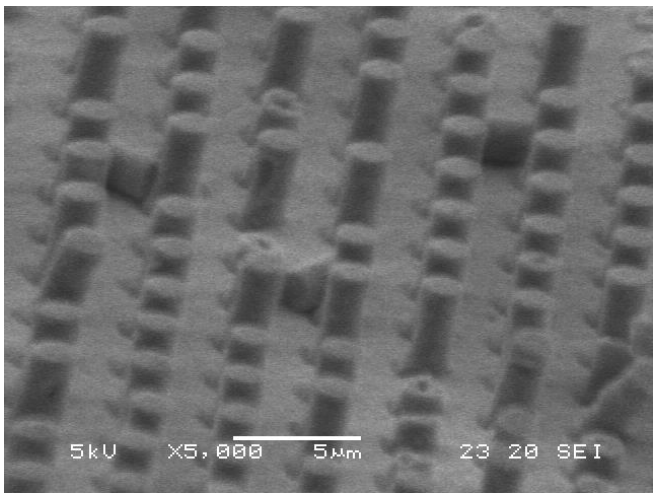

f. (PSS-PAH)80

Figure 8.4. SEM micrograph displaying PMMA (PSS-PAH-$CaCO_3$)40 after chemical infiltration of the sealed surface of PEM micro chambers on a silicon substrate; 2a: x1000 magnification, 10 micron scale bar, 2b-x8000 magnification and 5 micron scale bar.

8.7. SEM on (PSS-PDADMAC) Three-Dimensional Pillars

The (PSS-PDADMAC) PEM combination exhibits different polymeric properties when used for synthesis in layer-by-layer assembly. It is a polymer which behaves similarly to biological components present in nature with a high degree of swelling. This can be seen in figure 8.5a whereby the (PSS-PDADMAC) arrays have been formed with 8 bilayers, compared to its (PSS-PAH) 20 counterpart it exhibits a greater level of polymeric integrity. The pillars, prior to infiltration in this image appear to be loose, flaccid and elastic in nature. They have relaxed to one side and this can be attributed, once again, to the environmental effects; temperature, pressure and moisture which are present in the environment when sealing. The sample is analysed in a stable environment within the SEM and so these images are reflective of the structural integrity of the polymeric system. When compared to its infiltrated counterpart these infiltrated pillars seem smaller in size and have also collapsed on one side. However there is one notable difference, whereby the infiltrated arrays have consistently strong walls in within their arrays. This may be attributed to the infiltration pores, where some chemical infiltration has resulted in the growth of a minute an inorganic phase. The composition of the inorganic phase will be further discussed in TGA analysis, with an aim to quantify the volume of calcium-carbonate/ inorganic component within the structures.

As the PEM multilayer thickness is increased to n=14 within the (PSS-PDADMAC) system there is a continuous evolution of the appearance of the micro chambers. In this sample they are all standing upright in a consistent array, the surface of the sample is smooth and this may be attributed to the gel-like nature of PSS composite. As with the (PSS-PAH) 20 sample the pillars tend to taper in the mid-section consistently with a hollow region at the top.

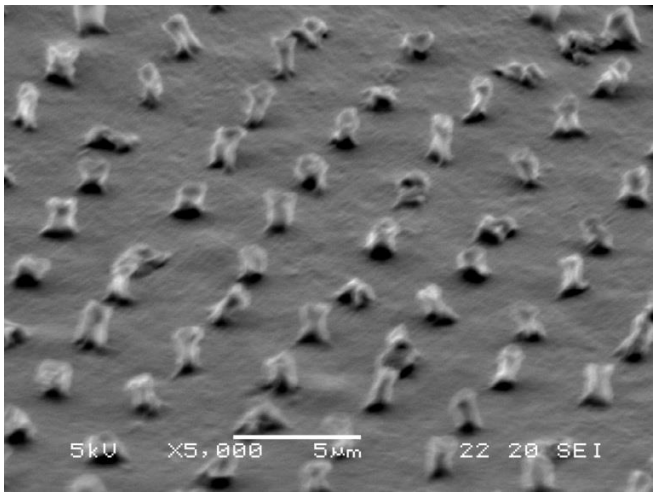

a. (PSS-PDADMAC-$CaCO_3$) 8

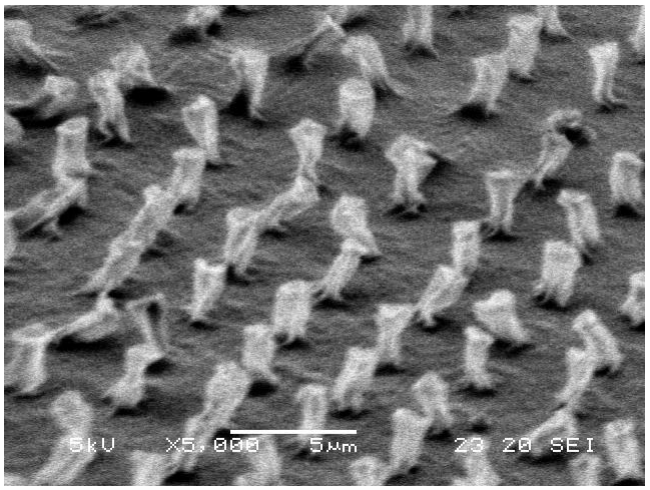

b. (PSS/PDADMAC) 8

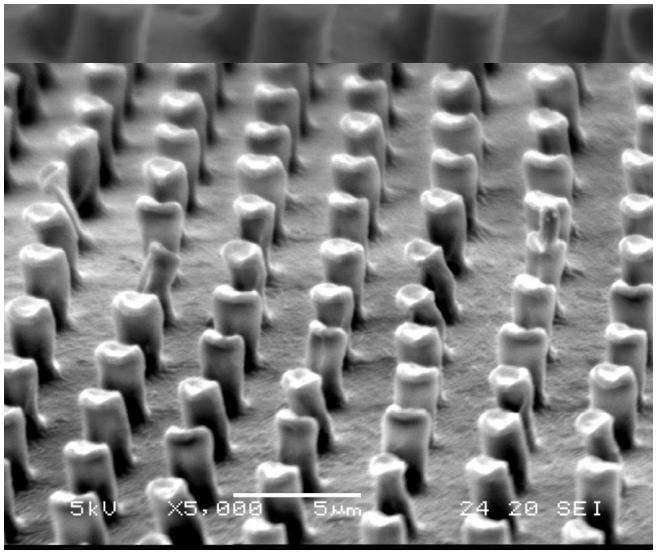

c. (PSS-PDADMAC-$CaCO_3$) 14

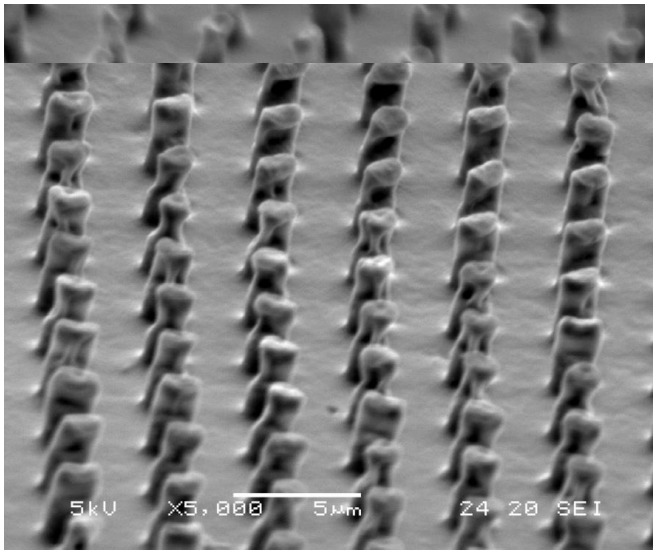

d. (PSS-PDADMAC) 14

Figure 8.5 . Three Dimensional Assemblies: (PSS/PDADMAC) PEM's before and after chemical infiltration of the sealed surface of PEM micro chambers on a silicon substrate.

When compared to its infiltrated counterpart the (PSS-PDADMAC-$CaCO_3$)14 – the micro chambers are significantly bulkier and thicker in nature. The micro chambers appear to increase in diameter and it appears the 'bulk' is present on the width of the pillar rather than on the top or the bottom only. There is not a significant level of tapering of the pillars in this sample, this indicates the possibility of inorganic

component growth within the pillars. This growth will occur in the walls of the chamber rather than at one end of the PEM. It can be seen that the tops of some of the pillars have collapsed inwards, this is due to the reasoning that these are hollow chambers and any infiltration is taking place within the walls of the PEM.

The SEM images for the (PSS-PDADMAC-$CaCO_3$) composite with 20 bilayers continue to show the same trend. The pillars have significantly increased in their width when compared to their non-infiltrated counterpart This is attributed to the growth of calcium carbonate particles which will be discussed further. Due to the swelling nature of the polymer, the maximum number of infiltration cycles conducted were 20.

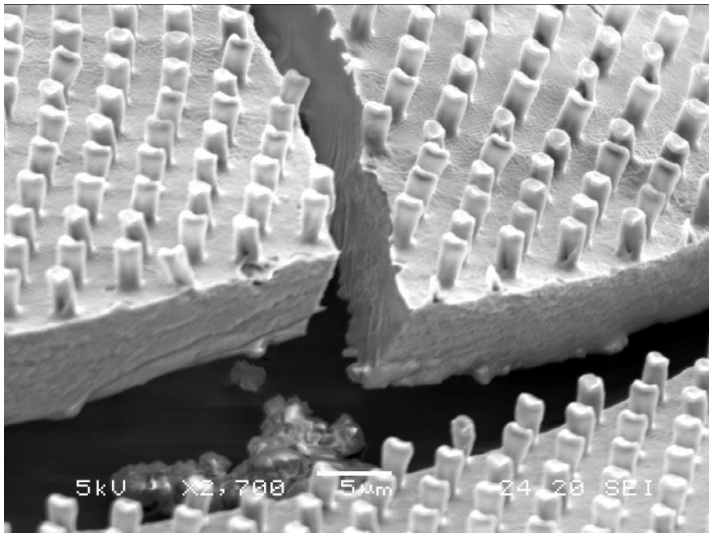

Figure 8.6. (PSS-PDADMAC-$CaCO_3$)- 20 bilayer PEM.

Figure 8.6 displays the cross section of this sample, the growth of the film also occurs on the non-patterned edge, the pillars are static and withhold their structural integrity whilst attached to the surface of the polyelectrolyte film.

The SEM images generally show an uneven and rough surface on the modulated samples. The increased surface roughness is evident on the (PSS-PDADMAC)n samples. There are several explanations to this behaviour, wettability is one of the factors that can influence the structural integrity and synthesis of the multi-layered heavily influences the way in which the polyelectrolytes adheres to the substrate surface.

The increase in layers corresponds to the increasing thickness for both sample types and this evidently suggests that both samples have successfully attached to the surface. However the images from the (PSS/PDADMAC) 60 layer samples indicates that it has a lower hydrophilicity. A lower hydrophilicity leads to less wettability of a polyelectrolyte and less surface contact with the layer below. This could be one of the reasons for its unevenly distributed structure. As discussed earlier, the overcompensation of the oppositely charged PSS and PDADMAC polyelectrolyte resulted from a higher surface roughness.

A greater surface roughness increases the wettability of a polyelectrolyte on a surface, hence allowing the build-up of more than one layer. A plausible factor to consider is the strength of the ionic bonding between the two charged polyelectrolytes. A flexible polymer with highly flexible polymer chains could be due to low ionic strength between the layers which result in the conformation of chains rather than elongation in a parallel conformation compared to the layer below. This is incoherent and not a valid suggestion because PSS/PDADMAC has been proven to have strong ionic interactions. The surface roughness visible in these samples supports the notion that conformational behaviour at a molecular level, is the reason for its formation.

The increase in thickness of the film and mechanical integrity can also be associated

with the existence of mineral bridges in the structure and distributed within the organic matrix (230) The presence of bridges reinforces the weak interfaces, such that the interfaces become just suitable for any deformity or crack to extend in itself thus reducing the mechanical integrity of the structure. Successive layers of inorganic component (aragonite in nacre) are not simply laying one over another but there are interlocks present between the layers. Simulations conducted display the existence of such interlocking has significant role in the deformation behaviour and the progressive failure of interlocks helps in limiting catastrophic failure of these high performance bio composite materials (230).

In addition to this, a single micro chamber was analysed under using the SEM, upon closer inspection of this sample in figure 8.7. The three-dimensional pillar appears to be forced onto a lower side, the stretching on the surface displays the thickness of the multilayer as part of the walls have been fractured, giving an insight on the rest of the structure. This proves that the multilayer is consistent throughout the pillar and is stable.

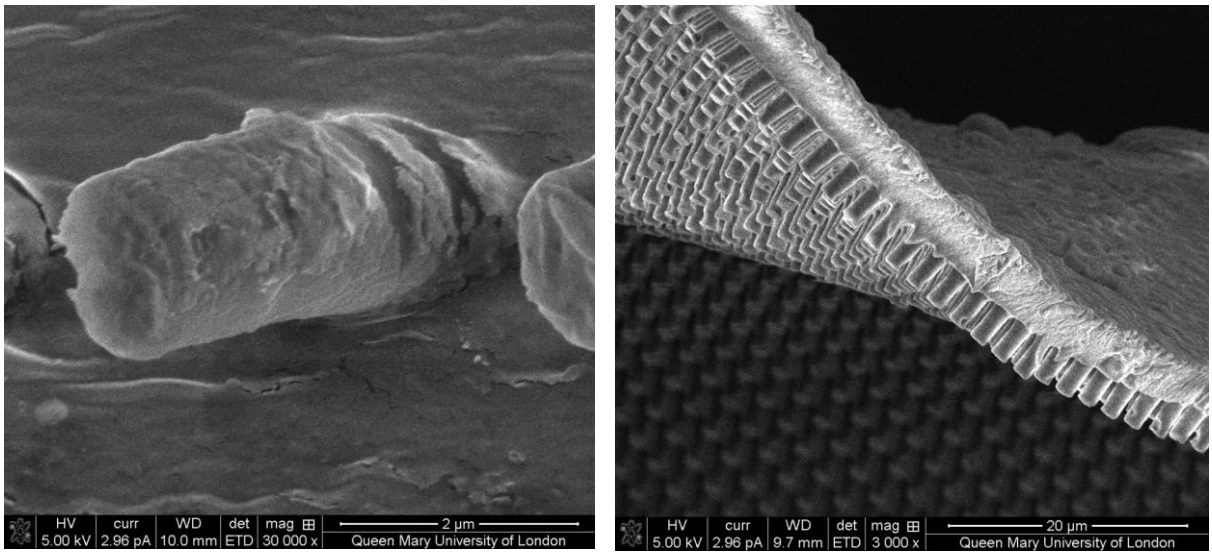

a. **b.**

Figure 8.7 (PSS-PDADMAC-$CaCO_3$) - individual micro chamber (a) 40 bilayer PEM (b).

Film growth and film thickness as well as the diffusion mechanism can influence the thickness of the PEM multilayer structures. From the SEM micrographs it is evident that there is a trend with the micro chamber growth before and after infiltration. The micro chamber appears to increase in diameter after infiltrations, whereas prior to infiltration the micro chamber just tapers thinly in the midsection, not only suggesting the hollow middle but also thinner walls. When debating the film thickness and growth of films exponentially or linearly, there are various parameters as to why the films will grow in either direction, upward or outwards.

In theory if there is an exact charge compensation in the film between the positive and negative charges carried by the polyanion and polycation then diffusion is still probable, as a result of the change in chemical potential of the free polyelectrolytes within the film and those in the solution. Both the polyanion and polycation should easily be able to diffuse in and out of the film. This explains the mechanical integrity of the chambers which have not been mineralized with the infiltration process. The mechanical integrity of the pillars increases with the increase in the number of multilayers in both the (PSS-PAH) and (PSS-PDADMAC)n systems.

The film thickness can also be affected by an uneven surface coverage of the polyelectrolytes during synthesis. When beginning the multilayer deposition it is possible that the surface is not covered uniformly by the solution and the attachment of the polyelectrolyte occurs only in regions on the surface of the substrate forming multiple islets. Upon increasing the deposition number the free space is fulfilled to produce a film. The toughness on the surface of the sample which is visible in the SEM images described previously suggests this fact and as the number of deposition

cycles are increased to 20, 40 or 60 the surface continues to become smoother, thus eliminating the spaces where there has been a lack of attachment.

The diffusion coefficient can vary for each polyelectrolyte and so the rate of diffusion will differ throughout the film. (231). The polyelectrolyte network may entrap larger molecules but be penetrable to smaller ones. The PEM film structure can have an influence on the transport mechanism which has been extensively studied (231), applying the general theory that ionic strength of the solution will heavily indicate individual layer thickness, a higher level of ionic strength, with additional salts used in this method allow the polyelectrolyte to conform into loop structures at the surface of the PEM. The thickness of the multilayer may also be affected by the possible defects within the system, this could be on the substrate, or during the processing technique which will ultimately hinder the permeability of the solutions within the PEM.

8.8. Nano-indentation

In addition to this nano-indentation was conducted on the sample to measure the Young's modulus and hardness of the sample. The mechanical properties of the composite films are not only of interest for possible future applications, but they also reflect the composition and the structural ordering and are hence important for the evaluation of composites prepared under various conditions. Since the composites are films of several micrometres thickness only, the Young's modulus and hardness have been determined by Nano-indentation. The indentation depth was restricted up to 200 nm for the thinner and to up to 600 nm for the thicker samples, respectively, in order to avoid any influence of the underlying substrate.

All the samples were sealed onto a silicon wafer, silicon is used for sealing as it has an atomically flat surface. In order to increase the adhesion of the film on the surface the silicon was treated with a (PSS-PDADMAC) 8 multilayer. The following graphs display a simple load-displacement curve attributed to the testing on the (PSS-PDADMAC)- 14 bilayer sample with and without chemical infiltration for comparison. The mechanical performance of the polyelectrolyte multilayer significantly increase when reinforced with the calcium carbonate. This is comparable to the process which was previously described in Nature, whereby the synergy between inorganic and organic phase of a material increases its mechanical performance at the structural level.

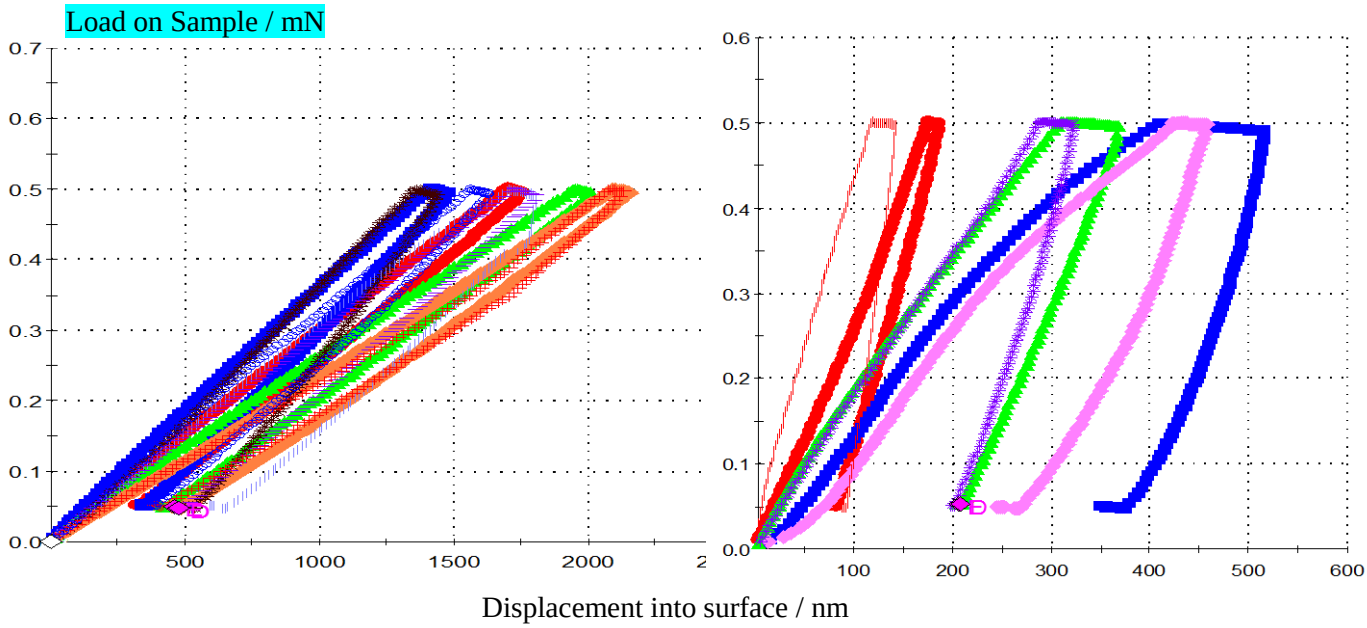

Figure 8.8. *a.* (PSS-PDADMAC)14 bilayers sealed on silicon wafer, average modulus is 70 MPa, average hardness is 30 MPa *b.* (PSS-PDADMAC-$CaCO_3$)14 bilayers sealed on silicon wafer, average modulus 2.1 GPa, average hardness is 200 MPa. Each point reflects a separate point on the sample.

When compared with naturally occurring materials like nacre which has a reported Young's modulus of (4 ± 1) GPa calculated from the elastic deformations reported.

It is also noteworthy to take into consideration that in naturally occurring materials like nacre, deformations are directed over large surface areas and due to this, higher stresses are required to slide platelets further, therefore resulting in various stress concentration points. Under tensile stress, the interfaces begin to yield in shear thus causing the structure to slide with local deformation as depicted in the curves obtained in figure 8.8. Once the sliding sites are exhausted, the material fails by pull-out of the inorganic components. This mechanism is considered to be the main source of the superior mechanical properties and is unique to nacre (232) and is a result of the reinforcing organic phase of the material.

A possible strengthening process is anchoring of the organic adhesive phase to the inorganic component is to understand the unfolding of chains, breaking of cross-links and perhaps permanent reorientation of the organic phase during deformation helps in the strengthening mechanism. An uncontrolled crack growth is prevented if a stress normal to the platelet plane is applied. This is due to the organic fraction that glues the crystals and shows high level of ductility. Importance of soft organic phase is clear as it plays a key role in alleviating impact damage to aragonite platelets (229), however, Meyers et al. has reported importance of organic layer in the growth of the aragonite crystal, while having only a minor role in the mechanical strength.

Another factor which may have influenced the mechanical performance of the composites includes; the changing conformation of the polymer. The polymer conformation is necessary for maximizing the interaction of the polyelectrolytes at the nanoscale and this control will have a direct influence on the bonding and mechanical integrity of the resulting film which has been considered true in previous

investigations (83,113) The conformation of the adsorbed polymer depends on the degree of protonation (and with that on the pH), but also on parameters like its concentration and adsorption kinetics, the importance of which have been discussed in Section 2.

8.9. Thermogravimetric analysis

TGA was conducted in order to identify the decomposition of calcium carbonate, ultimately identifying the yield of the calcium carbonate- organic component. In order to do this all samples were analysed using the TGA to analyse whether there is a correlation between the number of bilayers and growth of calcium carbonate. Also whether there is a significant change in calcium-carbonate growth dependent on the polymeric system used to synthesise the PEM multilayer in three dimensions. It is essential to monitor amount of $CaCO_3$ that had been infiltrated in the PEM films. This was carried out using (TGA) as this can provide the mass of the inorganic matrix. The technique is able heat up the sample to high temperatures up to 1000 °C and this will burn off the organic matrix leaving the ceramic that is able to withstand such temperature. The method will generate a curve of showing the correlation between temperature and mass. This in turn, will be able to quantify how much $CaCO_3$ has infiltrated the sample.

8.10. TGA on three-dimensional PEM's

When considering the decomposition of calcium carbonate, the reaction readily occurs on a small scale during pyro metamorphism and on larger scales subduction zones. The thermal decomposition of calcite is commonly called calcining or calcination and this is the process which took place when the samples were being analysed using TGA. Accurate control of thermal decomposition of calcium carbonate was necessary to achieve a high quality yield. The degradation was primarily associated with particle size, surface area and the porosity of calcium-oxide aggregates.

The TGA data identified the $CaCO_3$ composition for the various three-dimensional PEM microstructures. In addition to this the calcium-carbonate content for previously investigated films has been included. This assisted in identifying the

growth of calcium carbonate crystal in three dimensional assemblies in comparison to planar, free-standing multi-layered films.

From the previous chapter it was established that calcium carbonate growth does occur within the PEM for this reason, it is useful to now investigate the content of calcium carbonate which has mineralized through the infiltration process within the three dimensional arrays. This was investigated using the same TGA methodology as described previously. The content of TGA increases by weight percentage as the number of bilayers increases.

8.10.1. (PSS-PAH-$CaCO_3$)

Looking at Table 10, it was calculated that an increase in the number of bilayers of (PSS-PAH) from 20, 40 and 60 the content of calcium carbonate also increases from 14% to 25% in 40 bilayer and 28% in 60 bilayers. Although there is a significant increase of inorganic component from 20 bilayers to 40 bilayers; the content appears to plateau off at 60 bilayers. This could be due to the possibility that the space for mineralization within the pillars is fully saturated at 60 bilayers. This theory is supported by the SEM images as the pillars from 40 and 60 bilayer samples have very similar structures and characteristics. The analysis was conducted on several parts of the same sample to ensure reliability and consistency and this was a continuous trend. This can be attributed to the nature of the polymer and the way in which the electrostatic bonding played a role within the multilayer, the interaction energy between PSS and PAH is relatively strong compared to other polyelectrolytes. This is supported by previous research conducted on (PAH-PSS) films which continued to increase in thickness up to a 5 M NaCl in comparison to (PDADMAC-PSS) films whereby the polyamine with the amino groups which are replaced by the polymer

ammonium groups can reach a maximum thickness in 2 M NaCl. This indicates that there is a greater interaction energy between PSS and PAH in comparison to PDADMAC and PSS.

Conversely when compared to the planar surface it was also deduced that 20 bilayers in a planar surface evolved 32% calcium carbonate, just over double the mineralization content. (PSS-PAH-$CaCO_3$)40 had 33% calcium carbonate infiltrated, once again a trend is visible whereby reaching the 40 bilayers, the PEM was fully saturated and calcium carbonate had reached its maximum mineralization potential.

8.10.2. (PSS-PDADMAC-$CaCO_3$)

Thermo-gravimetric analysis was also conducted on the (PSS-PDADMAC-$CaCO_3$)n samples where n= 20 and 40 bilayers. It was established that there was 21% and 26% calcium carbonate present in the samples. Compared to their planar counterparts, this was much lower, 40 bilayers of the same sample on a non-patterned surface had a 33% yield of calcium carbonate. There is a given trend here that the patterned surfaces yield a lot less calcium carbonate infiltrated than their planar counterparts. In addition to this when comparing (PSS-PAH-$CaCO_3$)40 with (PSS-PDADMAC-$CaCO_3$)40 there was not much of a difference between the calcium carbonate yield between the two samples.

Table 10. Displaying the calcium carbonate content present in the free standing films in the various sample types identified.

Sample Composition & Structure	Temperature Range / ºC (mg weight loss in each range)				$CaCO_3$ / %
	25-250	250-400	400-500	500-900	
(PSS/PAH)20i- 3d arrays	0.04	0.62	1.3	0.11	14
(PSS/PAH)40i-3d arrays	0.05	0.32	1.19	0.21	25
(PSS/PAH)60i -3d arrays	0.02	0.21	0.68	0.13	28
(PSS/PDADMAC)20i -3d arrays	0.19	0.05	0.72	0.38	21
(PSS/PDADMAC))40i -3d arrays	0.20	0.14	0.80	0.521	26
(PSS/PAH)60 i -planar	0.03	1.01	0.39	0.65	32
(PSS/PDADMAC)40 i - planar	0.04	0.2	0.30	0.30	33
(PSS/PDADMAC)60 i -planar	0.12	0.09	0.12	0.54	62

The combination of (PSS-PDADMAC) PEM system leads to 'supralinear' growth of the multilayer. Ultimately, exponential growth is not only limited to weakly charged polyelectrolytes and linear growth to synthetic polyelectrolytes with a high charge density. This may be one of the factors contributing to the limited growth of calcium carbonate within the multilayer. In addition to this, (PSS/PDADMAC) complexes are much more hydrated than the PEM (PSS/PAH) systems made under the same conditions. This is due to the presence of pores in the PEM. A way to engineer the growth of the PEM is to incorporate a salt solution, the monovalent contributes to the film hydration, permeability and ability to swell. This demonstrates that the structures have a significant effect on the infiltration process and this could be due to the wetting

process whilst synthesizing the PEM. Another factor affecting the (PDADMAC/PSS) multilayers include, the temperature and ionic strength which can influence their structural integrity. From previous investigations (158) the Young's modulus of capsules diminished at an ionic strength above 3M due to the cohesive interactions between the polyelectrolytes compared to (PSS/PAH) which did not demonstrate this behaviour.

8.11. Conclusions

Layered composites of (PSS-PAH) and (PSS-PDADMAC) were prepared through layer-by layer assembly. The composites were synthesized on templates created through Nano-patterning techniques to attain a three dimensional array of structures on a modulated surface as surface in nature and natural environments are never flat. The poly-electrolyte multilayers created in 3D were then infiltrated with sodium carbonate and calcium chloride in order to initiate the growth of an inorganic phase within the multilayer in order to mimic the structural architecture of materials which are already present in nature, namely nacre.

The growth and structural features were studied along with their mechanical properties. Fabricated composite material looks morphologically similar to the nacre microstructure. The Nano-composite was analysed through SEM imaging and the structural integrity of the modulated surface was compared for both polymer complexes. In addition to this, TGA analysis was carried out in order to compare the level of mineralization between the two polyelectrolyte composites. It was found that the (PSS-PDADMAC-$CaCO_3$) composite evolved the highest level of inorganic component, this was supported by the structural integrity of the micro-pillars present in the modulated surface.

9. General conclusions

In conclusion, this thesis explains how the process of calcium carbonate infiltration is working in polyelectrolyte multilayers fabricated on flat and modular surfaces. In the complex system PSS-PAH/$CaCO_3$ both linear and exponential growth regimes can be observed at the nanoscale and have now been explained, via a correlation with thickness growth through the infiltration process. The results have verified that a relationship can be established between the number of deposition cycles and the structure of the film, influencing the overall mechanical properties.

Although the effect of the number of bilayers on layer thickness was the main focus of this project, the infiltration of calcium carbonate through a cyclic deposition method was also thoroughly investigated in an attempt to achieve a layer-by-layer mineralization process through diffusion kinetics and crystal nucleation. The effect of this was to produce a stable composite structure with a greater degree of mechanical integrity through reinforcement of an organic phase. It is necessary to be aware of other factors that also influence the thickness of films. These influences include the effect of temperature, ionic strength and the concentration of the organic solutions. The high concentration used is likely to be responsible for the clusters formed, thus rendering the film thicker with what appears to be high mechanical properties. In order to achieve homogenous layers within the composite.

Nanoporous charged polyelectrolyte multilayers (PEMs) were made from PAH/PSS and PDADMAC/PSS. The PEMs were then infiltrated with calcium and carbonate ions to nucleate and grow an inorganic phase inside the nanoporous polyelectrolyte

multilayer. The effect of multilayer thickness and also of the number of infiltration cycles was investigated. It was found that the yield of calcium carbonate within the PEM film increased with the number of infiltration cycles and could make up to a 60% increase in mass in some cases. Calcium and carbonate ions penetrated through the organic multilayer film and then formed an amorphous shell in voids of multilayers and also on surface. Mineralization of the PEM with the fraction of inorganic component (over 8 wt. %) caused a 263 % increase of the Young modulus reaching an average modulus value of 10.0 GPa. An even more drastic effect has been observed on hardness where higher degree of mineralisation increases it in 60 times. These results show the promise of using layer-by-layer PEM multilayers as mesoscale scaffolds to form mineralized composites in a biomimetic manner.

The use of natural polymers (instead of synthetic PEs) to mimic natural mineralization was investigated, hyaluronic acid and collagen were used as biological polyelectrolytes to form a compact biocomposite film. The number of multilayer depositions were controlled through the automated dipping process. The films were kept hydrated and infiltrated again with calcium carbonate to monitor the level of mineralization in the biocomposite and compared to that which is present in Nature. It was found that the planar films yielded a maximum of 37% of inorganic components-calcium carbonate. Hyaluronic acid and collagen were then used to create three-dimensional modulated surfaces. The yield of calcium carbonate in the three dimensional arrays (chapter 7) almost doubled to 67% and this was an extraordinary result. The research on modulated surfaces is still novel and therefore continued research and analytical techniques are required for further investigation.

The effects of including complex microscale modulations in topology were investigated with the use of (PSS-PAH) and (PSS-PDADMAC) polymers, the 3D

arrays were then analysed. The 3D PEMs were infiltrated with calcium and carbonate ions to nucleate and grow an inorganic phase inside the nanoporous polyelectrolyte modulated multilayer. The effect of multilayer thickness and also of the number of infiltration cycles was investigated. It was found that the yield of calcium carbonate within the modulated PEM increased with the number of infiltration cycles. Mineralization of the PEM with the fraction of inorganic component resulted in an increase of the Young's modulus. The TGA displayed a high level of mineralization within the micro chambers and this is a promising feature when considering naturally occurring materials like nacre.

10. Future work

The results of this thesis have initiated novel research in the field of biological nanocomposites in three-dimensional assembly with high mechanical strength. This opens up the applications of these high integrity 3D structures in the areas of defence, reinforcement and cargo materials. However, there are still many challenges left to be overcome for the improvement of these systems. Hurdles remain in the smooth transition of these experimental works into practical uses.

When identifying different polymeric material for use in the synthesis of these three dimensional structure it is important to consider the change in ionic strength of the PE solutions. This is necessary to monitor growth and behaviour patterns of the composite material. A high ionic strength can potentially result in thicker PEM multilayers ultimately increasing the mechanical integrity of the structure which is a necessity when considering high performance and versatile applications.

Statistical significance can also be evaluated using t-tests and the acquired data. The concentration of collagen can also be increased in order to obtain PEM films with a greater number of collagen fibrils on its surface. It is also possible to use layer-by-layer assembly in conducting the same experiment but with calcium phosphate crystals. This will also have shown significant changes in the results as the crystals of $CaCO_3$ are larger than $Ca_3(PO_4)_2$. It is also possible to create these structures on silicon wafers therefore creating free standing films that can be easily analysed for mechanical properties and also create the possibility for large scale production.

Profilometer studies can be conducted to further monitor the thickness of the samples and assess the change in thickness when changing the deposition cycles. Thickness measurement with the help of SEM is difficult due to the inaccuracy of cutting a cross section, and the danger of not having a reflective sample region. In addition to this other artefacts may hinder the analysis on the region being analysed, resulting in a high level of uncertainties being created. The thickness; thus be determined by employing a Profilometer. The force acting on the stylus of the Profilometer will manoeuvre over the surface and can be adjusted so as to not penetrate the material but to only scan the upper surface.

Considering the mechanical testing on films in hydrated conditions will be another area of research which can be investigated further, in order to obtain deeper understanding of their viscoelastic properties. This topic can also be achieved by considering the results of the quartz crystal microbalance (QCM), where findings can be evaluated in the Butterworth-Van Dyke fit (BVD fit), where resistance is found to be proportional to the viscoelasticity of the film. In addition to this it would be useful to determine the reversible properties of the PE chains. The synthesis method can be exploited whereby dehydrated films are fabricated and analysed, and the same film is subjected to an external stimuli (hydration, temperature or even different pH baths), before being analysed further. There are many exploration routes that materials scientists are yet to embark on with thin films, the basis of which starts at understanding the mechanisms behind the bottom up layer-by-layer process, for manipulation of physico-chemical properties of composite materials.

11. Works cited

1. Rho J.Y., Zioupos P., Mechanical properties and the hierarchical structure of bone., *Medical Engineering and Physic*s, 1998, Vol. **20,** pp. 92-102.

2. Decher G., Fuzzy nanoassemblies: Toward layered polymeric multicomposites, *Science,* 1997, Vol. **277**, pp. 1232-1237.

3. Gower L.B., Biomimetic Model Systems for Investigating the Amorphous Precursor, *Chemical Reviews,* 2008, Vol. **11**, pp. 4551-4627.

4. Xu A., Ma W., Colfen Y. R., Biomimetic mineralization, *Materials Chemistry,* 2007, Vol. **17**, pp. 415-449.

5. Cheng Q., Jiang L., Tang Z., Bioinspired Layered Composites Based on Flattened Double-Walled Carbon Nanotubes, *Advanced Materials,* 2012, Vol. **24**, pp. 1838-1843.

6. Goffin J.J., Rajadas J., Gerald G., Fuller I., Interfacial flow processing of collagen, *Langmuir* , 2010, Vol. **26,** pp. 3514-3521.

7. Li Y., Asadi A., Monroe M., Douglas E., pH Effect on collagen in vitro: Electrostatic interaction and phosphate binding, *Materials Science and Engineering,* 2009,Vol. **29**, pp. 1643-1649.

8. Erbil H., Surface chemistry of Solid and Liquid Interfaces. ISBN: 978-1-4051-1968-9**,** 2006, pp. 150-165.

9. Knoll W., Interfaces and thin films as seen by bound electromagnetic waves. *Review of Physical Chemistry*, 1998, Vol. **49,** pp. 569-638.

10. Yadavalli V.K., Svintradze D.V., Pidaparti R., Nano-scale measurement of the assembly of collagen to fibrils, *Biological Macromolecules*, 2010, Vol. **46**, pp. 458-464.

11. Schonhoff M., Layered polyelectrolyte complexes: physics of formation and molecular properties, *Journal of Physics: Condensed Matter*, 2003, Vol. **15**, pp. 49-56.

12. Silva H.S., Uehara T.M., Bergamaski K., Miranda P.B., Molecular Ordering in Layer-by-Layer Polyelectrolyte Films Studied by Sum-Frequency Vibrational Spectroscopy, *Nanotechnology*, 2008, Vol. **8** , pp. 3399–3405.

13. Dubas S., Schlenoff J.B., Factors controlling the growth of polyelectrolyte multilayers, *Macromolecules*, 1999, Vol. **32,** pp. 8153-8160.

14. Cheng Q., Wu M., Li M., Jiang L., Tang Z., Ultra tough Artificial Nacre Based on Conjugated Cross-linked Graphene Oxide, *Angewandte Chemie*, 2013, Vol. **125,** pp. 3838-3843.

15. Yao H., Fang H., Tan Z., Wu L., Yu S., Biologically Inspired, Strong, Transparent, and Functional Layered Organic–Inorganic Hybrid Films. *Angewandte Chemie*, 2010, Vol. **49,** pp. 2186-2191.

16. Yao H., Mao L., Yan Y., Cong H., Lei X., Yu S., Gold Nanoparticle Functionalized Artificial Nacre: Facile in Situ Growth of Nanoparticles on Montmorillonite Nanosheets, Self-Assembly, and Their Multiple Properties, *ACS Nano*, 2012, Vol. **6**, pp. 8250-8260.

17. Yao H., Fang H., Wang X., Yu S., Hierarchical assembly of micro-nano-building blocks: bio-inspired rigid structural functional materials, *Chemical Society Reviews*, 2011, Vol. **40**, pp. 3764-3785.

18. Yao H., Wu L., C C., Fang H., Yu S., Direct fabrication of photoconductive patterns on LAYER-BY-LAYER assembled graphene oxide/PDDA/titania hybrid films by photothermal and photocatalytic reduction, *Journal of Materials Chemistry*, 2010, Vol. **20**, pp. 5190-5195.

19. Yao H., Tan Z., Fang H., Yu S., Artificial Nacre-like Bionanocomposite Films from the Self-Assembly of Chitosan–Montmorillonite Hybrid Building Blocks, *Angewandte Chemie*, 2010, Vol **49**, pp. 10127-1031.

20. Wang C., Huang Y., Guo H., Cai S., Biomimetic structure design- a possible approach to change the brittleness of ceramics in nature, *Materials Science and Engineering*, 2000, Vol. **11,** pp. 9-12

21. University, Mc Guill,
Cited: www.thestar.com.my/Lifestyle/Features/2014/02/05/Mollusc-shells-inspire-superglass, Date accessed: 30/04/2014.

22. Weiss I., Tuross N., Addadi L., Weiner S., Mollusc larval shell formation: Amorphous calcium carbonate is a precursor phase for aragonite, *Journal of Experimental Zoology*, 2002, Vol. **293,** pp. 478-491.

23. Currey J.D., Mechanical properties of mother of pearl in tension, Proceedings of the Royal Society of London Series B-*Biological Sciences* , 1977, Vol. **196,** pp. 443-463**.**

24. Wu M., Shuai H., Chang Q., Jiang L., Bioinspired Green Composite Lotus Fibers, *Angewandte Chemie*, 2014, Vol. **53**, pp. 3358-3361.

25. Currey J D., Zioupos P., Davies P., Casinos A., Mechanical properties of nacre and highly mineralized bone, *The Royal Society*, 2001,Vol **268,** pp. 107-111.

26. Elliott D.H., Structure and Function of mamallian tendons, *Biological Reviews*, 1965, Vol. **40**, pp. 392-421.

27. Riley G., Tendinopathy, *Nature and Rheumatology*, 2008, Vol. **4,** pp.82-89.

28. Jackson A. P., Vincent J. F. V., Turner R. M., The mechanical design of nacre, *Proceedings of Royal Society*, 1988, Vol. **234,** pp. 415–440.

29. Wang J., Cheng Q., Lin L., Jiang L., Synergistic Toughening of Bioinspired Poly(vinyl alcohol)–Clay–Nanofibrillar Cellulose Artificial Nacre, *American Chemical Society*, 2014, Vol. **8**, pp. 2739-2745.

30. Cheng Q., Jiang L., Tang Z., Bioinspired Layered Materials with Superior Mechanical Performance, *Accounts of Chemical Research.*, 2014, Vol. **47,** pp. 1256-1266.

31. Nudelman F., Gotliv B., Addadi L., Weiner S., Mollusk shell formation mapping the distribution of organic matrix components underlying a single aragonite tablet in nacre, *Journal of Structural Biology*, 2006, Vol. **153**, pp. 176-187.

32. Deville S., Saiz E., Nalla R.K., Freezing as a path to build complex composites, *Science*, 2006, Vol. **311**, p. 515-520.

33. Jackson A. P., Vincent J. F. V., Turner, R. M., The mechanical design of nacre, *Royal Society*, 1995, Vol. **234,** pp. 415-450.

34. Evans J.S., Tuning mollusc shell nacre-prismatic-associated protein terminal sequences. Implication for biomineralization, *Chemical reviews*, 2008, Vol. **108**, pp. 4455-4462.

35. Rousseau M., Meibo A., Bourrat M., Angellier M., Lopez E., Dynamics of sheet nacre formation in bivalves, *Journal of Structural Biology*, 2009, Vol. **165,** pp. 190-195.

36. Tang Z., Kotov N., Magonov S., Ozturk B., Nanostructured artificial nacre, *Nature Materials*, 2003, Vol. **2**, pp. 413-418.

37. Becker A., Ziegler A., Epple M.,The mineral phase in the cuticles of two species of Crustacea consists of magnesium calcite, amorphous calcium carbonate, and amorphous calcium phosphate, *Dalton Transactions*, 2005, Vol **10**, pp. 1814-1820.

38. Burghard Z., Tucic A., Jeurgens L., Hoffman R., Aldinger F., Nanomechanical properties of bioinspired organic-inorganic composite films, *Advanced materials*, 2007, Vol. **19**, pp. 970-974.

39. Katti K., Katti S., Pradhan D. R., Bhosle S. M., Platelet interlocks are the key to toughness and strength in nacre, *Materials Research*, 2005, Vol. **20**, pp. 1097-1100.

40. Wan S., Li Y., Peng J., Hu H., Cheng Q., Jiang L., Synergistic Toughening of Graphene Oxide–Molybdenum Disulfide–Thermoplastic Polyurethane Ternary Artificial Nacre,. *American Chemcial Society Nano*, 2015, Vol. **9**, pp. 708-714.

41. Wang J., Cheng Q., Tang Z., Layered nanocomposites inspired by the structure and mechanical properties of nacre, *Chemical Society Reviews*, 2012, Vol. **41**, pp. 1111-1129.

42. Cui W., Li M., Liu J., Wang B., Zhang C., Jiang L., Cheng Q., A Strong Integrated Strength and Toughness Artificial Nacre Based on Dopamine Cross-Linked Graphene Oxide, *American Chemical Society Nano*, 2014, Vol. **8**, pp. 9511-9517.

43. Curry J.D., The design of mineralised hard tissues for their mechanical functions. *Experimental Biology*, 1999, Vol. **202**, pp. 3285-3294.

44. Weiner S., Traub W., Wagner H.Lamellar bone: Structure-function relations, *Journal of Structural Biology*, 1999, Vol. **126**, pp. 241-255.

45. Harris J.R., Soliakov A., Lewis R.J., In vitro fibrilogenesis of collagen type one in varying ionic and pH conditions, *Micron*, 2013, Vol. **49**, pp. 60-68.

46. O'Dubhthaigh-Orgel Joseph Patrick Rosen, The molecular structure of collagen, PhD thesis, *University of Stirling-UK*, 2000, pp. 84-96

47. Toth T., Vautier D., Haikel Y., Voegel J.C., Schaaf P., Chluba J., Viability adhesion and bone phenotype of osteoblast-like cells on polyelectrolyte multilayer films, *Biomedical Materials Research*, 2002, Vol. **60**, pp. 657-667.

48. Fratzl P., Gupta H.S., Paschalis E., Roschger P., Structure and mechanical quality of the collagen-mineral nano-composite in bone. *Journal of Materials Chemistry*, 2004, Vol. **14**, pp. 2115-2123.

49. Mainard D., Voegel J., Caruso F., Benikrane J., Active multilayered capsules for in vivo bone formation, *Proceedings of the National Academy of Sciences of the United States of America*, 2014, Vol. **107**, pp. 3406-3411.

50. Yadavalli V. K., David V. Svintradz, Pidaparti R.M., Nanoscale measurement of the assembly of collagen to fibrils, *International Journal of Biological Macromolecules*, 2010, Vol. **206**, pp. 458-464.

51. Yuping L.,The Mechanism of collagen self-assembly: Hydrophobic and Electrostatic interactions, PhD thesis, *University of Florida- USA.* 2009, pp.56-78

52. Holmes D. F., Chapman J. A, Prockop D. J., Kadler K. E., Growing tips of type I collagen fibrils formed in vitro are near paraboloidal in shape, implying a reciprocal relationship between accretion and diameter, *Proceedings of National Academy of Science.*, 1992, Vol. **89**, pp. 9855-9859 .

53. Wood G., Keech M.K., The formation of fibrils from collagen solution: The effect of experimental conditions : Kinetics and electron microscope studies, *Journal of Biochemistry*, 1960, Vol. **75**, pp. 588-598 .

54. Bosia F., Abdalrahman T., Pugno M., Investigating the role of hierarchy on the strength of composite materials: evidence of a crucial synergy between hierarchy and material mixing, *Nanoscale*, 2012, Vol. **4,** pp. 1200-1207.

55. Lavalle P., Voegel J., Vautier D., Senger B., Schaaf P., Ball V., Dynamic aspects of films prepared by sequential deposition of species: perspectives for Smart responsive materials, *Advanced Materials*, 2011, Vol. **23**, pp. 1191-1221.

56. Salomaki M., Vinokurov I. A., Kankare J., Effect of temperature on the build-up of polyelectrolyte multilayers. *Langmuir*, 2005, Vol. **21**, pp. 11232-11240.

57. Currey J.D., Strain Rate Dependence of the Mechanical-Properties of Reindeer Antler and the Cumulative Damage Model of Bone-Fracture, *Journal of Biomechanics*, 1989, Vol. **5,** pp. 469-475.

58. Rubner M., Materials Science: Synthetic Sea Shell. *Nature*, 2003, Vol. **423**, pp. 925-926.

59. Fratzl P., Barth F.G., Biomaterial systems for mechanosensing and actuation. *Nature*, 2009, Vol. **462**, pp. 442-448.

60. Curry J.D., Mechanical-Properties of Bone Tissues with Greatly Differing Functions. *Journal of Biomechanic*s, 1979, Vol. **12**, pp. 313-318.

61. Ariga K., Sasaki Y., Hoiguchi H., Kikuchi J., Layered nanoarchitectures between cationic and anionic materials - Composite assemblies of polyions, lipid bilayers, and proteins. *Soft Chemistry Leading to Novel Materials*, 2001, Vol. **191**, pp. 35-60.

62. Blodgett K., Films Built by Depositing Successive Monomolecular Layers on a Solid Surface, *Journal of American Chemistry*, 1934, Vol. **57,** pp. 1004-1022.

63. Podsiadlo P., Tang Z., Shim B., Kotov N., Counterintuitive Effect of Molecular Strength and Role of Molecular Rigidity on Mechanical Properties of Layer-by-Layer Assembled Nanocomposites, *Nano Letters*, 2007, Vol **7**, pp. 1224-1231.

64. Dobrynin A., Rubinstein M., Theory of polyectrolyes in solutions and at surfaces, *Polymer Science*, 2005, Vol. **30**, pp. 1049-1118.

65. Joussein E., Petit S., Churchman J., Theng B., righi D., Delvaux B., Halloysite clay minerals- a review, *Clay Minerals*, 2005, Vol. **40**, pp. 383-426.

66. Elbert D., Herbert C., Hubbell J.A., Thin polymer layers formed by polyelectrolyte multilayer techniques on biological surfaces. *Langmuir*, 1999, Vol. **15**, pp. 5355-5362.

67. Saubery Z., Immobilization for an aluminium nitride based biosensor, *Physics*, 1959, Vol.**155**, pp.206-222.

68. Donath E., Walther D., Shilov V., Knippel E., Budde A., Lowack K., Mohwald H., Non-linear hairy layer theory of electrophoretic fingerprinting applied to

consecutive layer-by-layer polyelectrolyte adsorption onto charged polystyrene latex particles, *Langmuir*, 1997, Vol. **13,** pp. 5294-5305.

69. Robert J., Contact angle, wetting, and adhesion: a critical review, *Adhesion Science and Technology*, 1992,Vol. **6**, pp. 1269-1302.

70. Decher G., Hong J.D., Build up of ultrathin mutilayer films by self assembly process, consecutive adsorption of anionic and cationic bipolar polyelectrolytes on charges surface. *Physical Chemistry*, 1991, Vol. **95**, pp. 1430-1435.

71. Caruso F., Niikura K., Furlong D., Okahata Y., Assembly of alternating polyelectrolyte and protein multilayer films for immunosensing, *Langmuir*, 1997, Vol. **13**, pp. 3427-3433.

72. Timoshenko S.P., Gere J.M., Theory of elastic stability. McGraw Hill, 2nd Edition, ISBN: 007858217, 1963, pp. 453-467.

73. McLeish T.C.B., Tube theory of entangled polymer dynamics, *Advances in Physic*s, 2002, Vol. **51,** pp. 1379-1527.

74. Bennadji-Gridi F., Smith A.,Biomimetics, learning from nature, M*aterials Science Engineering*, 2006, Vol. **130**, pp. 132-136.

75. Ieker P., Schnho M., Linear and Exponential Growth Regimes of Multilayers of Weak Polyelectrolytes in Dependence on pH , *Macromolecules*, 2010,Vol. **43**, pp. 5052-5059.

76. Iler R.K., Multilayers of colloidal particles. *Colloid Interfaces Science*, 1966, Vol. **21**, pp. 569-594.

77. Schlenoff J.B., Ly H., Li M., Charge and mass balance in polyelectrolyte multilayers, *American Chemical Society*, 1998, Vol. **10**, pp. 347-352.

78. Zhao Q., Qian J., An Q., Speedy fabrication of free-standing layer-by-layer multilayer films by using polyelectrolyte complex particles as building blocks, *Journal of Materials Chemistry*, 2009, Vol. **19,** pp. 8448-8455.

79. Samuel R. E., Shukla A., Paik D.H., Wang M.X., Fang J.C., Schmidt D.J., Hammond P.T., Osteoconductive protamin based polyelectrolyte multilayer functionalized surfaces, *Biomaterials*, 2011, Vol. **32**, pp. 7491-7502.

80. Higgs P., Joanny J., Theory of polyampholyte solutions. *Journal of Chemical Physics*, 1991, Vol. **94,** pp. 1543-1554.

81. Schlenoff J.B., Laurent H., Stepp J., Redox active polyelectrolyte multilayers. *Advanced Materials*, 1998, Vol. **10**, pp. 347-356.

82. Kuhn H., Mobius D., Systems of monomolecular Layers Assembling and physico-chemical behaviour. *Angewandte Chemie- International Edition*, 1971, Vol. **10**, pp. 620-628.

83. Guzman E., Ritacco H., Rubio J., Rubio R. G., Ortega F., Salt induced changes of polyelectrolyte multilayers, *Soft Matter,* 2009, Vol**. 5**, pp. 2130-2142.

84. Zhai L., Cebeci F., Cohen R., Rubner M., Stable superhydrophobic coatings from polyelectrolyte multilayers, *Nano Letters,* 2004, Vol. **4**, pp. 1349-1353.

85. Kumar S., Self-Healing Materials: Fundamentals, *Design Strategies, and Applications*, 2009, Vol. **4,** pp. 130-134.

86. Zhu F., Zhou Y., Yang C., Zhang R., Xie L., Molecular approaches to understand biomineralization of shell nacreous layer, *Progress in Molecular and Subcellular Biology,* 2011, Vol. **52**, pp. 331-352.

87. Weiner S., Biomineralization: A structural perspective. *Journal of Structural Biology,* 2008, Vol. **163,** pp. 229-234.

88. Weiner S., Dove P., An overview of biomineralization processes and the problem of the vital effect, *Biomineralization,* 2003, Vol. **54**, pp. 1-29.

89. Zolotoyabko E., Pokroy B., Biomineralization of calcium carbonate: structural aspects, *Crystengcomm*, 2007, Vol. **9,** pp. 1156-1161.

90. Addadi L., Joester D., Nudelman F., Weiner S., Mollusk shell formation: a source of: a source of new concepts for understanding biomineralisation processes, *Chemistry- A European Journal,* 2006, Vol. **12,** pp. 980-987.

91. Nudelman F., Gotliv B., Addadi L.. Weiner S., Mollusk shell formation: Mapping the distribution of organic matrix components underlying a single aragonitic tablet in nacre. *Structural Biology,* 2006, Vol. **153,** pp. 176-187.

92. Nishimura T., Imai H., Oaki Y., Sakamoto T., Kato T., Preparation of thin film hydroxyapatite/ polymer hybrids, *Chemical Letters,* 2011, Vol. **40,** pp. 458-460.

93. Mahamid J., Sharir A., Addadi L., Weiner S., Amorphous calcium phosphate is a major component of bone formation: Indications for an amorphous precursor phase. *Proceedings of the National Academy of Sciences*, 2008, Vol **105**, pp. 12748-12753.

94. Veis A., Mineralization in organic matrix frameworks, *Biomineralization,* 2003, Vol. **54**, pp. 249-289.

95. Wei Y., Zuo S., Microstructure observation and mechanical behaviour modeling for limnetic nacre. *Acta Mechanica*, 2008, Vol. **24**, pp. 83-89.

96. Ozin G., Arsenault A., A chemical approach to Nanomaterials. *The Royal Society of Chemistry,* 2006, Vol. **2**, pp. 15-20.

97. Waite J. H., Mussel adhesion: finding the tricks worth mimicking, *Journal of Adhesion*, 2005, Vol. **81**, pp. 297-301.

98. Olszta M., odom D., Douglas E., Gower L., A new paradigm for biomineral formation: Mineralization via an amorphous liquid-phase precursor, *Connective Tissue Research*, 2003, Vol. **44**, pp. 326-334.

99. Hammond P.T., Form and function in multilayer assembly: New applications at the nanoscale, *Advanced Materials*, 2004, Vol. **16**, pp. 1271-1293.

100. Lakes R., Materials with structural hierarchy, *Nature*, 1996, Vol. **361**, pp. 511-515.

101. Lapcik L., De Smedt S., Demeester J., Chabrechek P., Hyaluronan: preparation, structure, properties, and applications, Chemistry Reviews., 1998, Vol. **98**, pp. 2663-2684.

102. Cripps F., A review of analysis methods for sub-micron indentation testing. *Vacuum*, 2000, Vol. **58**, pp. 569-585.

103. Nudelman F., Pieterse K., George A., Bomans P., Brylka L., Hilbers P., Sommerdijk N., The role of collagen in bone apatite formation in the presence of hydroxyapatite nucleation inhibitors, *Nature Materials*, 2010, Vol. **9**, pp. 1004-1009.

104. Olszta M., Cheng X., Kumar R., Kaufman M., Douglas W., Gower L., Bone structure and formation: A new perspective, *Materials Science & Engineering Reports*, 2007, Vol. **58,** pp. 77-116.

105. Wang Y., Yang C., Chen X., Zhao N. Biomimetic formation of hydroxyapatite/collagen matrix composite, *Advanced Engineering Materials, 2*006, Vol. **8,** pp. 97-100.

106. Ashby M.F., Gibson L.J., Olive R., The mechanical properties of natural materials. I. Material property charts, *Proceedings of the Royal Society-Mathematical, Physical and Engineering Sciences*, 1995, Vol. **450**, pp. 123-140.

107. Landis W., Hodgens K., Arena J., Song M., McEwen B., Structural relations between collagen and mineral in bone as determined by high voltage electron microscopic tomography, *Microscopy Research and Technique*, 1996, Vol. **33**, pp. 192-202.

108. Sugawara A., Nishimura T., Yamamoto Y., Kato T., Self-organisation of orientated calcium carbonate/polymer composites: Effects of a matric peptide isolated from the exoskeleton of a crayfish. *Angewandte chemie*., 2006, Vol. **45,** pp. 2876-2879.

109. Beniash E., Aizenberg J., Addadi L., Weiner S., Amorphous calcium carbonate transforms into calcite during sea urchin larval spicule growth, *Proceeding of the Royal Society of London Series B- Biological Sciences*, 1997, Vol. **264**, pp. 461-465.

110. Jiang C., Markutsya S., Tsukruk V.V., Individual plasmon resonances in nanoparticle films obtained by spin-assisted layer-by-layer assembly. Langmuir, 2004, Vol. **20**, pp. 882-890.

111. Srivastava S., Kotov N., Composite Layer-by-Layer Assembly with Inorganic Nanoparticles and Nanowires. *Chemistry Research*, 2008, Vol. **41**, pp. 1831-1841.

112. Mamedov A., Kotov N., Prato M., Guildi D., Wicksted J., Hirsch A., Molecular design of strong single-wall carbon nanotube/polyelectrolyte multilayer composites. *Nature Materials*, 2002, Vol. **1**, pp. 190-194.

113. Samanta T., Mukherjee M., Swelling dynamics and swelling induced structural changes of polyelectrolyte ultrathin films. *Polymer*, 2014, Vol. 55, pp. 4385-4393.

114. Kotov N., Layer-by-layer self-assembly: The contribution of hydrophobic interactions, *Nanostructured Materials* 1999, Vol. **12**, pp. 789-796.

115. Mamedov A., Kotov N., Free standing layer-by-layer assembled films, magnetite nanoparticles, *Langmuir*, 2000, Vol. **16**, pp. 5530-5533.

116. Schlenoff J. B., Dubas S. T., Farhat T., Sprayed polyelectrolyte multilayers., *Langmui*r, 2000, Vol. **16,** pp. 9968-9969.

117. Porcel C., Lavalle P., Decher P., Senger G., Voegel B., Schaaf J.C., Influence of the polyelectrolyte molecular weight on exponentially growing multilayer films in the linear regime, *Langmuir*, 2007, Vol. **23**, pp. 1898-1904.

118. Etienne O., Picart C., Keller E., Schaaf P., Voegel J.C., Haikel Y., Egles C., Polyelectrolyte Multilayer Film Coating and Stability at the Surfaces of Oral Prosthesis Base Polymers: an in vitro and in vivo Study, *Journal of Dental Restoratives*,. 2006, Vol. **85**, pp. 44-48.

119. Schlenoff J., Ly H., Li M., Charge and mass balance in polyelectrolyte multilayers, *Journal of the American Chemical Society*, 1998, Vol. **120**, pp. 7626-7634.

120. Shiratori S., Rubner M., pH-dependent thickness behavior of sequentially adsorbed layers of weak polyelectrolytes. *Macromolecules*, 2000, Vol. **33,** pp. 4213-4219.

121. Sigma- Aldrich. 2014.
Cited: https://www.sigmaaldrich.com, Date accessed: 30/05/2014.

122. Runlan J.C., Lin A., Choi J.K., Antimicrobial behaviour of polyelectrolyte multilayer films containing cetrimide and silver, *Biomacromolecules*, 2005, Vol. **6**, pp. 1149-1153.

123. Tyreone P., Vautier D., Haikel J.C., Voegel J., Schaaf P., Chluba J., Viability, adhesion and bone phenotype of osteoblast-like cells on polyelectrolyte multilayer films, *Biomimedical Materials*, 2002, Vol. **15,** pp. 657-667.

124. Brunot C., Ponsonnet L., Lagneau C., Farge P., Picart C., Grosgogeat B., Cytotoxcity of polyethylamine (PEI), precursor base of polyelectrolyte multilayer films, *Biomaterials,* 2007, Vol. **28**, pp. 632-640.

125. He T., Chan V., Covalent layer-by-layer assembly of polyethyleneimine multilayer for antibacterial applications, *Biomedical Materials Research*, 2010, Vol. **95**, pp. 454-459.

126. Smith R., McCormick M., Barrett J., Reven L., Smith R., Spiess W., NMR studies of PAH-PSS polyelectrolyte multilayers adsorbed onto silica, *Macromolecules*, 2004, Vol. **37**, 4830-4838**.**

127. Schonhoff M., Layered polyelectrolyte complexes, physics of formation and molecular porperties. *Journal of Physics Condensed Matter,* 2003, Vol. **15**, pp. 781-785.

128. Marthe R., Meibo A., Geze M., Bourat X., Angellier M., Lopez E., Dynamics of sheet nacre formation in bivalves. *Journal of Structural Biology*, 2009, Vol. **3**, pp. 190-195.

129. Podsiadlo P., Tang Z., Shim B., Kotov N., Counterintuitive Effect of Molecular Strength and Role of Molecular Rigidity on Mechanical Properties of Layer-by-Layer Assembled Nanocomposites, *Nano Letters,* 2007, Vol. **7**, pp. 1224-1231.

130. Dahne C.S., Tailor-made polyelectrolyte microcapsules: From multilayers to smart containers. *Chemistry International,* 2004, Vol. **43**, pp. 3762-3783.

131. Podsiadlo P., Shim B., Kotov N., Clay and polymer/carbon nanotube hybrid organic-inorganic multilayered composites made by sequential layering of nanometer scale films, *Polymer Coordination Chemistry*, 2009, Vol. **253**, pp. 2835-2851.

132. Shafir A., Andelman D., Phase behaviour of polyelectrolyte-surfactant complexes at planar surfaces, *American Physical Society,* 2006, Vol. **74,** pp. 155-160.

133. Picart C., Lavalle P., Cuisinier F., Decher G., Schaaf P., Voegel J., Buildup Mechanism for Poly(l-lysine)/Hyaluronic Acid Films onto a Solid Surface, *Langmuir,* 2001, Vol. **17**, pp. 7414-7424.

134. Picart C., Mutterer J., Richert L., Luo L., Prestwich G., Schaaf J.C, Lavalle P., Molecular basis for the explanation of the exponential growth of polyelectrolyte multilayers, *Proceeding of the National Academy of Science of the USA*, 2002, Vol. **99**, pp. 12531-12535.

135. Hoda N., Larson R., Modeling the Buildup of Exponentially Growing Polyelectrolyte Multilayer Films, *Physical Chemistr*y, 2009, Vol. **113**, pp. 4232-4241.

136. Dejeu J., Membreys F., Dizian S., Bainier C., Spajer M., Charraut D., Foissy J., Study of Film Growth Properties of Self-Assembled Polyelectrolyte Films of Higher Thickness: Reflectometric and Focused Ion Beam Analyses, *Physical Chemistry*, 2008, Vol. **112**, pp. 10531-10537.

137. Hubsh E., Ball V., Senger B., Becher G., Voegel J., Schaaf P., Controlling the Growth Regime of Polyelectrolyte Multilayer Films: Changing from Exponential to Linear Growth by Adjusting the Composition of Polyelectrolyte Mixtures, *Langmuir*, 2004, Vol. **20**, pp. 1980-1985.

138. Lavalle P., Picart C., Muttterer J., Gergely C., Reiss H., Voegel J.C., Senger B., Schaaf J., Modeling the buildup of polyelectrolyte multilayer having exponential growth, *Phyical Chemistry*, 2004, Vol. **108**, pp. 635-648.

139. Salomaki M., Vinokurov I. A., Kankare J., Effect of temperature on the buildup of polyelectrolyte multilayers, *Langmuir* , 2005, Vol. **21**, pp. 11232-11240 .

140. Podsialo P., Michel M., Lee Jungwoo., Verploegen E., Kam N., Ball V., Hart A., Exponential growth of LAYER-BY-LAYER films with incorporated inorganic sheets. *Nano letters*, 2008, Vol. **8,** pp. 1762-1770.

141. Somasundaran P., Kramer G., Time-dependant conformational changes of polyelectrolyte complexes in solution Colloids and Surfaces, *Physicochemical* Engineering, 2004, Vol. **250**, pp. 189-193.

142. Lavalle P., Gergley C., Cuisinier F., Decher G., Schaaf P.,Picart C., Comparison of the structure of polyelectrolyte multilayer films exhibiting a linear and an exponential growth regime: An in situ atomic force microscopy study. *Macromolecules*, 2002, Vol. **35** , pp. 4458-4465.

143. Ostrander J., Mamedov A., Kotov N., Two modes of linear layer-by-layer growth of nanoparticle-polyelectrolyte multilayers and different interaction-layer-by-layer deposition. *American Chemical Society*, 2001, Vol. **123**, pp. 11232-11240.

144. Beruto D., Searcy A. W., Use off Langmuir method for kinetic studies of decomposition reactions: calcite, *Journal of Chemical Society*, 1974. Vol**. 70**, pp.2145-2153.

145. Burke S., Barrett C., Controlling phyiochemical properties of weak polyelectrolyte multilayer films through acid base equilibria, *Pure and Applied Chemistry*, 2004, Vol. **76,** pp. 1387-1398.

146. Mjahed H., Cado G., Boulmedais F., Senger B., Schaaf P., Ball V., Voegel J., Restructuring of exponentially growing polyelectrolyte multilayer films induced

by salt concentration variations after film deposition. *Journal of Materials Chemistry*, 2011,Vol. **21**, pp. 8416-8421.

147. Laugel N., Betscha C., Winterhalter M., Voegal J-C., Ball V., Relationship between the growth regime of polyelectrolyte multilayers and the polyanion/polycation complexation enthalpy, *Physical Chemistry*, 2006, Vol. **110**, pp. 19443-19449.

148. Ladam G., Schaad P., Voegel J.-C., Schaaf P., Decher G., In situ determination of the structural properties of initially deposited polyelectrolyte multilayers. *Langmuir*, 2000, Vol. **16**, pp. 1249-1255.

149. Kiryukhin M. V., Man S. M., Sadovoy A. V., Low H. Y., Sukhorukov G.B. Peculiarities of Polyelectrolyte Multilayer Assembly on Patterned Surfaces. *Langmuir*, 2011, Vol. **27**, pp. 8430-8436.

150. Kiryukhin M. V., Man S. M., Gorelik S., Subramanian G.S., Low H.Y., Sukhorukov G.B., Fabrication and mechanical properties of microchambers made of polyelectrolyte multilayers, *Soft Matter*, 2011, Vol. **7**, pp. 6550-6556.

151. Johnson T.J., Waddel E., Kramer G., Locascio L.E., Chemical mapping of hot-embossed and UV-laser ablated microchannels in poly(methyl methacrylate) using carboxylate specific fluroscent and UV laser-ablated microchannels, *Applied Surfaces Science*, 2001, Vol. **181**, pp. 148-159.

152. Tang Z., Wang Y., Podsiadlo P., Kotov N., Biomedical applications of layer-by-layer assembly: from biomimetics to tissue engineering, *Advanced Materials*,2006, Vol. **18**, pp. 3203-3224.

153. Nolte A. J., Rubner M. F., Cohen R. E., Determining the young's modulus of polyelectrolyte multilayer films via stress-induced mechanical buckling instabilities, *Macromolecules*, 2005, Vol. **38**, pp. 5367-5370.

154. Park W., Kim D. H., Jung S.-W., Yi G.-C., Metalorganic vapor-phase epitaxial growth of vertically well-aligned ZnO nanorods, *Applied Physics Letters*, 2002, Vol. **80**, pp. 4232-4237.

155. Mann S., Biomimetic Materials Chemistry, ISBN: 9780471185970, *John Wiley and Sons*, 1997, pp. 315-355.

156. Bertrand P., Jonas A., Laschewsky A., Legras R., Ultrathin polymer coatings by complexation of polyelectrolytes at interfaces: suitable materials, structure and properties, *Macromolecular Rapid Communications*, 2000, Vol. **21**, pp. 319-348.

157. Kiryukhin M., Man S.M., Tonoyan A., Low H., Sukhorukov G., Adhesion of polyelectrolyte multilayers- sealing and transfer of microchamber arrays, *Langmuir*, 2012, Vol. **28**, pp. 5678-5686.

158. Heuvingh J., Zappa M., Fery A., Salt softening of polyelectrolyte multilayer capsules, *Langmuir*, 2005, Vol. **21**, pp. 3165-3171.

159. Hiller J., Mendelsohn J.D., Rubner M.F., Reversibly erasable nanoporous anti-reflection coatings from polyelectrolyte multilayers, *Nature Materials*, 2002, Vol. **59**, pp.59-63.

160. Krol S., Guerra S.D., Grupillo M., Diaspro, Gliozzi A., Marchetti P., Multilayer nanoencapsulation. New approach for immune protection of human pancreatic islets. *Nano Letters*, 2006, Vol. **6**, pp. 1933 – 1939 .

161. Fischer H., Materials Science and Engineering, Polymer nanocomposites: from fundamental research to specific applications, *Materials Science*, 2003, Vol. **23**, pp.763-772.

162. Shi J., Tae-Gon C., Jonathan C., Alfred R., Diggs, Jong Hyun Choi, Marshall D., Porterfield, Microbiosensors based on DNA modified single-walled carbon nanotube and Pt black nanocomposites., *Analyst*, 2011, Vol. **136**, pp. 4916-4924.

163. Gieshaber D., MacKenzie R., Voros J., Reimhult E., Electrochemical biosensors, sensor principles and architectures, *Sensors*, 2008, Vol. **8**, 1400-1458.

164. Toshiaki K., Atsushi K., Noda I., Nagasawa M., Conformation of Polyelectrolyte in Aqueous solution, *Macromolecules*, 1980, Vol. **13**, pp. 57–63.

165. Singamenini S., Mc Conney M., Tsukruk V., Spontaneous self- folding in confined ultrathin polymer gels. *Advanced Materials*, 2010, Vol. **11,** pp.1263-1268.

166. Grunlan J.C., Choi J.K., Lin A., Antimicrobial behavior of polyelectrolyte multilayer films containing cetrimide and silver, *Biomacromolecules*, 2005, Vol. **6,** pp. 1149-1153.

167. Chou S., Krauss P., Renstrom P., Nanoimprint Lithography, *Journal of Vaccine Science and. Technology*, 1996, Vol. **14**, pp. 4129-4133.

168. Guzman E., Ritacco H., Rubio J., Ortega F., Salt-induced changes in the growth of polyelectrolyte layers of poly(diallyl-dimethylammonium chloride) and poly(4-styrene sulfonate of sodium), *Soft Matter*, 2009, Vol. **5**, pp. 2130-2142.

169. Lee D., Nolte A., Kunz A., Rubner M., Cohen J., pH-induced hysteretic gating of track-etched polycarbonate membranes: Swelling/deswelling behavior of polyelectrolyte multilayers in confined geometry, *Journal of the American Chemical Society*, 2006, Vol. **128,** pp. 8521-8529.

170. Alem H., Blondeau F., Glinel K., Demoustier-Champagne., Layer-by-Layer Assembly of Polyelectrolytes in Nanopores, *Macromolecules*, 2007, Vol. **40**, pp. 3366-3372.

171. Dobrynin A., Colby R., Rubinstein M., Scaling Theory of Polyelectrolyte Solutions, *Macromolecules,* 1995, Vol. **28,** pp. 1859-1871.

172. Ashby M., Brecher Y., Cebon D., Salvo L., Selection strategies for materials and processes, *Materials and Design*, 2004, Vol.**25**, pp.51-67.

173. Ramsden J.J., Lvov Y.M., Decher G., Determination of optical-constants of molecular films assembled via alternate polyion adsorption, *Thin Solid Films,* 1995, Vol **254**, pp. 343-344.

174. Decher G., Eckle M., Schmitt J., Struth B , Layer-by-layer assembled multicomposite films. *Current Opinion in Colloids & Interface Science,* 1998, Vol. **3**, pp. 32-39.

175. Dua A., Equilibrium and dynamics of dilute polymer solutions. *Polymer,* 2010, Vol. **7,** pp.1253-1403.

176. Roberts G.G., An applied science perspective of Langmuir-Blodgett films, *Advances in Physics,* 1985, Vol. **34**, pp.475-512.

177. Ferguson E., Kleinfield E.R., Stepwise formation of multilayered nanostructures from macromolecular precursors, *Science,* 1994, Vol. **265,** pp. 370-373.

178. Center of Science Education Resource. What is X-ray Diffraction [Online]www.serc.carleton.edu/research_education/geochemsheets/techniques/XRD.html. [Accessed: 06-2014]

179. Humphreys J., Beanland R., Electron microscopy and analysis. *Taylor and Francis*, 2001, Vol. **6**, pp. 122-169.

180. Goodhew P.J., Humphreys J., Beanland R. New York : Taylor and Francis, Electron microscopy and analysis, *Springer Science & Business Media*, 2009, Vol. **3**, pp.640-646.

181. Chescoe D., Goodhew P.J., The operation of transmission and scanning electron microscopes. New York : *Oxford University Press,* 1990, pp. 47- 80.

182. Bagambisa F., Joos U., Schilli W., A scanning electron microscope study of the ultrastructural organisation of bone-mineral. *Cells and Materials,* 2006, Vol. **3**, pp. 93-102.

183. Bertrand P., Jonas A., Laschewsky A., Legras R., Ultrathin polymer coating by complexation of polyelectrolyes at interfaces: suitable materials, structures and properties. *Macromolecule Rapid Communcations*., 2000, Vol. **21**, pp. 319-348.

184. Reimer L., Kohl H., Transmission electron microscopy: Physics of image formation, *Springer Series in Optical Sciences,* 2008, Vol. **5**, pp. 420-429.

185. Braga P.C., Ricci D., Atomic Force Microscopy, Biomedical methods and applications, *Methods in Molecular Biology,* 2004, Vol. **242**, pp. 13-20.

186. Avarro C., Ruiz-Agudo E., Luque A., Rodriguez A., Huertas M., Thermal decomposition of calcite: Mechanisms of formation and textural evolution oof CaO nanocrystals, *American Mineralogist,* 2009, Vol. **94**, pp. 578-593.

187. How does TOF-SIMS work? Max Plank Institute. [Online] 2015. www2.fkf.mpg.de/ga/machines/sims/How_does_TOF_SIMS_work.html [Accessed: 06/2014].

189. Kim Y., Douglas E., Gower l.Patterning inorganic thin films via a polymer-induced liquid-precursor process, *Langmuir,* 2007, Vol. **23**, pp. 4862-4870.

190. Tan W. S., Cohen R. E., Rubner M. F., Sukhishvili S. A., Temperature-Induced, Reversible Swelling Transitions in Multilayers of a Cationic Triblock Copolymer and a Polyacid, *Macromolecules,* 2010, Vol. **43**, pp. 1950-1957.

191. Wang N. M., Liechti K., White J., Winter R., Nano-indentation of polymeric thin films with an interfacial force microscope. *Mechanics and Physics of Solids,* 2004,Vol. **52**, pp. 2329-2354.

192. Kranenburg J., Tweedie C., Vliet J., Schubert U., Challenges and Progress in High-Throughput Screening of Polymer Mechanical Properties by Indentation. *Advanced Materials,* 2007, Vol.**21**, pp. 3551-3561.

193. Hall. A, Orientated hydroxyapatite, *Crystengcomm,* 2011, Vol **13,** pp. 2077-2083.

194. Poole C., Ownes F., Introduction to Nanotechnology, New York, John Wiley and Sons, ISBN: 0471079359, 2003, pp. 257-310.

195. Wang L., Nancollas G., Pathways to biomineralization and biodemineralization of calcium phosphates: the thermodynamic and kinetic controls, *Dalton Transactions,*2008, Vol. **15**, pp. 2665-2672.

196. Wang Y. J., Yang C. R., Chen, X. F., Zhao N. R., Biomimetic formation of hydroxyapatite/collagen matrix composite. *Advanced Engineering Materials,* 2006, Vol. **8**, pp. 97-100.

197. Bigi A., Gandolfi M., Roveri N.,Valdre G., In vitro calcified tendon collagen: An atomic force and scanning electron microscopy investigation. *Biomaterials,* 1997, Vol. **18** , pp. 657-665.

198. Baagambisa F.B., Joos U., Schilli W., Scanning microsope study of the ultrastructural organisation of bone mineral . *Cells and materials,* 1993, Vol. **3,** pp. 93-103.

199. Johansson J., Halthur T., Herranen M., Lennart S. Build up of collagen and hyaluronic acid polyelectrolyte multilayer, *Biomacromolecules,* 2005,Vol. **6**, pp. 1353-1358.

200. Lowack K., Molecular mechanisms controlling the self-assembly process of polyelectrolyte multilayers. *Macromolecules*, 1998, Vol. **31**, pp. 823-833.

201. Decher G., Eckle M., Sschmitt, J., Struth B., Layer-by-layer assembled multicomposite films. *Current Opinion in Colloid & Interface Science*, 1998, Vol. **12**, pp. 32-39.

202. Wegst U. G. K., Bai H., Antoni E., Ritchie R., Bioinspired structural materials, *Nature Materials*, 2015,Vol. **84**, pp. 23-26.

203. Jackson, A. P., Vincent, J. F. V., Turner R. M., Comparison of nacre with other ceramic composites, *Journal of Materials Science*, 1990, Vol. **25**, pp. 3173-3178.

204. Espinosa H. D., Merger of structure and material in nacre and bone—perspectives on de novo biomimetic materials., *Materials Science*, 2009, Vol. **54**, pp. 1059-1100.

205. Schaffer T., Ionescuzanetti C., Proksch R., Walters D., Zaremba C., Belcher A., Morse D., Hansma P., Does abalone nacre form by heteroepitaxial nucleation or by growth through mineral bridges, *Chemistry of Materials*, 1997, Vol. **9**, pp. 1731-1740.

206. Gao H., Ji J., Jager B.H., Arzt I.L., Fratzl P., Materials become insensitive to flaws at nanoscale: Lessons from nature, *Medical Engineering and Physics*, 2003, Vol. **100,** pp. 5597-5600.

207. Olzsta M. J., Douglas E. P., Gower L. B., Scanning electron microscopic analysis of the mineralization of type I collagen via a polymer-induced liquid-precursor (PILP) process, *Calcified Tissue International*, 2003, Vol. **73**, pp. 583-591.

208. Olszta M. J., Odom D. J., Douglas E. P., Gower L. B., A new paradigm for biomineral formation: Mineralization via an amorphous liquid-phase precursor, *Connective Tissue Research*, 2003, Vol.**44**, pp. 326-334.

209. Picart C., Lavalle P., Hubert P., Cuisinier F. J. G., Decher G., Schaaf P., Voegel J. C. Buildup Mechanism for Poly(l-lysine)/Hyaluronic Acid Films onto a Solid Surface, *Langmuir*, 2001, Vol. **17**, pp. 7414-7424.

210. Wood KC., Chuang H.F., Batten R.D., Lynn D.M., Hammond P.T., ontrolling interlayer diffusion to achieve sustained, multi-agent drug delivery from layer-by-layer thin films, *National Academy Science USA*, 2006, Vol. **103**, pp. 10207.

211. Tan J.P.K., Wang Q., Tam K.C., Control of burst release from nanogels via layer-by-layer assembly, *Journal of Controlled Release*, 2008, Vol. **128**, pp. 248–254.

212. Wang J., Lin L., Cheng Q., Jiang L., A Strong Bio-Inspired Layered PNIPAM–Clay Nanocomposite Hydrogel, *Angewandte Chemie*, 2012, Vol. **51,** pp. 4676-4680.

213. Song F., Soh, A. K., Bai, Y. L., Structural and mechanical properties of the organic matrix layers of nacre, *Biomaterials*, 2003, Vol. **24**, pp. 3623-3631.

214. Venkat K., Lin W., Sitaraman K., Polymer Thin Films for Biomedical Applications Nanomaterials for the Life Sciences, *Nanostructured Thin Films and Surfaces*, 2010, Vol. **5**, pp.2511-2516.

215. Zhang W., Liao S., Cui F.,Hierarchical self-assembly of nano-fibrils in mineralized collagen, *Chemistry of Materials*, 2003, Vol. **15**, pp. 3221-3226.

216. Liu Y., Kim Y., Dai L., Khan S., Pashley D., Tay F., Hierarchical and non-hierarchical mineralisation of collagen, *Biomaterials*, 2011, Vol. **32,** pp. 1291-1300.

217. Lowack K., Helm C., Molecular mechanisms controlling the self-assembly process *Macromolecules*, 1998, Vol. **31,** pp. 823-833.

219. Lvov Y., Decher G., Sukhorukov G.,Assembly of thin films by means of successive deposition of alternate layers of DNA and poly(allylamine), *Macromolecules*, 1993, Vol. **26**, pp. 5396-5399.

220. Luo Y., Kirker K.R., Prestwich G.D., Cross-linked hyaluronic acid hydrogel films: new biomaterials for drug delivery, *Journal of Controlled Release*, 2000, Vol. **69**, pp.169–184.

221. Bigi A., Boanini E., Panzavolta S., Roveri N., Biomimetic growth of hydroxyapatite on gelatin films doped with sodium polyacrylate, *Biomacromolecules*, 2000, Vol. **1**, pp. 752-756.

222. Bigi A., Gandolfi M., Roveri N., Valdre G., In vitro calcified tendon collagen: An atomic force and scanning electron microscopy investigation, *Biomaterials*, 1997, Vol. **18**, pp. 657-665.

223. Zhang J., Senger B., Vautier D., Picart C., Schaaf P., Voegel J., Lavalle P., Natural polyelectrolyte films based on collagen and hyaluronic acid, *Biomaterials*, 2005, Vol. **26**, pp. 3353-3361.

224. Johansson J., Halthur T., Herranen M., Soderberg L., Elofsson U., Hilborn J., Build-up of collagen and hyaluronic acid polyelectrolyte multilayers, *Biomacromolecules*, 2005, Vol. **6**, pp. 1353-1359.

225. Bonderer L. J., Studart A. R., Gauckler L., Bioinspired design and assembly of platelet reinforced polymer films, *Science*, 2008, Vol. **319**, pp. 1069-1074.

226. Watanabe H., Viscoelasticity and dynamics of entangled polymers. *Polymer Science*, 1999, Vol. **24**, pp.1253-1403.

227. Meldrum F., Calcium carbonate in biomineralisation and biomimetic chemistry, *International Materials Reviews*, 2003, Vol. **48**, pp. 187-224.

228. Wei H., Ma N., Shi F., Wang Z.Q., Artificial nacre by alternating preparation of layer-by-layer polymer films and $CaCO_3$ strata, Chemistry Materials, 2007, Vol. **19**, pp. 1974-1978.

229. Wei H., Shen Q., Zhao Y., Wang W.J., Xu D.F., Crystallization habit of calcium carbonate in the presence of sodium dodecyl sulfate and polypyrrolidone, *Crystal Growth*, 2003, Vol. **260**, pp. 516-524.

230. Katti, K. S., Katti, D. R.,Why is nacre so tough and strong, *Materials Science and Engineering*, 2006, Vol. **26**, pp. 1317-1324.

231. Klitzing R., Mohwald H,. A realistic diffusion model for ultra thin polyelectrolyte films, *Macromolecules*, 1996, Vol. **29**, pp. 6901-6906.

232. Lutkenhaus J. L., Hrabak, K. D., McEnnis K., Hammond P. T., Elastomeric Flexible Free-Standing Hydrogen-Bonded Nanoscale Assemblies, *Journal of the American Chemical Society* 2005, Vol. **127**, pp.17228-17234.